University of St Andrews

The University of St Andrews

The Synthesis and Characterisation

Of

Supported Dendrimer Systems.

Thesis submitted in accordance with the requirements
Of the University of St Andrews for the degree
Of Doctor of Philosophy.

Emma Modrate

April 2004

Th E702

Declaration

I Emma Modrate, hereby certify that this thesis, which is approximately 40000 words in length, has been written by me, that is the record of work carried out by me and has not been submitted in any previous applications for a higher degree.

Date: 8|9|4   Signature of candidate:

I was admitted as a research student in October 2000and as a candidate for the degree of PhD in October 2000; the higher study for which this is a record was carried out in the University of St Andrews between 2000 and 2004.

Date: 8|9|4   Signature of candidate:

I hereby certify that the candidate has fulfilled the conditions of the Resolution and Regulations appropriate for the degree of PhD in the university of St Andrews and that the candidate is qualified to submit this thesis in application for that degree.

Date   30 August 2004   Signature of supervisor:

In submitting this thesis to the University of St Andrews I understand that I am giving permission for it to be made available for use in accordance with the regulations of the University Library for the time being in force, subject to any copyright vested in the work for not being affected thereby. I also understand that the title and abstract will be published, and that a copy of the work may be made and supplied to any *bona fide* library or research worker.

Date: 8|9|4   Signature of candidate:

Acknowledgments

Table of Contents

Chapter 3: The adsorption of thiocresol on Au surfaces

Chapter 4: The synthesis of vinyldimethyl-p-thiophenylsilane and the investigation of its adsorption on Au{111}.

Chapter 5: The adsorption of Generation 2 dendrimer thiol on Au surfaces

CHAPTER 1

BACKGROUND

1.1 Introduction

The use of dendrimers as homogeneous catalysts is a rapidly expanding research area. There are certain advantages of the heterogenisation of such catalysts - perhaps the most obvious of which is the ease of product separation from the catalyst. This research deals with the synthesis and characterisation (by NMR and GC) of thiol terminated dendrimers. These thiol terminated dendrimers are then adsorbed onto Au surfaces and their interaction with the surface is analysed by STM, RAIRS, TPD, AES, and XPS.

1.2 Dendrimers

Dendrimers are a unique class of polymers that can be distinguished from all other synthetic macromolecules by their globular shape. This shape occurs due to their perfectly branched architecture and their unique monodispersed nature[1]. Dendrimers have a regular and highly branched three-dimensional architecture. They were originally called cascade or arborol molecules and were first successfully synthesised in 1978 by Vögtle[2]. Dendrimer is a Greek word meaning tree part and it is used to describe how the molecule looks. The word cascade however is a more suitable description of the molecular nomenclature. The size weight and chemical functionality of individual dendrimers can be easily controlled by the synthetic methods used in their preparation. There are two different synthetic approaches for making a

dendrimer, divergent synthesis and convergent synthesis. With both of these approaches a branch point is inserted into the dendric structure at each synthetic step. Figure 1.1 shows the growth of a typical dendrimer molecule with a degree of branching of 100% (when there are no branch defects).
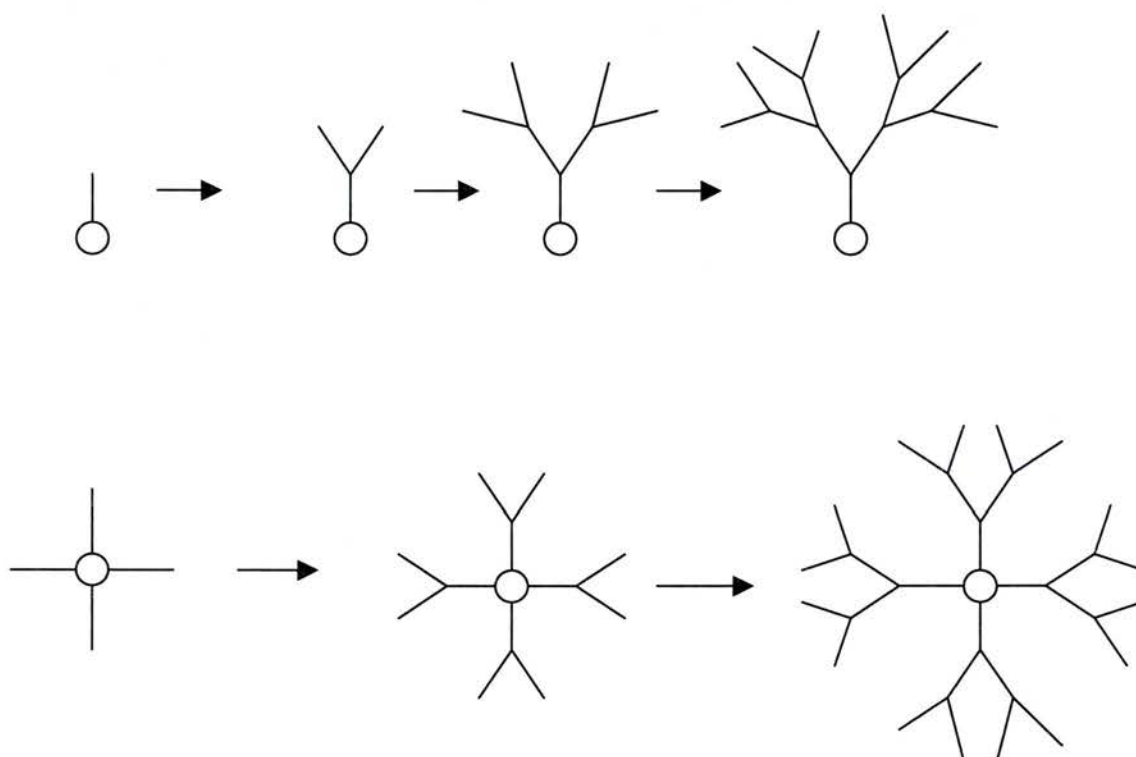
Figure 1.1 A diagram showing a very simple example of the growth of Dendrimer molecules

The highly branched dendric architecture shown in figure 1.1 causes the molecules to adopt a three-dimensional globular conformation which minimises free energy, with an immediate effect on macromolecular properties. The compositions of the chain ends of a dendrimer molecule also have a determining effect on many of the physical properties of the dendrimers, such as solubility or viscosity[1].

After Vögtle, [3]Denkewalted patented the synthesis of ℓ-Lysine based dendrimers in the early 1980's. These were said to have many generations however this was never proven because there was never any size exclusion chromatography data and no detailed characteristics of the materials were known. Progress in dendrimer research was initially slow, but in the early 1990s it took off rapidly. This was due to the synthesis of the first properly received dendrimers, for example, poly(amido amine) (PAMAM) dendrimers that were synthesised by Tomalia et al[3,4] and the introduction of Newkome's arborol system[5]. Both of these were divergently synthesised, however also in the 1990's Fréchet introduced the convergent synthesis approach and synthesised aromatic polyether dendrimers[6].

1.3 Convergent and Divergent synthesis

As mentioned above there are two different types of dendrimer synthesis, divergent synthesis and convergent synthesis. Divergent synthesis starts at the central core. The dendrimer is grown step by step until steric effects make bonding impossible. This means that numerous reactions have to be performed on a single molecule and so every reaction has to be very selective in order to ensure the integrity of the final product. This type of synthesis has some problems. For example, incomplete reactions at the end-groups are possible and so structural defects accumulate as the generations build up. Also each new divergently produced dendrimer cannot be purified and so these defects

cannot be avoided. Divergent synthesis is the macromolecular approach to dendrimer synthesis, where the purity is governed by statistics[7].

In convergent synthesis the opposite course has been taken and the difficulty of many reactions being performed on one molecule has been overcome as the synthesis is started at the periphery and ends at the core. This means that there are a low number of reaction sites warranted in every reaction step throughout the synthesis and so only a small number of side products can be formed. Also unlike in divergent synthesis every new generation can be purified by a technique such as gel permeation chromatography. Convergently produced dendrimers are dendrimers prepared by an organic chemistry approach and are defect free. However this type of synthesis does not allow the formation of as many generations as the divergent synthesis due to the steric problems arising from the reaction segments and the core molecule[7].

1.4 Dendrimer research

Until now research on dendrimers has been mostly confined to the preparation and molecular characterisation of a wide variety of dendrimers. For example it is now possible to produce dendrimers with a higher number of generations than before[2]. This is possible because these molecules are modelled on natural globular biomacromolecules. These large molecules are able to perform certain functions due to their three-dimensional formation and because of hydrogen bonding. The three dimensional structures are of great interest because they

are very different to biological macromolecules (such as proteins) in terms of their three dimensional covalently linked skeleton. For example if it is assumed that divergent synthesis makes each branch direct radially towards the outside and that the end-groups lie on the surface of an ellipsoid, the macromolecules transform into a special shape from a certain generation upwards, this is called "starburst dense packing". Recently, there have been many new types of dendrimer synthesised either through the synthesis of functional representatives of some already established dendric skeletons or from the production of new molecular skeletons. These new dendrimers can be as large as 10 generations (G10). In order to generate large generation dendrimers the combinatorial chemistry approach is now often used[7].

Over the past 16 years a wide range of "designer" dendrimers have been developed and these have been well studied and characterised. However the focus of dendrimer research has started to change and research is now being carried out on dendrimers for specific functions and particular applications for dendrimers are now being studied. Dendrimers have many different applications. For example, they are used in medicine, in molecular biology, host guest chemistry and catalysis. They are used most widely in medicine as drug delivery systems and they also come in the form of saccharide clusters from natural carbohydrate building blocks where they intervene in the body's specific adhesive phenomena thus preventing bacterial or viral infection[7].

The main applications of interest for this research are the application of dendrimers in catalysis and dendrimers at surfaces and interfaces. Dendrimers have nanoscopic dimensions and so can be molecularly dissolved. It is this combination of features that allows dendrimers to bridge the gap between homo- and heterogeneous catalysts. This means that dendrimers have the catalytic advantages of both homo- and heterogeneous catalysis. For example if the dendrimer is soluble and has well defined catalytic sites it may be possible to remove it from a homogeneous reaction mixture using simple separation techniques, e.g. ultra filtration. Very recently there have been studies on the uses and applications of dendrimers at surfaces and interfaces[1]. This will be discussed more fully below.

Research on dendrimers is diverse and is expanding rapidly. It is possible that dendrimers may be used in new devices because they are highly defined molecules, with precise submicron dimensions, and will be of great interest to the newer scientific fields, bio- and nanotechnology.

1.5 Dendrimer Catalysis

In liquid phase chemistry dendrimer catalysts combine the advantages of both homogeneous and heterogeneous catalysts. Putting these dendrimer catalysts onto solid supports may bridge the gap between these two branches of catalysts.

At the interface between heterogeneous and homogeneous catalysis there is great scope for developing new materials that can combine the advantages and/or minimise the disadvantages of each of the two classes of catalyst[8]. Homogeneous catalysts have many advantages over heterogeneous catalysts[9]. For example they have faster kinetics and an accessible metal centre. They are also considerably more selective than heterogeneous catalysts. However, they have one major drawback and that is they are very difficult to separate from a reaction mixture. Heterogeneous catalysts on the other hand are very easy to separate from a reaction mixture. Unfortunately their catalytic sites are often inaccessible; also they often have mass transfer problems which can vastly affect the activity of the catalyst, although this can be avoided by using open pore materials. Ideally by combining the strengths of both these catalysts, a catalyst would be produced that has fast kinetics, an available metal centre and is easily removable from a reaction once it is finished.

The first attempt at bridging the gap between the two catalytic types was to anchor catalytic metal sites to a polymer[10]. However this was not very successful as there is a great difficulty in accurately controlling the location and number of the metal sites. It did however show some catalytic possibilities and although not reusable, was able to be extracted from the reaction. It was after this research that dendrimers were considered. The reason why they were considered is because they are similar to polymers, *i.e. they are large structures built up of molecular building blocks*. However unlike polymers the position and amount of the active sites is easier to control. This is because the unique molecular structure of the dendrimer positions the active sites on its periphery branches. The first ever dendrimer functionalised to be a catalyst was by Knapen et al. in 1994[8]. Initially polysilane dendrimers were used and their periphery branches were functionalised with catalytically active metal sites. These dendrimers showed regiospecific catalytic activity for the Kharasch addition process, *i.e. the addition of CCl_4 to methyl methacrylate under standard conditions*. However although this was a breakthrough the catalyst used could still not be recycled or reused.

Initially dendrimers were used because of their shape and size[11]. The catalytically active sites are positioned on the periphery branches of a dendrimer because of the globular shape of the dendrimer. Also due to their molecular weight, size (~25Å) and again, globular shape they should be

retainable by either ultrafiltration or by using a membrane. It was also initially hoped that they would be able to find one that was completely reusable. [12]Later on researchers also hoped that another advantage of using dendrimers would be that crowding in the periphery might lead to constrained geometries in the metal binding and this then might affect the activity or even the selectivity of the catalyst.

In recent years there have been many different attempts at making the perfect dendrimer catalyst. There have been some non metal active sites but mostly it is metalladendrimers that have been worked on. Metalladendrimers can have active sites either on the periphery or in the core of the molecule but mostly on the periphery. Other than the work mentioned above one of the first dendrimer catalysts was developed by Knapen et al[8]. During their research they made two new dendrimer catalysts (G0{SiMe$_2$-ArNiBr}$_4$) and (G1-{SiMe$_2$-ArNiBr}$_{12}$). These represented nanoscopic catalysts with physical characteristics such as size, shape, solubility and dispersity of catalytic sites unlike those on related systems of conventional polymers which are not as well defined. These dendrimers were then successfully applied as a catalyst for the Knapen reaction. However unlike the example of dendrimer catalyst mentioned above these were removed, and although some activity was lost they were also reusable.

In 1999 Brinkmann et al[11]. used Pd active dendrimers as active catalysts where the dendrimers had Pd complexes on their periphery branches. The results of this research were positive and the dendrimers were recyclable. However after being used in the desired reaction the palladium, that origionally had 86% of the expected number of Pd atoms available, now only had 80% of the Pd atoms available. These results signify that the catalyst must have leached Pd into the reaction product and solution.

Recently work in this field has been carried out by Maraval et al[13]. They too looked at palladium complexes of dendrimers and compared them with already tried and tested catalytic systems such as $(Ph_3P)PdCl_2$. Under the desired reaction conditions, after 2.5 hours at room temperature the palladium complexed dendrimer induced 95% conversion of the reactants into the product whereas the $(Ph_3P)PdCl_2$ catalyst only induced 81% after 20 hours at 68°C. The dendrimer was easily removed from the product solution as an orange precipitate. There was no significant loss in activity and was reusable as it stood.

As was also mentioned above the production of a selective dendrimer catalyst is also very desirable. This has recently been achieved by Ropartz et al[12]. During their research they prepared dendrimers based on polyhedral oligomeric silsesquioxane cores e.g.
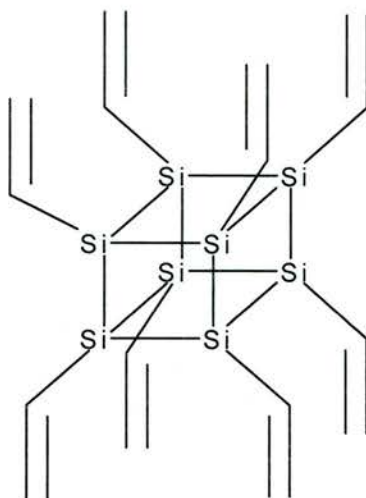
Figure 1.2. A polyhedral oligomeric silsesquioxane dendrimer core.

Dendrimers such as the one shown in figure 1.2 have sufficient steric crowding and so make bidentate co-ordination favourable. These rings then enhance the linear selectivity in hydroformylation reactions.

The work to be discussed in this thesis involves preparing thiol terminated dendrimers and then adsorbing them onto Au surfaces. When researching the literature on this subject there appears to be few examples of dendrimenr adsorbed onto Au{111} ever being investigated. The reasoning behind this research is that if the dendrimer catalysts are attached to a solid support then they will be even more easily removed from the reaction solution and hopefully completely reusable. The choice of thiol terminated dendrimers and Au{111} was dictated by the fact that Au is easily usable in atmospheric pressure and the growing field of self assembled monolayers show that thiol adsorption on Au surfaces can lead to well defined surfaces being produced.

1.6 Dendrimers on Surfaces

The study of self assembled monolayers of dendrimers on solid surfaces has enhanced the understanding of novel properties that are only accessible through surface confinement[1]. One of the first examples of research on dendrimers on surfaces showed the formation of multilayers when PAMAM dendrimers were sequentially deposited onto glass[14], e.g.

NH₂   NH₂   NH₂

K₂PtCl₄ 1) (D)-NH₂ 2) K₂PtCl₄

(repetitive sequence)
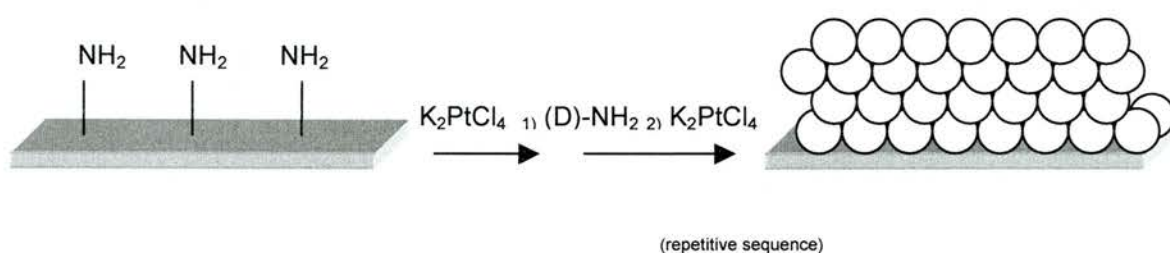
Figure 1.3 This shows the deposition of amine terminated dendrimers onto a Pt^{2+} bearing surface followed by reactivation by K_2PtCl_4. This example was published in 1994 by Watanabe and Regen[14].

This particular reaction used solutions of G6 or G4 PAMAM dendrimers. The ellipsometric film thickness was measured and the surfaces were studied by X-ray photoelectron spectroscopy (XPS). These techniques both confirmed the construction of the multilayered assemblies. This research led to the discovery of new classes of thin films[49] and other new research such as the creation of novel gel electrophoretic media which possess a relatively uniform pore structure capable of exceptionally high resolution, for use in the fabrication of heterogeneous catalysts that exhibit size selectivity.

This research also led to the investigation of the condensed phase behaviour of dendrimers, and the ordering of dendrimers on the surface. Dendrimers on surfaces are usually imaged using AFM and in 1996 Collaund et al.[15] performed a systematic AFM study on ultra thin films of mesogen substituted carbosilane dendrimers. The films investigated were non-equilibrium structures. Three different dendrimer generations were used, G1, G2 and G3, and deposition was carried out using different concentrations of the dendrimer. The AFM images showed that films produced from high concentrated dendrimer solutions were extremely flat, and lower concentration dosing solutions produced rough surfaces. However, at even lower concentrations the surface produced was also flat. No order was observed from the films produced through high concentration dendrimer solutions, however from the low concentration solutions the monolayers showed a cellular hole pattern. At the time of this research it was not possible to image individual dendrimer molecules as the AFM tip resolution at that time was not sufficiently accurate.

Research then lead on to the imaging of individual dendrimers. This was carried out in 1998 by Hierlemann et al.[16] using G4 and G8 PAMAM dendrimers. In this study Au substrates were dipped into 1×10^{-7}M dendrimer solution for 45s. Individual dendrimer molecules were successfully imaged by tapping mode AFM. However this was not the main aim of this research. After the dendrimer molecules were deposited onto the substrate it was soaked in a

1mmol hexadecanethiol solution for 24 – 110 hours. This formed focally substituted organothiol dendron adlayers on gold by chemisorption. This phenomenon occurred as the amine – Au interactions from the dendrimers are not as strong as the thiol – Au interactions from the alkanethiol, so in some cases the alkanethiol completely replaces the dendrimer and in other cases focally substituted organothiol dendron adlayers are formed. Infrared spectroscopy, X-ray photoelectron spectroscopy and ellipsometry were all used to interpret the nature of this adsorption and they all proved that chemisorption took place.

Many of the studies of dendrimers at surfaces and interfaces, investigate the adsorption characteristics and the various surface characteristics, *i.e. if they form ordered monolayers and how that order can be improved.* One example of this is Bo et al.[17], who change the normal terminal group on a Fréchet dendrimer to a thiol terminated group and then deposit it onto Ag and Au substrates. This research was carried out in 1998 and it was so successful that in 1999 Chechik and Crooks[18] substituted the amine terminal group on a PAMAM dendrimer.

PAMAM dendrimers possessing a thiol terminating group adsorb strongly to Au and Ag. This means they can be used to prepare dendric monolayers on planar and colloidal Au substrates. Research by Chechik and Crooks showed that the thiol terminated dendrimers formed stable monolayers on planar Au substrates.

XPS studies showed that most of the thiol groups had a direct interaction with the Au surface, this implied that the dendrimer molecules are flexible. These types of materials are of great interest, for example the ease of preparation of these materials along with the permeability of the dendrimer stabiliser makes them a possibility for use in sensing devices and in catalysis.

Later in 1999 Crooks et al.[19] imaged amine terminated dendrimers monolayers on Au and mixed dendrimer/alkanethiol monolayers on gold with tapping mode AFM (TM-AFM). Using this method they did not image the individual G4 dendrimers as the AFM cantilever apex was large compared to the size of the G4 dendrimer and also because the dendrimer coverage was high and the small inter-dendrimer spacing prevented any height measurement. The research here was to take images by AFM of the time dependent absorption of the alkanethiols to the already dendrimer modified gold surfaces. The results showed that after some time the alkanethiols with long methylene chains such as C_{16} and more completely displaced the dendrimer from the surface of the gold, whereas the alkanethiols with less methylene groups displaced only some of the dendrimer. They also show that agglomeration of dendrimers occur when the films are exposed to the thiol figure 1.4 shows some of the images taken by Crooks et al[19].
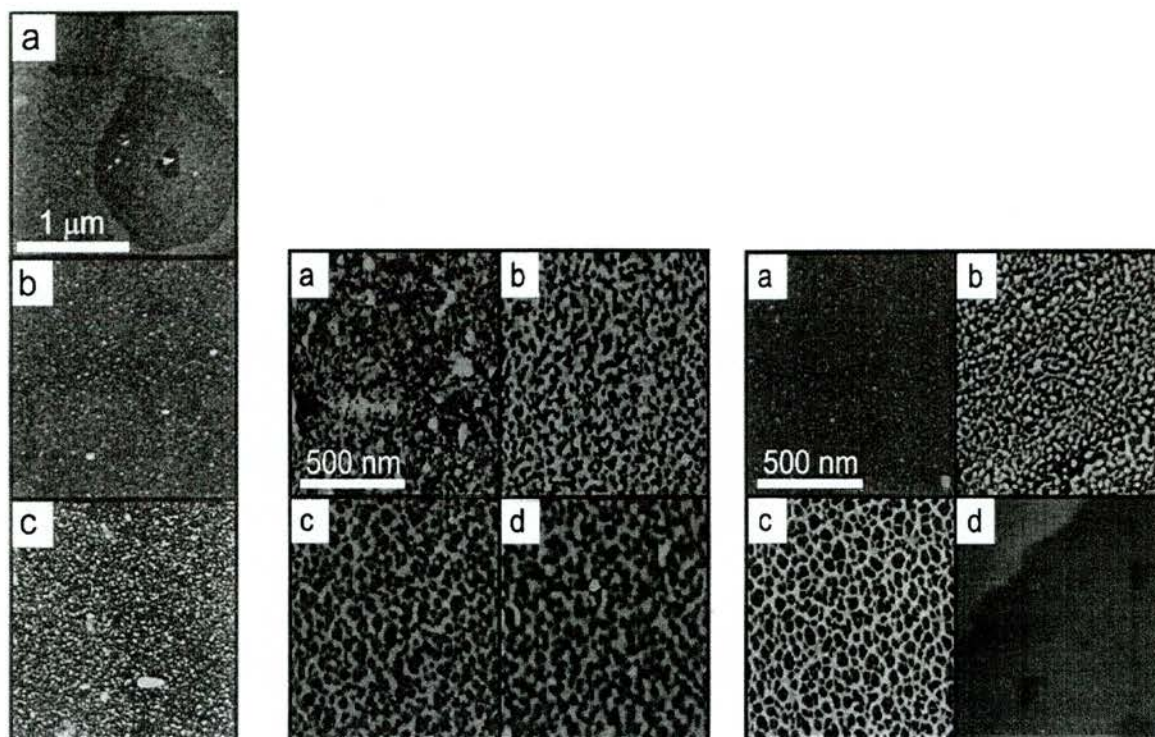
Figure. 1.4 The first of these three pictures shows gold fully covered by a)G4-NH, b)G6-NH, c)G8-NH. The second two images show the G4-NH covered gold immersed in a thiol solution (C5SH for first image and C16SH for second image) after certain periods of time a) 1min, b)1h, c)24h and d)96h. This clearly shows that for the C5SH (where the light grey parts of the image are the dendrimer and the dark parts are the thiol) the dendrimer is only partly displaced and agglomeration has occurred by 96h and for the C16SH the dendrimer is fully displaced and agglomeration has occurred after just 1h[19].

The displacement observed in figure 1.4 is due to the sulphur end group having a stronger affinity for the gold than the amine end group of the dendrimer. The Au-S bond is a lot stronger than the NH-Au bond between. To test this theory Crooks et al[19]. synthesised thiol terminated dendrimers and carried out the same experiments. This showed that the displacement of the dendrimer was less and agglomeration did not occur. It was also observed that solvent plays a large part in the dendrimer displacement. This is important for this thesis as it is essential to find an end group that will attach itself firmly to an Au substrate.

Dendrimers have the potential to be used for many different applications. However in order to fulfil their potential they must be analysed closely so that their characteristics and properties can be fully investigated. The important characteristics are uniformity of size and shape, degree of rigidity and ease of removal. In 2000 Ponomarenko et al.[20] used AFM to investigate these properties. Their studies focused on the properties of PAMAM dendrimers deposited on a mica surface and to do this they used AFM. They investigated the size shape and rigidity of the deposited dendrimers. The first observation was that the uniformity of the monolayer is dependent on concentration of the dendrimer regardless of the generation. When the concentration is high the excess dendrimer molecules form globules on the surface of the dendrimer film and so the film is not uniform. They found that it was possible to image individual dendrimers by AFM but only if the molecule is G4 or above. The AFM images shown in figure 1.5 also show that after G4 the dendrimers coated on the mica has no order and in fact the dendrimers are spaced quite far apart after G7, *e.g.*
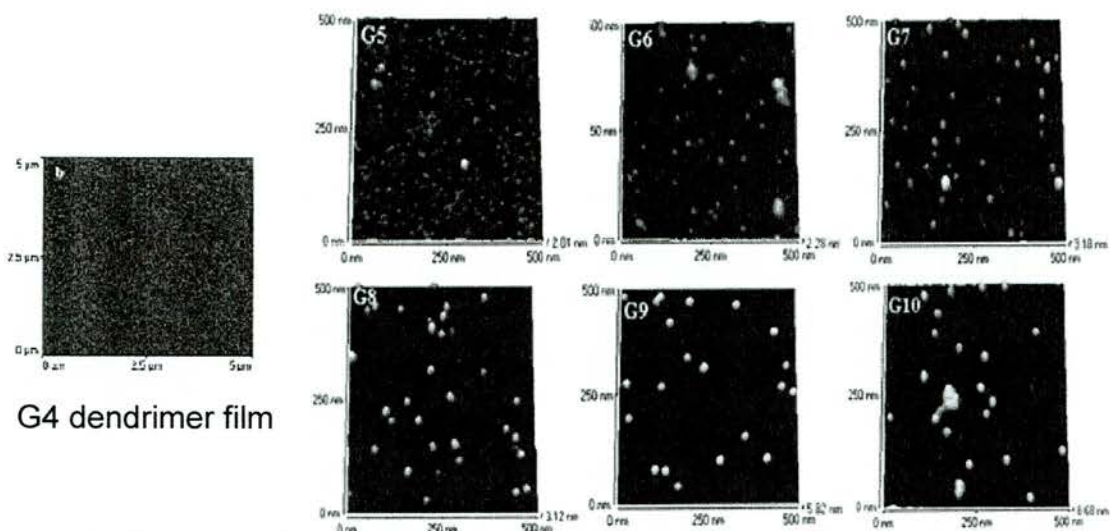
G4 dendrimer film

Figure.1.5. These images show that it is not possible to image the individual G4 dendrimers and that it is possible to image the G5 dendrimers and above. It also shows that the larger dendrimers do not form ordered films[20].

After Ponomarenko et al[20]. imaged the slides with AFM they were able to measure the heights and diameters of the dendrimers on the film. The results showed that the diameters were larger than the heights. This showed that the dendrimers were no longer spherical. There was also an increase in diameter with increasing generation and by G10 the dendrimer was no longer curved. These results showed that the rigidity of the dendrimers decreases with increasing generation. This was expected due to the surface group dense packing. However, this also showed that the surface adsorption forces between the mica and the dendrimer increases with increasing generation. What the images show is that the dendrimers spread out on the surface showing they are relatively soft molecules not solid spheres. This showed them that G4 dendrimers could not be imaged individually because they are not rigid enough.

In 2000 Zhang et al.[21] imaged G4 dendrimers using non-contact AFM (NC-AFM). This was possible because the solution of the dendrimer used in deposition of the monolayer was very low in concentration (1.47×10^{-8}M of G4-Td dendrimer in CH_2Cl_2). Heights of the individual dendrimers were calculated and they were the same as expected so in G4 dendrimers there is no flattening of the molecule. This study showed that on comparison to the mica surface the individual molecules showed high stiffness and low adhesion properties. These properties are determined by their rigid structures, hydrophobic surfaces and the adsorbed thin film of water on the surface of the mica before deposition of the dendrimer.

Zhang et al.[22] then imaged the topography and found information on the local stiffness and adhesion properties of individual G2 core-shell tecto dendrimers. The images showed small white spherical dots on the surface of the mica, the heights of these were measured however these heights showed that these dots were in fact dendrimer aggregates and were of the order of three dendrimer molecules high. This was not the case for the G4 dendrimers as the heights of the imaged spots were the same as the expected height of a single G4 core-shell tecto dendrimer. This difference was due to the functionality of the two dendrimers and was proven as they found that coating mica with a higher concentration of G4 dendrimer solution G4 dendrimer aggregates were observed. The final results for the adhesion and stiffness of these two dendrimers showed that both the G2 and G4 dendrimer aggregates showed a

lower adhesion than the mica substrate. This is explained by the hydrophobicity of the outer rings of both the dendrimers; however G2 is less hydrophobic than G4. The stiffness results show that both of these dendrimers are relatively soft.

How dendrimers of different generations behave on different surfaces is important. As when the dendrimers synthesised for this thesis are coated onto the gold it will be possible to make comparisons and find differences. The focus of this research to use STM and RAIRS to image Au surfaces coated with G1 and G2 dendrimers so to investigate their surface properties and characteristics, and from this to develop new dendrimer catalysts.

For this research dendrimer and dendrimer precursor molecules were carefully chosen. These molecules are shown in figure 1.6.
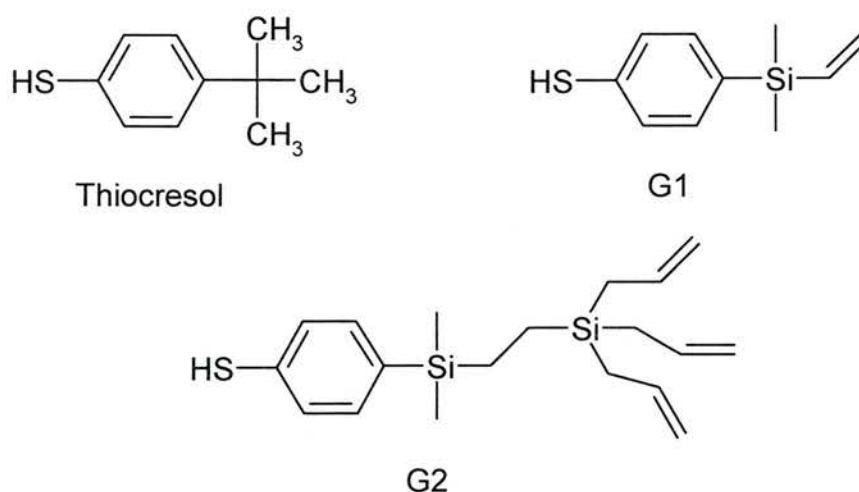
Figure 1.6 A schematic diagram of the three molecules being discussed in this thesis, thiocresol G1 dendrimer and G2 dendrimer.

The molecules G1 and G2 were chosen for their dendric properties and also because the thiolated end group would enable the molecule to be bound to a Au surface. These molecules were chosen to see how they would bind to the Au surface, how they orientate on the surface and their nearest neighbor interaction. They were also chosen as the vinyl end group would allow the possibility of further growth of the molecule and thus synthesis of further generations of dendrimer would be possible. The binding of the molecule to the surface is important as future work may include the attachment of this or larger generation thiolated dendrimer molecules to gold colloids. The vinyl groups in this molecule are also very important as they would eventually be used to attach the active catalyst to the molecule.

The thiocresol molecule was chosen after the initial investigation on the G1 molecule as a model molecule, as it is similar to the G1 dendrimer molecule. Thiocresol on Au{111} has surprisingly not been studied before even though it is commercially available. The only previous study was carried out on Pt{111}[23]. Its p-substituent makes it an interesting model molecule for comparison with the G1 dendrimer molecule. The molecule thiophenol (TP) and its interactions with Au{111} have been extensively studied and there is a lot of data on this subject available for the comparison to the thiocresol molecule on Au{111}[24,25,26] and on other surfaces such as Ag{111} and Cu{111}[27]. We were interested to see if the effect of the para substitution on the thiocresol makes the molecule behave any differently to TP.

1.7 Self Assembled Monolayers (SAMs)

Self assembly can be described as the spontaneous formation of ordered complex structures on specific substrates, for example, thiol molecules on Au {111} or organosilanes on oxidated mica[28]. As the formation of thiol monolayers on Au{111} is used for the work in this thesis, this is the area of self assembly that will be discussed in this section. Since 1983 the self assembly of alkanethiols on Au has been of great interest to surface scientists[29,30].
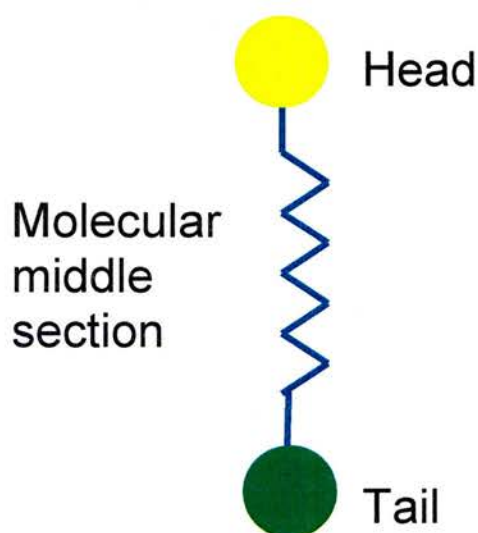
Figure 1.7 Schematic diagram of an alkyl thiol showing the head, tail and molecular middle section.

Molecules that form SAMs consist of a head group that adsorbs to the surface, a molecular middle part such as an alkyl chain or a benzene ring and a tail group which is on the free end of the molecule and can be functionalised before or after deposition of the thiol (see figure 1.7). The head group is normally a molecule that is known to strongly chemisorb to the substrate being used, for example, thiol (S – H) head groups are used with Au{111} surfaces[28]. SAMs are widely studied as they offer a unique chance to increase the fundamental

understanding of self organisation[30]. Being able to tailor both the head groups and the tail groups of the constituent molecule makes SAMs excellent systems in the understanding of phenomena affected by competing intermolecular and molecular – substrate interactions.

When thiols adsorb onto gold an oxidative addition reaction is thought to take place with the simultaneous release of hydrogen gas and the hydrophobic interactions between the aliphatic chains increase the stability of the film. There are two different ways of preparing thiol on Au monolayers. These are solution deposition and gas phase deposition. Solution deposition is where thiol SAMs are formed spontaneously by the immersion of a Au substrate into a solution of the active surfactant for example an alkane thiol or an aromatic thiol which has been diluted by an organic solvent. Many different solvents are used but ethanol is the most common solvent used in thiol deposition. The alkanethiol solutions used normally have very low concentrations, *e.g.*10^{-3}-$10^{-6}M$. Figure 1.8 shows how a thiol SAM forms on a Au surface.
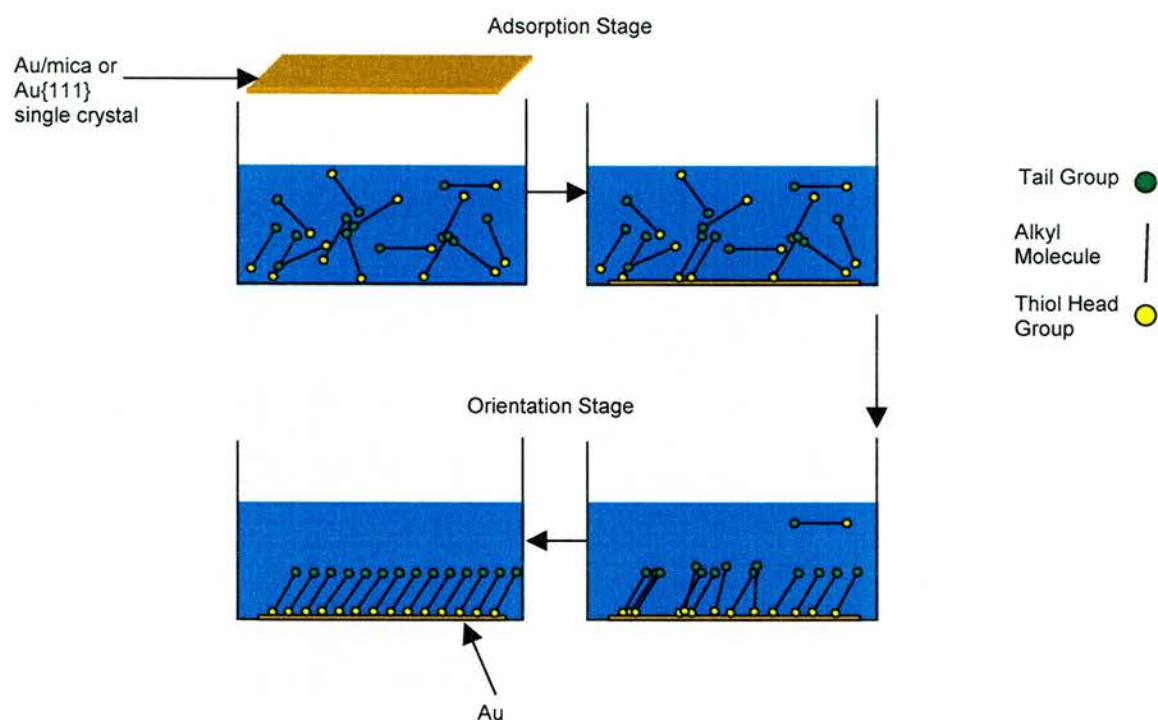
Figure.1.8 A Schematic diagram of the solution deposition of thiol molecule onto an Au{111} single crystal or onto an Au/mica film.

There have been extensive studies carried out on the adsorption of thiols onto Au substrates[30] and these have shown that there are two very distinct types of adsorption kinetics. Figure 1.8 shows these two adsorption kinetics as two different stages of SAM. The first stage is a very fast step that takes only a few minutes and at the end of which contact angles are close to their limiting value and thickness (80-90% of maximum)[31]. This first stage of SAM growth is where most of the molecules randomly attach to the surface. This part of the SAM growth takes up to an hour, it is called the adsorption stage.

There is then a second slower step which lasts several hours. In the case of alkanethiol SAMs over 15 hours, and in this time the contact angles have reached their final values[30,31]. The leading step is diffusion controlled Langmuir adsorption. There is also a further step that occurs for some but not all thiols and hence is not shown in Figure 1.8. This further stage is referred to as surface crystallisation. This is where the alkyl chains order to a 2-d periodic structure.

As mentioned the molecules can also be chemisorbed onto the surface through gas phase deposition. Gas phase deposition is carried out in an Ultra High Vacuum (UHV) system (see chapter 2). Figure 1.9 is a schematic diagram of gas phase deposition. For gas phase deposition the undiluted molecule is dosed on to the substrate through gas lines in UHV system. Ordering does occur more quickly after gas phase deposition but for certain molecules leaving them for a period of time after deposition will allow order to occur. The difference between solution and gas phase deposition is that during the deposition time if a thiol molecule desorbs from the surface in the solution phase it will go back into solution and could be re-adsorbed onto the substrate. However, for gas phase deposition if a thiol molecule desorbs off the surface during or after deposition it will get pumped away by the UHV system.
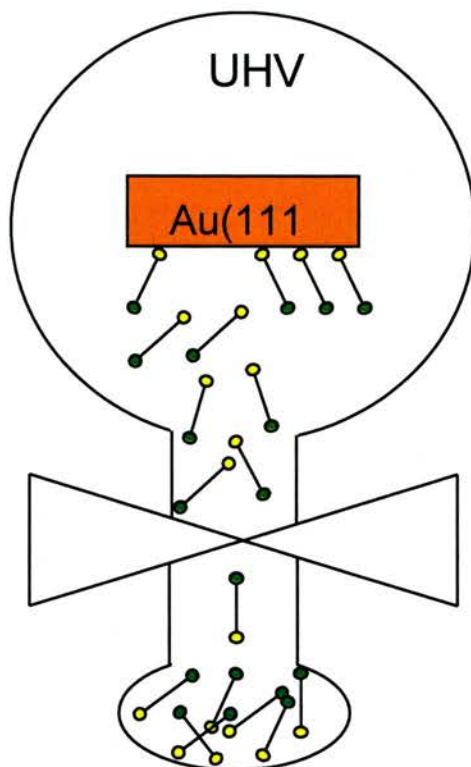
Figure 1.9. A schematic diagram of thiol gas phase deposition onto an Au{111} single crystal from pure thiol liquid or solid.

The chemical reaction of thiols when they adsorb onto the gold surface is highly exothermic[28,31]. Some of the sites (approx. 1/3) on the gold are thought to be occupied, and because the binding sites are close together van der Waals forces become important. This is why thiol SAMs were originally thought to stand vertical to the sample surface[31]. Thiol SAMs have now been thoroughly characterised using a vast array of different surface techniques such as RAIRS[32], ellipsometry[33], XPS[34] and SPM (scanning tunneling microscopy (STM[32]) and atomic force microscopy (AFM[35])). The technique most used in the characterisation of SAMs is STM and in fact the invention of STM[36] and the initial research on thiol SAMs coincides.

SAMs in general are a valuable type of sample for investigation by STM, and STM studies on them have helped reveal the molecular structure of the SAMs. These studies have been used to prove the previous assumptions and have shown that SAMs with chain lengths of 12 or more methylene units form well ordered, dense monolayers on Au(111). The thiols attach primarily to the threefold hollow sites of the gold surface losing a proton in the process leading to the formation of a $(\sqrt{3} \times \sqrt{3})R30°$ overlayer structure[30,37]. The distance between sites in this geometry is ~5Å and so the available area for each molecule is 21.4Å^2, however since the van der Waals diameter of the alkyl chain is too small for it to occupy the area, the chains are tilted to about 30°[28]. These observations confirm the above assumptions.

Alkanethiol self assembled monolayers are important to this research because the initial part of the research will be to attach dendrimers that are terminated with thiols onto Au surfaces (either {111} single crystal or Au/mica). It is possible that these might self assemble but due to their size and to the restrictions of the benzene ring – sulphur bond it will possibly attach onto the gold in a random manner.

1.8 Au{111} Surface (√3x23) Reconstruction

Unlike other fcc close packed {111} surfaces, Au{111} undergoes a surface reconstruction when it is clean[38]. This reconstruction is commonly referred to as herringbone reconstruction or sometimes the "chevron" reconstruction. Figure 1.10 shows good examples of Au{111} herringbone reconstruction from this work.
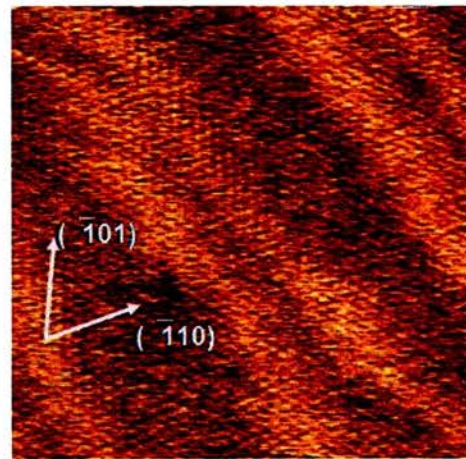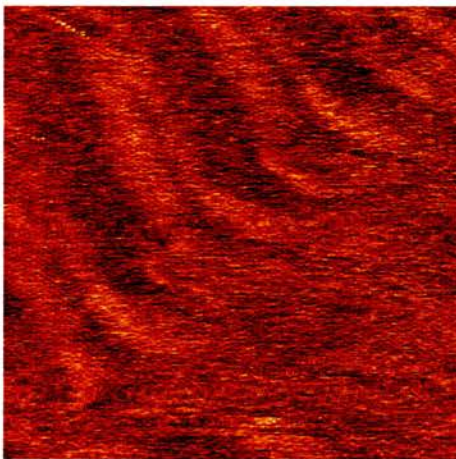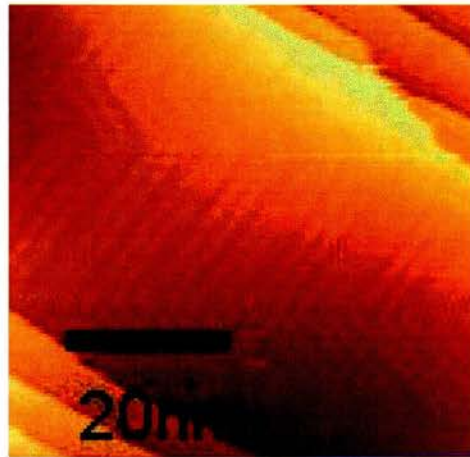
Figure 1.10 STM images of Au{111} reconstruction starting form a 200nm scan to show how it is across the whole surface.

In figure 1.10 reconstruction is easily seen as straight stripes that are ~6.3nm wide (assuming a width of 22 gold atoms). These straight lines are occasionally seen to bend at a 120° angle[39].

Many different techniques have been used to study this phenomenon, for example, LEED studies, which have produced several models for this structure[40] and Helium Atom Scattering which was the first technique to reveal this structure has a 22 x√3 unit cell[41]. However STM studies of gold first carried out in 1989[39] conclusively showed, with its direct atomic scale observations, that the unit cell is 22 x√3 and that the short end of this unit cell is 4.99Å long (this is √3 times the Au-Au distance) and it lies along the next-nearest-neighbour direction of Au atoms in the {111} plane. The long edge of the unit cell is as mentioned above ~6.3nm long and it is aligned along the nearest-neighbour direction of gold atoms in the {111} plane[38,39,42]. On looking closely at figure 1.10 what is observed is dark and light stripes. The lighter lines are known as the bridging sites. Figure 1.11 shows this more clearly[39].
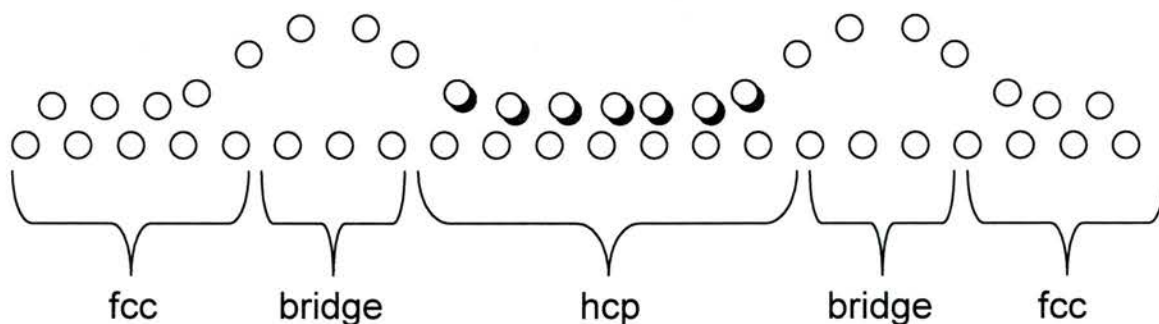
Figure 1.11 An exaggerated schematic model of the reconstruction viewed from within the Au surface end on.

Figure 1.11 shows that the environment of the Au atoms changes along the unit cell. It changes from face centred cubic (fcc) to hexagonally close packed (hcp) via a transitional stage which is known as the bridging site[38,39]. Then it changes again via a bridging site back to fcc. The Au atoms in the bridging sites have been shown to be vertically displaced by 0.2Å and the Au atoms in the middle hcp sites are shown to be vertically displaced by 0.12Å.

The herringbone reconstruction is generally thought to be destroyed when the Au is no longer clean[43] and so until recently it was assumed that the reconstruction had no effect on a resulting monolayer after deposition. However recently there have been many different studies that have revealed that the reconstruction is not always lifted after dosing and that it can sometimes have a profound effect on the molecular orientation of the molecules as when they are adsorbed onto a surface[39,44,45]. It is for this reason and many others that this phenomenon is still greatly studied.

1.9 Thiol adsorption on Au – Etch pit effects.

Etch pits or vacancy islands were first observed by Haussling et al[46]. They are holes or depressions that are imaged on gold surfaces after thiol adsorption. They are normally measured to be ~2.5Å deep which is consistent with a single Au atom step height[47]. There are several different theories to why etch pits occur. It was originally assumed that etch pits or vacancy islands were formed

by adsorbate induced shrinkage of the surface lattice constant. Other theories include the idea that during the desorption of the thiol, vacancy islands occur to accommodate for the ejection of excess atoms when the reconstruction is destroyed[38,48], this seems to be most likely as data exists which indicates that the surface lattice constant is actually increased during the monolayer assembly[48]. On investigation by the Poirier research group in 1997[47] evidence was found showing the existence of mobile Au adatoms during monolayer assembly. This then suggests that the vacancy islands are formed by the ejection of excess Au atom density from the surface during relaxation of the Au {111} herring bone reconstruction. If this was true then there would be Au atoms left behind in the thiol solution. This means that etch pits should only occur in SAMs that have been dosed from solution and not from gas phase deposition. More recent evidence however has been found for etch pits on Au after gas phase deposition. Research on this phenomenon is still on going.

References

[1] D. C. Tully, J. M. J. Fréchet Chem. Comm. **14** (2001) 1229

[2] M. Fischer, F. Vögtle Agnew. Chem. Int. Ed **38** (1999) 884

[3] D. A. Tomalia, A. M. Naylor, W. A. Goddard III.
Agnew. Chem. Int. Ed. **29** (1990) 138

[4] D. A. Tomalia, H. Baker, J. R. Dewald, M. Hall, G. Kallos, S. Martin,
J. Roeck, J. Ryder, P. Smith. Polym. J. (Tokyo) **17** (1986) 2466

[5] G. R. Newkome, Z-Q. Yao, G. R. Baker, K. Gupta.
J. Org. Chem **50** (1985) 2003

[6] C. J. Hawker, J. M. J. Fréchet J. Am. Chem. Soc **112** (1990) 7638

[7] A. W. Bosman, H. M. Janssen, E. W. Meijer. Chem. Rev. **99** (1999) 1665

[8] W. J. Knapen, A. W. van der Made, J. C. de Wilde, P. W. N. M. van Leeuwen,
P. Wijkens, D. M. Grove, G. van Koten. Nature **372** (1994) 659

[9] P. I. Couper, P-A. Jaffres and R. E. Morris.
J. Chem. Soc. Dalton Transactions. **13** (1999) 2183

[10] L. A. van de Kuil, et al. Chemistry of Materials **8** (1994) 1675

[11] N. Brinkmann, D. Giebel, G. Lohmer, M. T. Reetz and U. Kragl.
Journal of Catalysis **183** (1999) 163

[12] L. Ropartz, R. E. Morris, D. F. Foster and D. J. Cole-Hamilton.
Chem. Comm. **4** (2001) 361

[13] V. Maraval, R. Laurent, A-M. Caminade and J-P Majoral.
Organometallics **19** (2000) 4025

[14] S. Watanabe, S. L. Regen. J. Am. Chem. Soc. **116** (1994) 8855

[15] M. C. Coen, K. Lorenz, J. Kressler, H. Frey, R. Mülhaupt.
Macromolecules **29** (1996) 8069

[16] A. Hierlemann, J. K. Campbell, L. A. Baker, R. M. Crooks, A. J. Ricco.
J. Am. Chem. Soc. **120** (1998) 5323

[17] Z. Bo, L. Zhang, B. Zhao, X. Zhang, J. Shen, S. Höppener, L. Chi, H. Fuchs. Chemistry Letters **12** (1998) 1197

[18] V. Chechnik, R. M. Crooks Langmuir **15** (1999) 6364

[19] W. M. Lackowskie, J. K. Campbell, G. Edwards, V. Chechik R. M. Crooks. Langmuir **15** (1999) 7632

[20] S. A. Ponomarenko, N. I. Boiko, V. P. Shibaev. Langmuir **16** (2000) 5487

[21] H. Zhang, P. C. M. Grim, P. Foubert, T. Vosch, P. Vanoppen, U. M. Weisler, A. J. Berresheim, K. Müllen, F. C. De Schryver. Langmuir **16** (2000) 9009

[22] H. Zhang, P. C. M. Grim, T. Vosch, U-M. Weisler, A. J. Berresheim, K. Müllen, F. C. De Schryver Langmuir **16** (2000) 9294

[23] Z.Mekhalif, P.Lang, F. Garnier. J. Electroan. Chem. **399** (1995) 61

[24] C. M. Whelan, C. J. Barnes, C. J. H. Walker, N. M. D. Brown. Surface Science **425** (1999) 195

[25] S. Frey, V. Stadler, K. Heister, W. Eck, M. Zharnikov, M. Grunze. Langmuir **17** (2001) 2408

[26] L-J. Wan, M. Terashima, H. Noda, M. Osawa. J. Phys. Chem. B. **104** (2000) 3563

[27] L-J. Wan, K. Itaya. Langmuir **13** (1997) 7173

[28] F. Schreiber. Progression in Surface Science **65** (2000) 151

[29] J. T. Woodward, M. L. Walker, C. W. Menus, D. J. Vanderah, G. E. Poirier, A. L. Plant. Langmuir. **16** (2000) 5347

[30] A. Ulman. Chem. Rev. **96** (1996) 1533

[31] J. Lukkari, M. Meretoja, I. Kartio, K. Laajalehto, M. Rajamäki, M. Lindström , J. Kankare. Langmuir **15** (1999) 3529

[32] C. M. Whelan, C. J. Barnes, C. J. H. Walker, N. M. D. Brown. Surface Science **425** (1999) 195

[33] S. R. Wasserman, G. M. Whitesides, I. M. Tidswell, B. M. Ocko, P. S. Pershan, J. D. Axe. J. Am. Chem. Soc. **111** (1989) 5852

[34] C.M. Whelan, C.J. Barnes, C.Grégoire, J.-J. Pireaux.
Surface Science **454-456** (2000) 67

[35] A. Ulman (Ed.), Self-assembled monolayers of thiols, Thin Films, **24**
Academic Press, San Diego (1998)

[36] G. Binnig, H. Rohrer. Surface Science **152** (1985) 17

[37] E. Delamarche, B. Michel. Thin Solid Films. **273** (1996) 54

[38] S. B. Darling, A. W. Rosenbaum, Y. Wang, S. J. Sibener.
Langmuir **18** (2002) 7462

[39] M.H. Dishner, J.C. Hemminger, F.J. Feher. Langmuir **13** (1997) 4788

[40] J. Perdereau, J. P. Biberian, G. E. Rhead. J. Phys. F. **4** (1974) 798

[41] U. Harten, A. M. Lahee, J. P. Toennies, C. Woll.
Phys. Rev. Lett. **54** (1985) 2619

[42] N. J. Tao, S. M. Lindsay. J. App. Phys. **70** (1991) 5141

[43] G. E. Poirier, E. D. Pylant. Science **272** (1996) 1145

[44] J. A. Meyer, I. D. Baikie, E. Kopatzki, R. J. Behm. Surf. Sci. **365** (1996) L647

[45] D. D. Chambliss, R. J. Wilson, S. Chiang. Phys. Rev. Lett. **66** 1721

[46] L. Haussling, B. Michel, H. Ringsdorf, H. Rohrer.
Angew. Chem. Int. Ed. Engl. **30** (1991) 569

[47] G. E. Poirier. Chem. Rev. **97** (1997) 1117

[48] G. E. Poirier. Langmuir. **13** (1997) 2019

[49] D. A. Osullivn Chemical & Engineering News **71** (1993) 20

CHAPTER 2

Experimental Methods

2.1 Introduction

Since the 1960s there have been a growing number of surface scientific studies and surface science techniques[1], along with a growing awareness that studying surfaces, and understanding surface properties, can mean understanding many specific applications in the 'real world' *e.g. heterogeneous catalysis, material corrosion and semiconductors.*

When investigating a surface the main priorities in characterisation are the surface structure, its chemical composition, and information on its electronic structure. There are many different surface techniques that allow these factors to be determined. During this work the following were used, Scanning Tunneling Microscopy (STM) (in air and UHV), Reflection Absorption Infrared Spectroscopy (RAIRS), Auger Electron Spectroscopy (AES), X-Ray Photoelectron Spectroscopy (XPS) and Temperature Programmed Desorption (TPD).

Traditionally surface science techniques are performed in stainless steel vacuum chambers under ultra high vacuum (UHV) conditions. Ultra High Vacuum conditions are used to control the condition of the surface *e.g. to keep*

off dust, to stop oxidation, etc. The conditions of the surfaces have to be controlled as to study the properties of a well defined surface at an atomic level the composition of the surface must remain as near constant as possible over time[1]. [2]For example, during an experiment of one hour it is a reasonable requirement that no more than a few percent of an atomic layer of atoms attach themselves to the surface in the gas phase. The conditions satisfying this requirement may be calculated from the kinetic theory of gases. An expression for the rate of arrival of atoms (r) from a gas density (n) where the average velocity is c_a is

$$r = \tfrac{1}{4}nc_a \qquad \text{(equation 2.1)}$$

Then comparing the kinetic energy of the particle's mass(m), with a root mean square velocity c_{rms}, to their thermal energy (determined from absolute temperature (T) and the Boltzman constant k_B) gives the

$$c_{rms}^2 = 3k_BT/m \qquad \text{(equation 2.2)}$$

So then using relationship between the two velocities

$$c_a = (8/3\pi)^{\frac{1}{2}}c_{rms} \qquad \text{(equation 2.3)}$$

and the fact that the pressure P is shown as

$$P = nk_BT \qquad \text{(equation 2.4)}$$

the expression for the rate of arrival can be derived as

$$r = P(1/2\pi k_BTM)^{\frac{1}{2}} \qquad \text{(equation 2.5)}$$

So to completely cover $1m^2$ of metal atoms with one molecule per metal atom requires $\sim 1.6 \times 10^{19}$ molecules and therefore using expression 2.5 it is possible

to work out that, and if every impinging molecule sticks to the surface at a pressure of 10^{-9} torr it would take 75 minutes to completely cover the surface. This is obviously a worse case scenario as not all molecules will stick however in order to keep the surface less than 10% covered with contaminant molecules for one hour a pressure of about 10^{-10} torr is necessary. This is why UHV is used although it is not suitable for the analysis of catalysts under true catalytic conditions. [1]Figure 2.1 is a schematic diagram of a typical UHV.
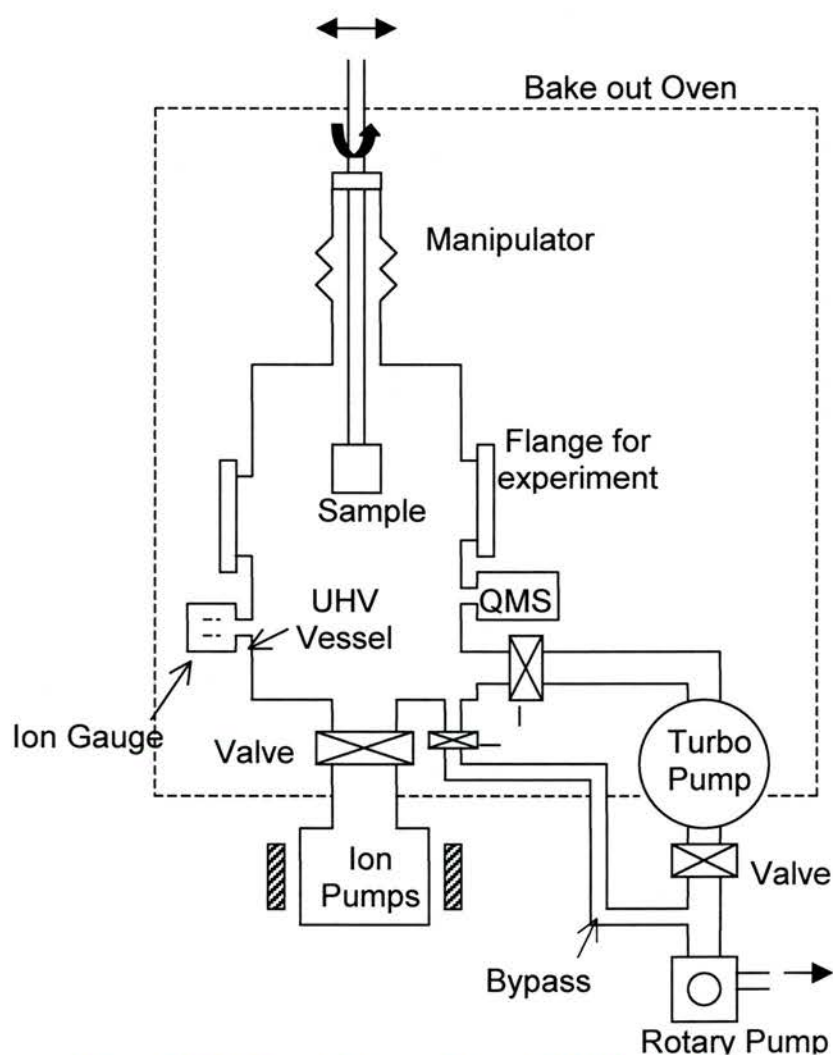
Figure. 2.1 A schematic diagram of a typical UHV chamber.

Basically the role of a UHV chamber is to ensure that the surfaces are in no way influenced by the arrival of ambient atoms or molecules.

Some surface techniques that were originally developed in UHV can be carried out in air or even at the liquid/solid interface. For example modern STM techniques have been developed for use out of UHV. This allows the solution deposition of a molecule to a substrate be investigated over time. It also allows electrochemical investigations to be carried out. STM can be carried out in air as well as the solid liquid interface but only on metals that are not easily oxygen contaminated (such as Au).

2.2 Scanning Tunneling Microscopy (STM)

2.2.1 Introduction

Scanning Tunneling Microscopy (STM) is a Scanning Probe Microscopic (SPM) technique. In SPM the image of a surface is produced from the information received when a mechanical probe travels over the surface. STM was invented in 1981 by Gerd Binnig and Heinrich Rohrer[3,] for which they were awarded the Nobel Prize for Physics in 1986. Although invented in 1981 the real breakthrough through was in 1982 when the first atomic resolution image of Si{111}-(7x7) surface was recorded, this was in fact the first ever well atomically resolved image of a surface structure[4], thus making STM the first technique to provide the real space images of individual atoms. Since its

invention it has been modified in many different ways and developed into a wide range of other SPM techniques, including Atomic Force Microscopy (AFM), Magnetic Force microscopy (MFM), and Scanning Near-Field Optical Microscopy (SNOM). STM is a very important and revolutionary technique and it has certain characteristics that are extremely important[5],

1)   It gives 3D images of surfaces in real space and of atomic scale in all three dimensions (x,y,z),

2)   It makes use of only bound particles and uses no lenses,

3)   It can be operated in UHV, ambient pressure, at the liquid-solid interface and at cryogenic temperatures and at elevated temperatures.

The invention of the STM has significantly changed researchers' perception of surface chemistry. There are two types of STM that will be discussed in this section Ultra High Vacuum STM (UHV STM) and in-situ/air STM.

2.2.2 Operation

[6]The tip, which is conductive, is approached towards the sample surface using a piezoelectric drive. This creates a small vacuum potential barrier, which suggests, classically, that there should be no current flowing between the tip and the sample. However, when a small voltage bias is applied between the tip and the sample a tunneling current begins to flow as electrons individually cross this barrier. However this is only measurable for barriers ~/nm, this is shown schematically in figure 2.2. This phenomenon is called quantum mechanical tunneling.
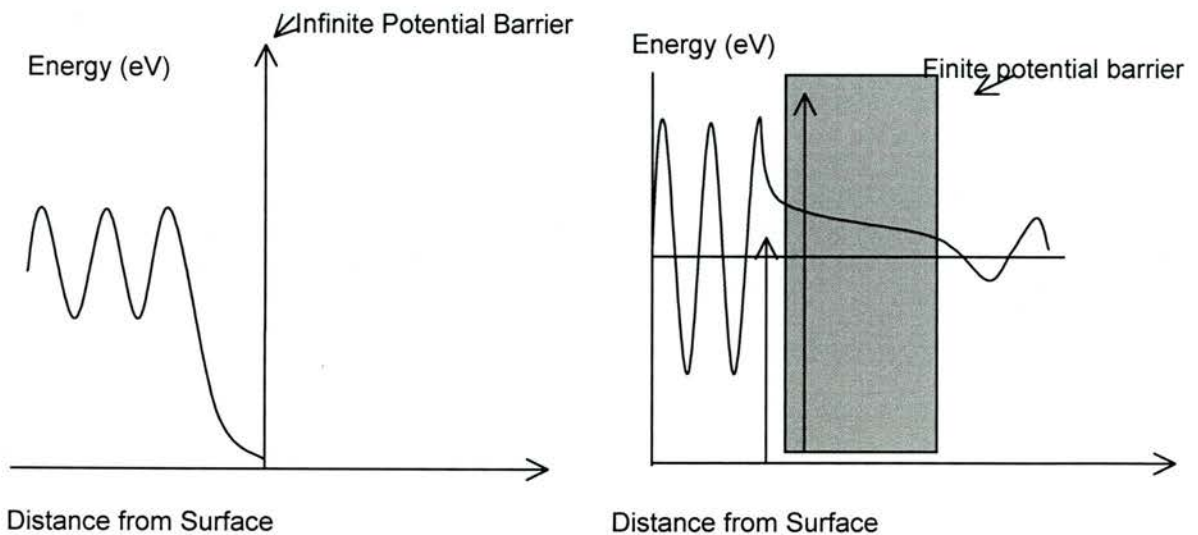
Figure.2.2 A wave function diagram of tunneling process[5].

[5]Quantum mechanical tunneling has only recently been completely understood. It is now known that when two metals are placed only a few angstroms apart their surrounding electron clouds overlap, therefore by applying a small voltage between these metals a measurable current is induced[7]. This is the tunnel current J, which is typically ~1nA. Until the voltage is applied the electrons can move in any direction but once it is applied they only move anode to cathode or vice versa. J, is a measure of the wavefunction overlap and is very dependent on the distance between the two metals, S. It also is dependent on the decay length k_0 and so hence follows the rule,

$$J \propto \exp(-Ak_0{}^s).$$ (equation 2.6)

In this case

$$k_0 = \sqrt{\tfrac{1}{2}(\phi_1 + \phi_2)}$$ (equation 2.7)

for two uniform metals where ϕ_1 and ϕ_2 are the respective work functions and where k_0^s also denotes the average barrier height. So as the distance between the sample and tip decreases the more likely it is that electrons will tunnel through the barrier, also when the overlap is large the current is large, and vice versa. This is the tunneling effect and it is this mechanism that underpins the STM. Figure 2.3 below is a diagram showing the tunneling current between the tip and the sample.
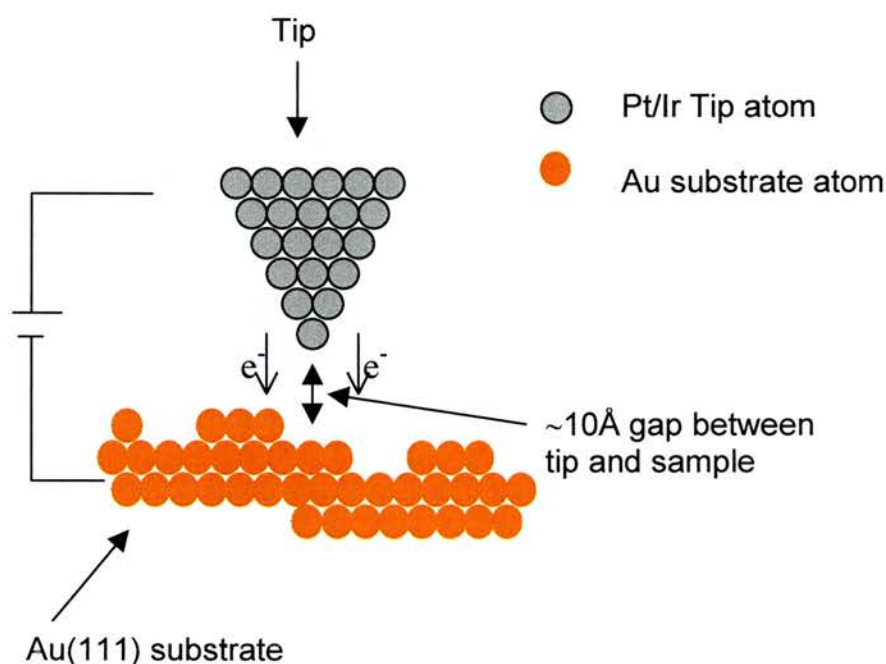
Figure.2.3, Schematic diagram showing the tunneling of electrons between tip and sample.

Once the desired tunneling current is reached the tip is then raster scanned across the sample in the x direction using a saw tooth wave form, and a ramp voltage moves the raster signal in the y direction. A third voltage adjusts the z direction, which either ensures a constant height of the tip above the sample, or a constant current between the tip and the sample. These are the two main

ways of imaging, constant height mode and constant tunneling current mode. [3]In constant current mode (which is the most widely used STM mode) a constant current is maintained while the tip scans the surface and the height between the tip and the sample changes. The height adjustment of the tip is performed as the appropriate voltage is applied to the z piezo drive. In this case an image is obtained when tip height is plotted against lateral tip position. In constant height mode the height of the tip is fixed this means that the tunneling current will be large at higher points on the surface and smaller at hollow points. To create an image from this the tunneling current versus the tip position is plotted. Neither of these two modes is possible without a feedback control system, as this is what keeps the tip no more than 10 angstroms from the surface and it is the tunneling current that provides the input for this system.

[4]One of the main problems in STM is the technique is extremely sensitive to both mechanically and electrically derived vibrations because any vibrations from the surroundings that are transmitted to the tip may cause the tip to crash into the surface. This will not only ruin the tip but could also break the piezo drives. This means that vibration isolation is very important. The most conventional way of doing this is to use a spring/damping table (see figure 2.4). This stops the vibrations and acoustic noise that comes through the floor. Or another way is a foam covering over the instrument or an isolation chamber lined with foam.
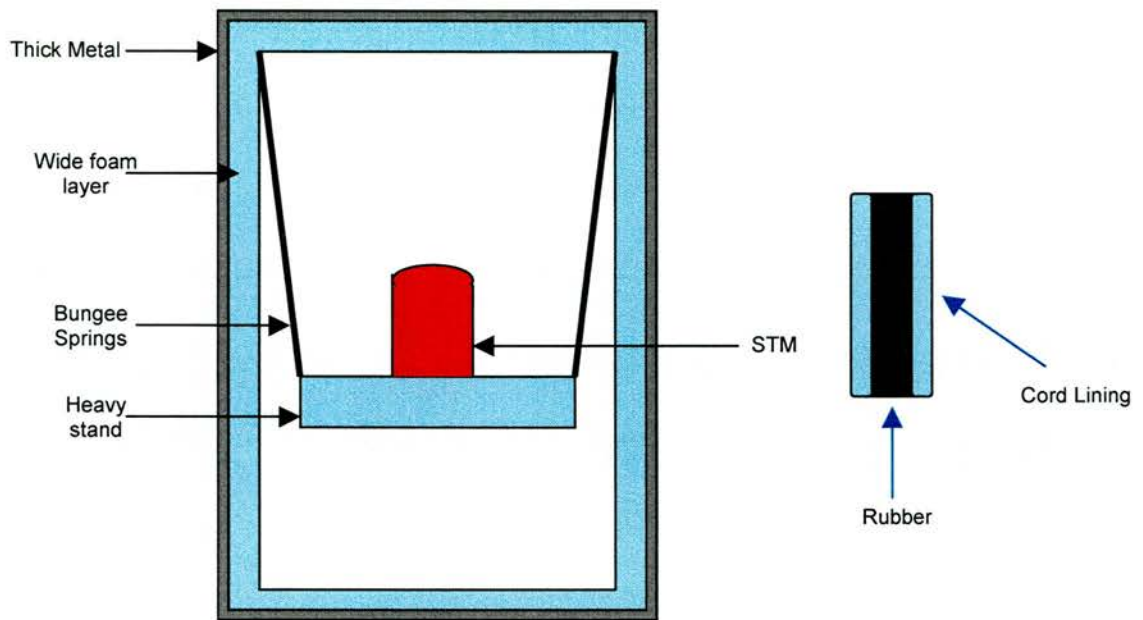
Figure 2.4 A schematic diagram of an STM vibration platform and close up of rubber bungee cord .

Another major problem is the environment. Although STM can now be used very effectively in ambient air and liquid it does work a lot better in UHV. Although the springs in figure 2.4 work for in-situ STM they do not in UHV STM as the parts are not compatible so another method was developed and in UHV STM a magnetic stage is used to dampen the vibrations. In this case strong magnets are used to hold the sample stand rather than bungee springs.

2.2.3 Instrumentation

Below is a schematic diagram of an STM.
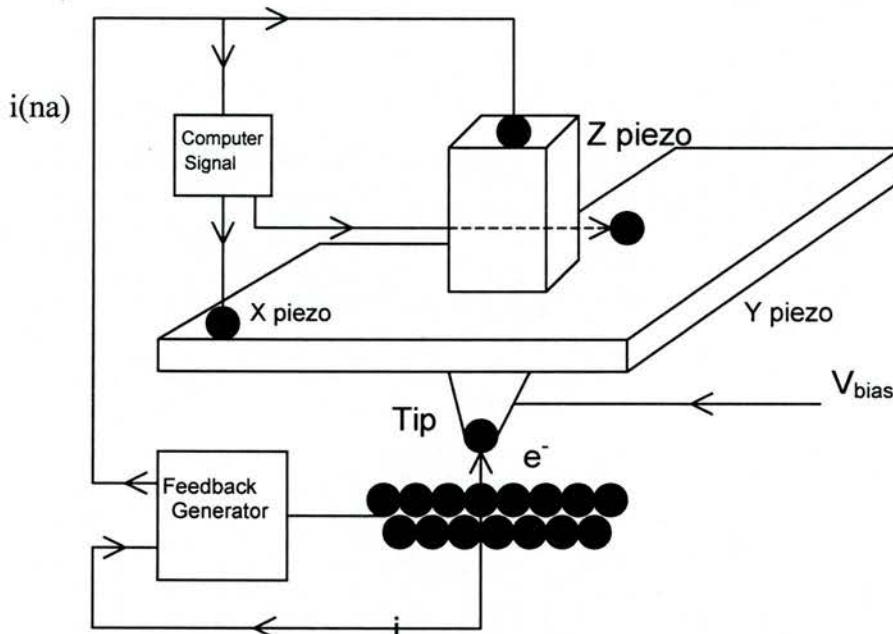
Figure.2.5 A schematic diagram of STM instrumentation

An STM consists of three major parts;

1) The mechanical part;

The mechanical part of an STM is a piezoelectric scanner/transducer that is made of piezoceramic material[8]. The piezoelectric scanner is pivotal to the operation of the STM as it provides the finely controlled motion essential for the workings of the STM which allows the instrument to have a small scanning range; it also provides a coarse positioning mechanism, which too is very important. The piezoelectric drive controls the sample distance during the scan ensuring that the tip height or tunneling current stays constant. A piezoceramic material is a material that either expands or contracts when a voltage is applied across it[4]. So in an STM when a voltage is applied the scanner expands by

about 1Å per millivolt and it is this that ensures how precisely the tip position is maintained relative to the surface. The piezoelectric scanner consists of three different parts, three different piezoelectric transducers, and these allow motion in three different directions, x, y, and z.

2) The tip;

[8]The tip is the most important part of an STM. It is this that is used to measure the surface topography directly. Firstly it has to be made of a conductive material, *i.e. a metal.* For atomic resolution of flat surfaces the STM tip must be extraordinarily sharp meaning the end of the tip should consist of a single atom. The shape of the tip is extremely important and the closer it is to the ideal shape (see figure 2.6) the better the tunneling conditions are.

(a)   (b)
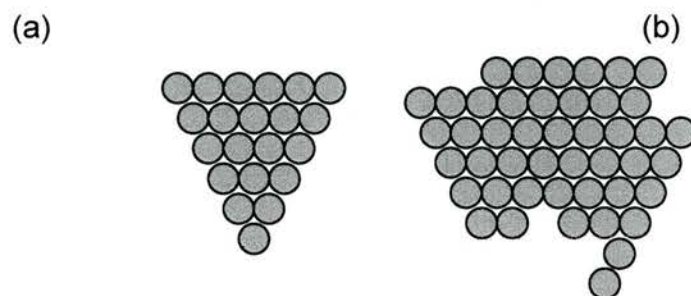
Figure 2.6 (a) Shows ideal tip shape (b) shows normal tip shape

The ideal shape of the tip however is not very hard to achieve and a normal tip shape is also shown in figure 2.6. This however will not make much difference to the resolution of an image[3] as the tip is still terminated with one atom but it will be less stable. The resolution from a normal tip is still sharp because the tunneling current is exponentially dependent on the tip-surface separation,

therefore the tip atom closest to the substrate always gives the major contribution to the tunneling current, however if the end of the tip consists of several atoms then the image will not be able to show atomic resolution and the molecular resolution will be blurred. Tips that contain a single atom at the end can be formed in many different ways. For example, an atomically sharp Pt/Ir tip can be formed by just cutting the wire with scissors or wire cutters, or atomically sharp tungsten wires can be made by electrochemical etching (2.8-6.3v) of the wire using an etching solution such as 10M KOH or NaOH. The quality of any tip can be tested by imaging a standard flat material such as Highly Ordered Pyrolitic Graphite (HOPG). This tip is mounted on the piezoelectric tube scanner discussed above.

3) The electronics;

[8]The electronics allow the measurement of the tunnelling current and the control the tip height. The electronics consist of an electrometer, a feedback loop, a bias voltage control and a piezodriver. The electrometer allows the tunnelling current to be converted into a voltage and amplifies it. It is a very noise sensitive device. The feedback generator is an essential part of the electronics which controllers the tip-sample distance. The bias voltage is the voltage applied between the tip and the surface and is used mainly in constant current mode, and the piezo driver "drives" the piezo scanner.

STM is used primarily to image conductive materials such as gold, graphite and semiconductors. However, it cannot be used to image insulating materials. It is also possible to use the STM to image organic molecules that have been adsorbed onto the surface of the conducting materials for example tartaric acid that has been adsorbed onto nickel[9] or thiols that have been adsorbed onto gold to form self assembled monolayers[10].

UHV STM was always carried out in constant current mode using an Omicron VT-STM, UHV chamber with a base pressure of 1×10^{-10} torr. Work was done using an etched W tip with the piezo drive connected to a PC using Scala Pro 2.5 analysis software. In air STM work was carried out in constant current mode using Pt/Ir tip that was cut with a pair of sharp wire cutters. The piezo drive was connected to a PC using Picoscan analysis software.

2.3 Reflection Absorption Infrared Spectroscopy (RAIRS)

2.3.1 Introduction

IR spectroscopy is a well known and highly used analytical technique in organic chemistry. [7]There are many different forms of this technique of which transmission infrared spectroscopy is the most common. However although this is useful for the measurement of solid, liquid and gaseous samples it is no use for studying thin films on metal (or other) surfaces, for this RAIRS is used.

[7,11]In RAIRS the infrared beam is directed to the surface at a grazing angle that can be seen in Figure 2.7.
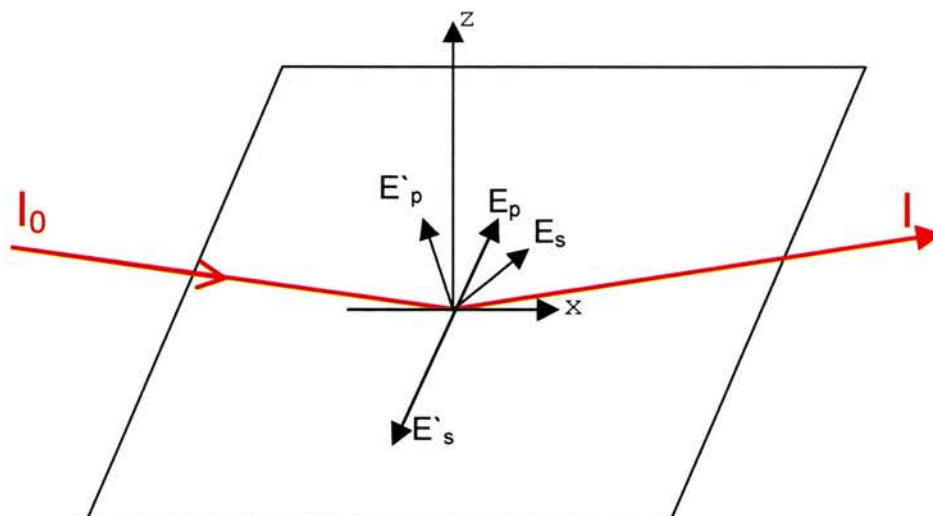
Figure 2.7 Red lines show grazing angle of IR beam.

It is the reflected light that then gives the absorption spectrum of the material that has formed a thin film on the surface of the reflective material. It is even possible with this method to be able to distinguish the adsorption geometry of an adsorbed molecule.

[12]To be able to use spectroscopic techniques to study surfaces the equipment needs to exhibit a very high sensitivity. IR spectroscopy was in fact one of the first vibrational techniques ever to be used in the field of Surface Science. In 1954 Eischens et al[13]. measured the vibrational spectra of CO that had been absorbed onto Si and supported by Cu, Ni, Pb, and Pt catalysts by transmission through the thin wafer of material. However RAIRS as we know it today was

48

first developed and used in the early 1960s by Pritchard et al[14], who studied adsorbates on reflective metal single crystals. RAIRS today is the most powerful application of vibrational spectroscopy that is used in the structural analysis of an adsorbate layer.

2.3.2 Theory and Operation

[7]In RAIRS, the excited surface vibrations of adsorbates on a reflective substrate are measured after a beam of infrared radiation is bounced off it. By measuring the reflected losses in radiation as the thin film on the surface is scanned, a reflection absorption infrared spectrum of the adsorbed layer is acquired.

[7]The theory behind RAIRS can be explained.

$$I \sim |\langle f | E.\mu | i \rangle|^2 \delta(\omega_0 - \omega) \quad \text{(equation 2.8)}$$

Equation 2.8 shows for electric dipole excitation the intensity of a vibrational transition from an initial state $| i \rangle$ to the final state $| \langle f$ where E is the electric field vector, μ is the dynamic dipole moment and ω_0 is the vibrational frequency. The equation shows maximum absorption occurs where E is parallel to the dipole[7]. This is very important in RAIRS as the component of the electric field, when in parallel with the metal surface, is perfectly hidden, only the component that is perpendicular to the surface is observed and in fact this component is

normally enhanced by almost a factor of two for grazing angles of incidence. In Figure 2.7 the two components are called P and S and these are perpendicular (⊥) and parallel (∥) to the reflected light wave *e.g. if the light wave I is parallel to the surface then P is (⊥) to the surface and S is (∥) to the surface* . However E_p can also be split into $E_p(⊥)$ and $E_p(∥)$[7].

The metal surface does not only screen the (∥) field, it also hides any dynamic dipole moment that appears on the induced image in the dipole metal. Figure 2.8 below shows two different dipoles one (∥) to the surface and the other(⊥). This demonstrates the surface dipole selection rule which states that vibrations will only be observed if the dynamic dipole moment has a component that is perpendicular to the surface (figure 2.8)[7].
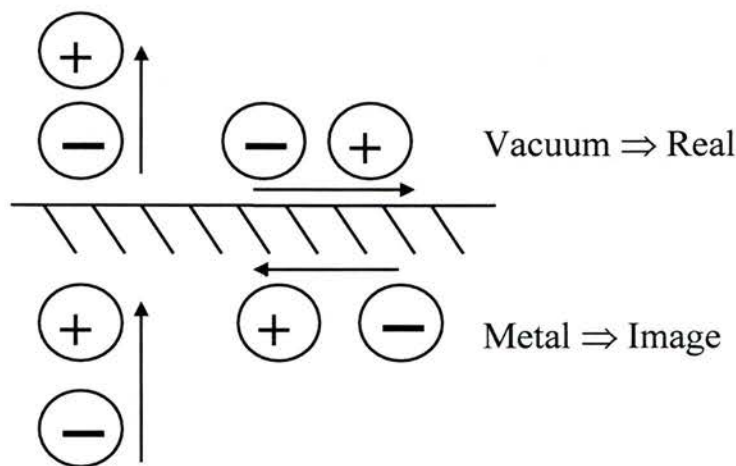
Figure 2.8 A schematic diagram of instantaneous dipoles perpendicular and parallel to a metal surface with that has been dosed with an adsorbate[7].

Looking at the diagram it is clear to see that if the dipole moment is parallel to the surface then the image dipole will cancel out the actual dipole and no vibration will be observed. However if dipole change has a component perpendicular to the surface then the image dipole reinforces the actual dipole and vibrations will be observed. This means that equation 2.8 will be reduced to[12];

$$I \sim | <f| E_2 \mu_2 | i> |^2 \delta(\omega_0 - \omega) \quad \text{(equation 2.9)}$$

[12]According to Boltzmann statistics, only the vibrational ground state $|0>$ of the molecule is populated so long as $kT < h\upsilon$ which means for RAIRS the vibrational ground state can be substituted for the initial state in equation 2.9. So using group theory both $|0>$ and z must be a completely symmetric representation of the point group and this means that $| <f$ must be completely symmetric for equation 2.9 to be non zero. This is another way of expressing the surface selection rule.

The surface selection rule and the general high resolution attainable through a RAIRS system make it a formidable technique in the field of surface science.

2.3.3 Instrumentation

RAIRS spectroscopy is carried out in a UHV chamber similar to the one described for the UHV STM system. In a RAIRS spectroscopic set up, infrared radiation is produced from an infrared source such as a temperature stabilised ceramic filament operating at around 1500K. It is then sent to a mirror which directs the beam into the interferometer. A beamsplitter then splits it into two separate beams. One of the beams is then sent to a fixed mirror while the other is sent to a moving mirror. These two mirrors send the secondary beams back to the beamsplitter where they are recombined. This causes the beams to interfere with each other constantly. When the infrared beam exits the interferometer, it is deflected by two mirrors before it reaches the detector. The detector produces an electrical signal in response to the encoded radiation striking it. The detector then measures the total intensity of infrared radiation reaching it across all frequencies. This measurement is read many times per second to generate the interferogram. When a sample is placed in the path of the IR beam, certain frequencies of the recombined beam might be absorbed or partially absorbed and as a result, the beam that comes out of the sample (or is reflected off the sample) is different to the one that went in. This is what gives the IR Spectra.

[6]Early RAIRS instruments used multiple reflections, at high angles of incidence, acquired from closely spaced mirrors. These mirrors were made from the sample to be analysed that has been evaporated on to a piece of glass or metal

foil. This technique however is no longer used because too many reflections reduce the total magnitude of the absorption signal. This is because "at any given wavelength the optimum number of reflections is small when the angle of incidence corresponds to the maximum reflection absorption in a single reflection"[6]. In most cases the change in reflection from a single reflection is at least half the optimum value. This provides the evidence that a single sample reflection instrument like the one shown in figure 2.9 is much better.
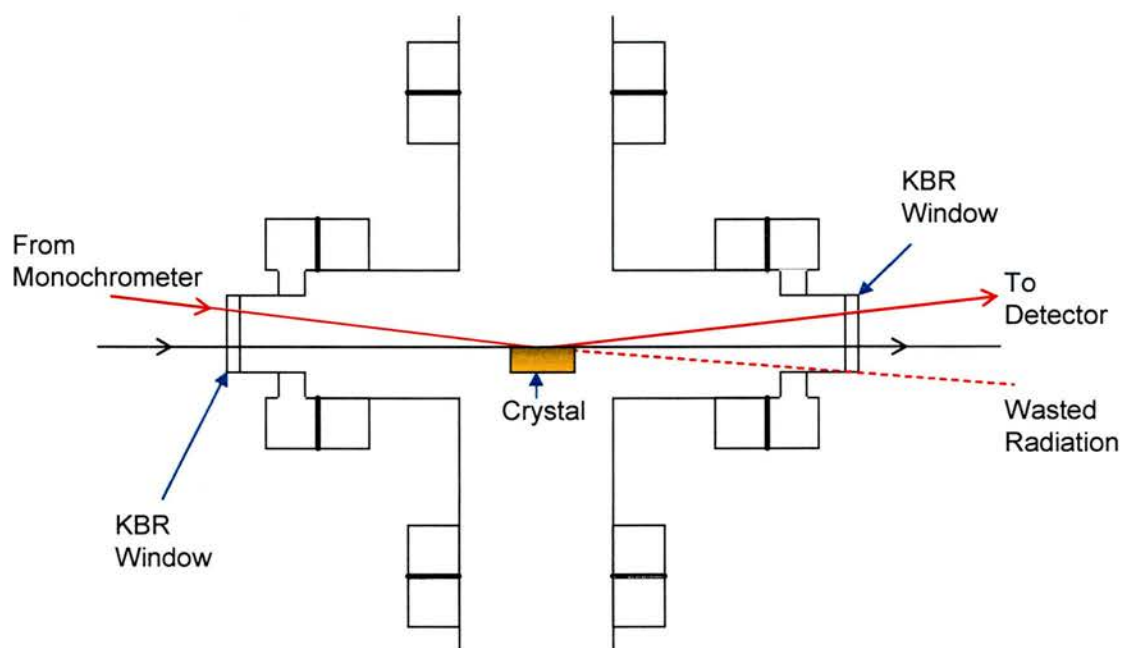
Figure 2.9 Diagram of UHV chamber holding RAIRS single reflection instrument.

The usual mode of operation for a RAIRS instrument is to record the reflection intensity both after and before the molecule has been adsorbed onto the surface. The ratio these two spectra is then measured to give the spectra of the adsorbate. This means that the stability of the IR source is very important which

is why normally double beam spectrometers are used as they show much better stability.

All experiments for this work were carried out in an Omicron UHV system operated at a base pressure of 1×10^{-10} torr. A Nicolet Magna-IR 860 spectrometer was used with a mercury cadmium telluride detector but two different MCT detectors were used. This was linked to a computer and ran using Omnic ESP software.

2.4 X-Ray Photoelectron Spectroscopy (XPS)

2.4.1 Introduction

XPS is one of the most frequently used surface analytical techniques. It was developed in the mid 1960s by K. Siegbahn [15,16] and his co-workers and in 1981 he was eventually awarded the Nobel Prize in physics for his work. XPS is used to gain information from a sample surface on elemental composition and the oxidation states of these elements. It is also possible in some cases to get depth information from flat layered samples. This is done by varying the angle between the sample surface and the analyser. XPS was originally intended to be used in gas analysis however it was quickly noticed that it was not working to its full potential. It was in fact the in the early seventies with the first UHV instruments being made commercially available that the first accurate data on mean free paths was obtained. Figure 2.10 below[4] shows the inelastic

mean free path (IMFP) v kinetic energy (KE) plot showing how the mean free path of an electron varies with its kinetic energy.
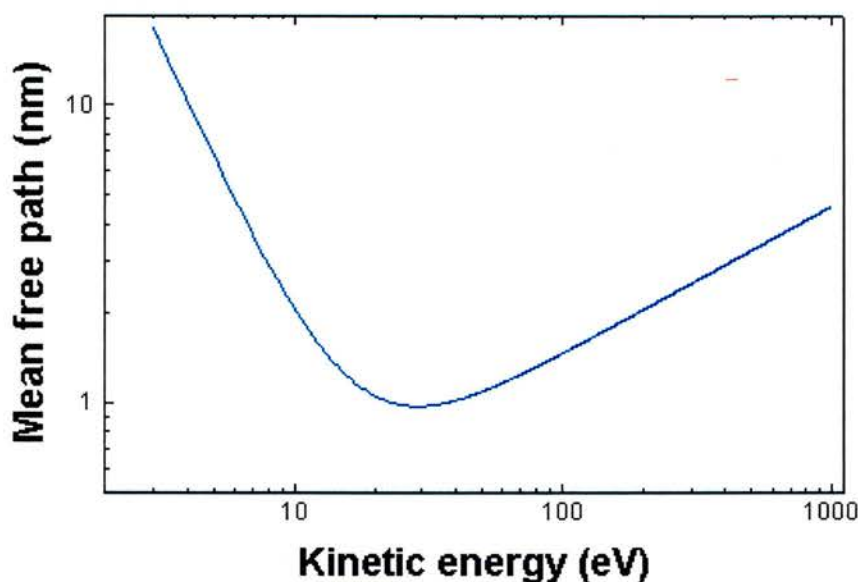
Figure 2.10 Universal curve showing how the inelastic mean free path of an electron in a solid varies with its kinetic energy[4].

2.4.2 Theory and Instrumentation

The theory of XPS is based on the photoelectric effect that was outlined by Einstein in 1905. [17]This is where the concept of the photon is used to describe the ejection of electrons from a surface when photons are impinged on it. The basic theory of this effect is that an atom absorbs a photon of energy, $h\nu$, and then a core or valence electron with a binding energy E_b is ejected with kinetic energy. Figure 2.11 shows this process more fully.
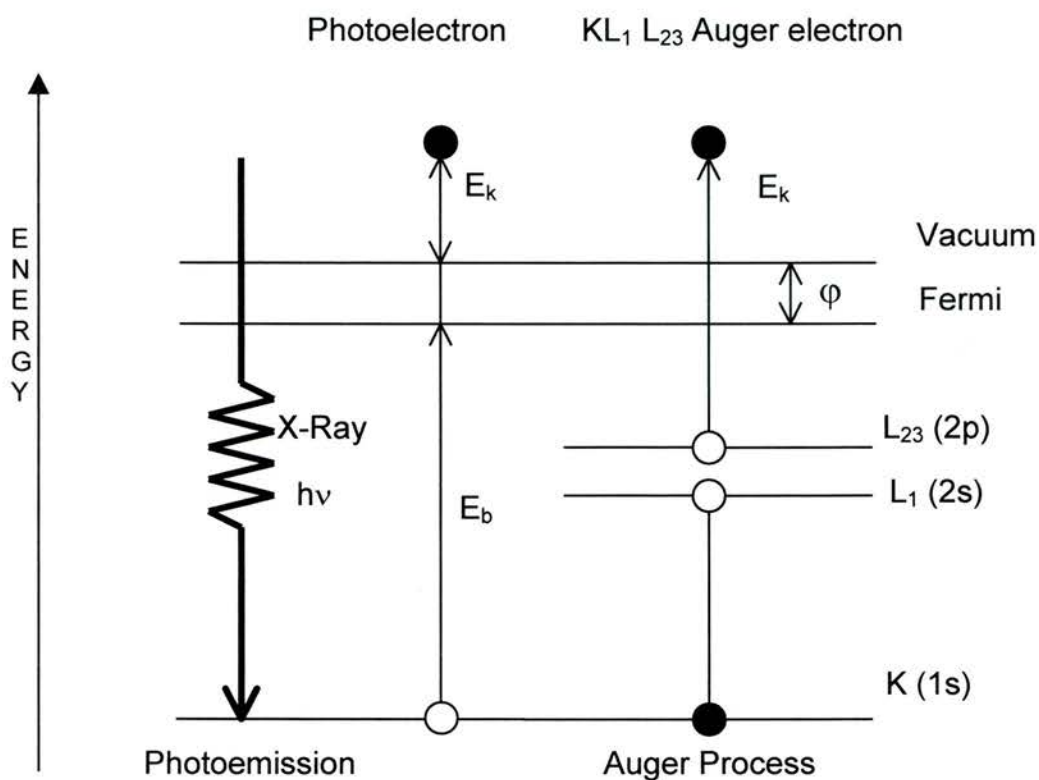
Figure. 2.11 An energy diagram showing the electronic transitions underlying the techniques of XPS and AES.

The equation for the photoelectric effect in the context of the XPS is

$$E_k = h\nu - E_b - \varphi \qquad \text{(equation 2.10)}$$

Where E_k =   The kinetic energy of the photon

     h   =   Planck Constant

     ν =   The frequency of exciting radiation

E_b =   Binding energy with respect to the sample Fermi level.

φ =   The work function of the spectrometer

XPS is a vacuum technique that uses X-Ray photons to bombard a sample surface. The most common X-Ray sources used are Mg Kα (1253.6eV) and Al Kα (1486.3eV) and these can also be combined to make a switchable twin

anode. Other X-Ray lines such as Ti Kα (2040eV) can also be used. The emitted photoelectrons will therefore have kinetic energies in the range of ca. 0 – 1250eV (Mg Kα mode) or 0 – 1480eV (Al Kα)[16]. In this energy range electrons have very short inelastic mean free paths (IMFP's) (~1nm) in solids and so the XPS technique is very surface sensitive (see figure 2.10)

In XPS it is the intensity of photoelectrons N (E) as a function of their kinetic energy that is measured. [7]However the XPS spectrum is actually a plot of N (E) versus E_k or even more likely E_b. The binding energies of energy levels in solids are conventionally measured with respect to the Fermi-levels of the solid rather than the vacuum level. The binding energy of each peak is characteristic of a specific element, i.e. there is a characteristic binding energy associated with each core atomic orbital. This is why it is possible to be able to investigate the elemental composition of a sample surface.

It is also possible when looking at an XPS spectrum to see Auger peaks as well as XPS peaks. The Auger peaks arise from de-excitation of the ion by Auger transitions (see figure 2.11). Auger electrons have fixed kinetic energies independent of X-Ray energy. However they are still plotted on the binding energy scale[16] if the Auger peaks are being observed as part of an XPS experiment. Because of this phenomenon it is possible that the Auger peaks may overlap the XPS peaks. However this can be solved relatively easily because by changing the XPS source, e.g. Al to Mg, the Auger peaks will shift

along the binding energy scale where as the XPS peaks do not move as their binding energy does not change.

As well as the X-Ray source an XPS also has an analyser. This is almost always a hemispherical analyser. In the entrance tube of this analyser the electrons are accelerated to a high speed at which they are able to travel through a hemispherical filter[6]. This defines the pass energy. The lower the pass energy the smaller the number of electrons that make it to the detector, however, the lower the pass energy the more precisely the energy of the electrons is determined. The detector is behind the energy filter and it is normally an electron multiplier or a channeltron. Both of these amplify the incoming photoelectrons to measurable currents. This then shows on a computer recorder the XPS spectra.

A very common occurrence in XPS is chemical shift[4]. The existence of chemical shifts analogous with different local chemical and electronic environments is of a practical value in XPS. The chemical shifts come from the sum of two different effects, one of which is the final state effect of relaxation and the other is an initial state effect that is often referred to as the true chemical shift. This is a shift from the original binding energy to the changed electronic environment. The relative size of these effects can vary vastly. All peaks in the same spectrum shift to higher binding energies by the same amount, this means that the shift can be calculated. Chemical shifts are used to

tell how molecules have interacted to the surface and thus are a very important effect in XPS.

The line width in XPS for Al and Mg is normally around 1eV however it is normally improved to around 0.3eV if the photon beam is monochromated. On an XPS the monochromator contains a quartz crystal that is positioned at the required Bragg angle for Al Kα radiation. Not only is the line now narrower but it is also focused better on the sample cutting out any unwanted X-Ray satellites[16].

XPS is a relatively good technique but it has some minor problems. One problem that often occurs is peak shifting. This occurs because sometimes there is a positive charge on the sample during the measurement. However these are only minor problems and XPS is a widely used technique in surface science for both quantitative and qualitative surface analysis. It is also possible for peaks to broaden if the charge on the sample is inhomogeneous.

The XPS measurements were carried out on an X-Ray photoelectron spectrometer in a stainless steel UHV chamber which was operated at base pressures in the low 1×10^{-9} torr range. The experiments were carried out using an Al Kα X-Ray source operated at 12kV and 20mA operated at a pass energy of 50eV. The measurements are calculated from the peaks produced. 70% of these peaks are gaussian and 30% are Lorentzian. Firstly the areas of the

peaks are calculated and then these are multiplied by a relative sensitivity factor (R.S.F.). Then the percentage is calculated using equation 2.13[18].

$$\% = \frac{A\chi \times RSF\chi}{\sum A\chi \times RSF\chi} \, x100$$
Equation 2.11

2.5 Auger Electron Spectroscopy (AES)

2.5.1 Introduction

[7]Auger electron emission has been discussed before in the section 2.3 on XPS (see figure 2.11). The Auger process is a way in which photo ionised atoms relax to ions of a lower energy. Earlier it was discussed how Auger peaks are a by product of XPS however they are also highly sensitive primarily element specific electrons that form the basis of another popular spectroscopic technique in the field of surface science called Auger Electron Spectroscopy.

The Auger effect was discovered in 1925 by Pierre Auger[1]. He observed that traces of electrons on photoplates that had been exposed to X-Ray radiation and he interpreted the formation of these electrons to be due to a radiationless transition in atoms excited by the primary X-Ray photons, whereby the emission of an electron from an outer level with an energy equal to that released by filling the core holes competes with the emission of characteristic X-Ray radiation. [16]Then in 1953 Lander studied the energy distribution of

secondary electrons emitted from solid samples that had been irradiated by slow electrons. On doing this Lander observed small distinctive peaks that he attributed to Auger electrons. It was Lander who suggested that these electrons may be of some use as a tool in surface analysis; however it was not until 1967 that the first surface AES was built.

2.5.2 Theory and Operation

[4]The technique of AES is carried out by the excitation of the sample with a beam of primary electrons. These electrons have a kinetic energy between 1 and 10keV, the electrons fired create core holes in the atoms of the sample. The excited atoms then relax by filling these core holes with an electron from a higher shell, this energy is then either liberated as an X-Ray or as an Auger transition which is the emission of a second electron, *i.e. the Auger electron*[7]. Figure 2.11 shows that the kinetic energy of the Auger electron is determined by the electron levels involved in the Auger process and not by the energy of primary electrons.

Auger electrons are observed to be small peaks on an intense background of secondary electrons when observed on an electron excited spectra. These Auger peaks of course originate from the primary beam. In order that the small peaks can be analysed they have to be presented in derivative mode as this makes the Auger peak more readily observable. The energy of an Auger transition (for example for KLM equation 2.12 [4]).

$$E_{KLM} \approx E_K - E_L - E_M - \delta E - \varphi \qquad \text{(equation 2.12)}$$

Where E_{KLM} is the Kinetic energy of the Auger electron

E_K is the binding energy of an electron in the K shell etc.

φ is the work function and

δE is the energy shift caused by relaxation effects.

The technique of AES works because Auger energies are as elementally specific as binding energies are in XPS. It is more difficult to obtain information on chemical shift information from AES data. However Auger electron emission is a process which involves the filling of core holes of low binding energies which then gives rise to relatively low kinetic energy Auger electrons of a short mean free path[16]. This detection outside the solid provides AES with a surface sensitive probe of chemical composition. Even although the initial core holes in this process might be created by incident photons or incident electrons. The ease and efficiency of creating sufficiently energetic electron beams (1.5-5keV) which are of high intensity (1-100μA) means that AES is normally performed with incident electron beams. Most AES studies use the Auger spectrum as a fingerprint of chemical composition. In general XPS is the chosen technique for studying oxidation states.

2.5.3 Instrumentation

AES instrumentation consists of three essential parts which in fact make up most spectroscopic techniques these are, a source of primary excitation, a sample and an analyser and detector system.

The Source

This is normally a primary type of radiation such as an electron beam which now is the standard type of AES source. A straight forward electron gun with focussing and deflection electrodes readily provides a beam of the required intensity. It is not necessary for any filtering of the electron beam because in AES it is not necessary for the energy from the primary electrons to be homogeneous. There are many electron guns that are commercially available and these produce emission currents of up to 200µA with an energy of 3-5keV. Although these are the main source used an X-Ray source like the one used in XPS can also be used[16]. However maintaining an X-Ray source in UHV is more complicated than an electron gun and the time needed to record a AES spectrum is much longer.

Analyser and Detector System

The most common analyser used is the Retarding Field Analyser (RFA)[4]. This type of analyser can also be used for LEED measurements. In this case the sample sits in the centre of concentric spherical grids. The grid nearest the sample is set at ground potential ensuring that the electrons that leave the sample travel in a field free region. A fluorescent screen is then used to collect

the electrons and the grid in front of this screen is set at a potential V_0 which corresponds to a minimum pass energy of

$$E_0 = eV_0 \qquad \text{(equation 2.13)}$$

This means that only electrons of energies greater than E_0 are able the reach the screen and be counted whilst the electrons of lower energy are retarded. The electrons that reach the screen have a kinetic energy between the energy of the retarding voltage V_0 and the primary energy beam E_p[4]. The expression for the current that arrives at the detector is shown in equation 2.14.

$$\int_{E_0}^{E_P} N(E)\,dE \qquad \text{(equation 2.14)}$$

N(E) is Number of electron states with energy E. If this current is differentiated it is therefore possible to obtain the desired energy distribution of the different electron energies. This is accomplished by applying an additional, small, modulation voltage, $\Delta V\sin\omega t$, to the retarding voltage, V. Therefore the expression for the current arriving at the detector is given by

$$\int_{E_0}^{E_P + \Delta E} N(E)\,dE \qquad \text{(equation 2.15)}$$

and this results in an energy distribution $N(E_0)\Delta E$ which means that the number of electrons possessing a particular kinetic energy can be counted.

All AES experiments were carried out using Omicron RFA spectraLEED optics. The electron beam was produced by thermionic emissions from a LaB_6 filament. The equipment was run by a computer using DAT 100 software.

2.6 Temperature Programmed Desorption (TPD)

2.6.1 Introduction

[7]Temperature programmed reaction methods are a class of spectroscopic techniques where a solid sample is heated with a linear heating ramp during which time the desorption of the surface species is monitored. Temperature Programmed Desorption (TPD) is one type of analysis within this field of techniques.

The theory behind TPD is relatively simple. It occurs when a metal such as gold is rapidly heated in a UHV system. When a metal is heated gases are desorbed from its surface. During TPD analysis it is observed that the rate of gas evolution from the surface changes markedly with temperature[4]. As a result of this there is an instantaneous rise in the gas density and a pressure rise within the UHV chamber. From this it should be possible to derive information on the nature and number of the adsorbed species as well as kinetic information from the evolution.

2.6.2 Instrumentation

Figure 2.12 is a simple schematic diagram of a TPD set[10].
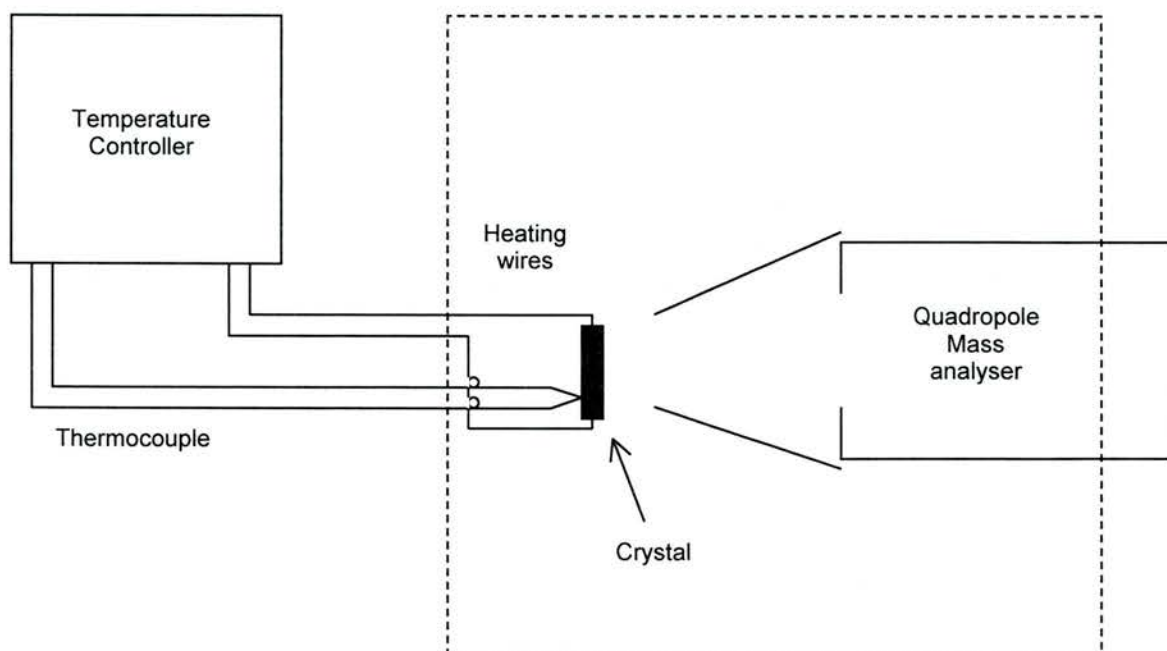
[10]Figure 2.12 The experimental set up of a UHV TPD instrument.

This diagram shows that the crystal is mounted onto a manipulator in a UHV chamber. It is possible to heat the sample crystal resistively by the heating wires which are normally made from high melting point metals such as tantalum or tungsten. The temperature is then measured by a thermocouple that is attached to the back of the metal crystal. Heating rates for TPD are normally 0.1-25K per second[7]. The partial pressure of the desorbing species is then monitored by a mass spectrometer that is positioned in such a way that, to a first approximation, it is only the desorbing species from the crystal that are measured. The pump from the UHV system pumps away the excess gases after desorption to ensure no readsorption of the molecules on the surface.

2.6.3 Theory and Operation

On most samples the TDS technique can give data on adsorbate coverage, adsorption energy, which is the same as the activation energy of desorption, lateral interactions between adsorbates through the coverage dependence of the adsorption energy and lastly the pre-exponential factor of desorption[6]. However obtaining these types of results is very difficult and most research does not need all of this type of information, which is why the most accessible spectral features, such as the energy of desorption, are normally investigated. To obtain these, the most commonly used method is the Redhead method, where the activation energy of desorption is given by[4] equation 2.16:

$$E_{des} = RT_{max} \left[\ln \left(\frac{\upsilon T\, max}{\beta} \right) - 3.46 \right]$$ (equation 2.16)

Where E_{des} is the activation energy of desorption

R is the gas constant

T_{max} is the peak maximum temperature

υ is the pre-exponential factor

β is the heating rate dT/dt

This expression is approximately correct for first order desorption and for values of υ/β between 10^8 and $10^{13} K^{-1}$, where the temperature T_{max} is independent. This reaction is very often applied to determine E_{des} from a single TPD spectrum.

This is a relatively straightforward technique however its execution does experience a few difficulties that can affect its data[11]. One difficulty is wall effects where molecules might be desorbed off the chamber walls. Others are temperature inhomogeneity across the sample during a temperature cycle and lastly the readsorption of gases onto the surface due to poor pumping speeds thus leaving a pressure rise during the heating cycle.

All TPD experiments were carried out using a temperature ramp of $\sim2Ks^{-1}$. The desorbing species was then monitors using a Spectra Microvision Plus MS (0-300 mass range) that was ran using a PC with the Spectra RGA software.

2.7 Gold Films

In STM experiments, having a flat gold surface such as an Au{111} single crystal is important. In UHV the single crystal is cleaned by argon sputtering and is then annealed to ensure flatness, however, for air STM this was not practical so an alternative had to be found. This alternative is normally a gold film on glass, silica or mica. The gold films have to be very flat as any molecular features dosed onto the films would be better imaged from a flat substrate. The most popular way of producing a gold film is to evaporate a thin film of chromium, and then a thin film of pure gold onto a glass microscope slide[19]. However when these slides are imaged using both Atomic Force Microscopy and STM the resulting film is not atomically flat. These slides have a rough surface. The AFM images in figure 2.13 show this. Previous Au/glass films

made before were good for the purpose they were made for such as IR and XPS as for these techniques the surface does not need to be flat. However for STM it is beneficial or atomic resolution would not be possible.

(a)

(b)
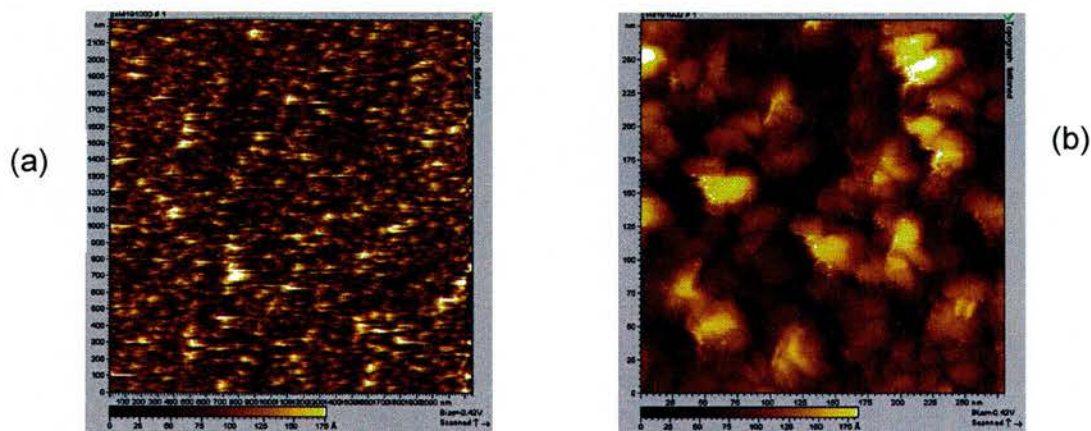
Figure 2.13 These images show gold coated on glass from 2500nm (a) and 300nm (b)

To make gold films flatter they are normally annealed[20,21,22]. This can be done in many different ways but in principle it involves the heating up of the gold surface to between 300 and 750°C. Samples are normally annealed using a Bunsen burner or a blow torch. STM imaging of an annealed Au/glass slide shows that there is no flattening of the gold and there is also noticeable warping of the glass.

This problem is due to the flatness of the glass. Figure 2.14 shows that glass is not atomically flat *i.e. it does not have any steps and terraces,* and thus the gold that covers it will not become flat. However when freshly cleaved mica is

imaged by AFM (see figure 2.14) it does show areas that are very flat. Thus an Au/mica slide is the best substrate for preparing a Au slide.

(a)   (b)
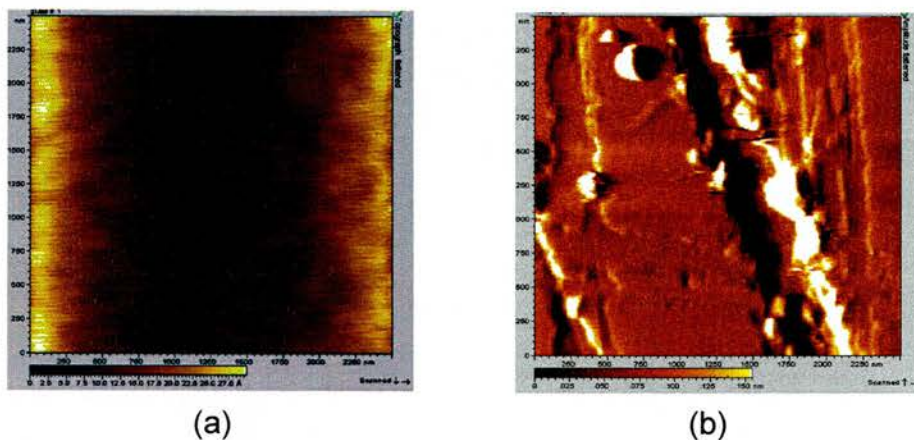
Figure 2.14 Image (a) is AFM image of clean glass and image (b) AFM image of freshly cleaved mica

Unlike for a glass slide Au can be directly evaporated onto the mica slide. This is because Au binds strongly to mica and will not be washed off by the solvent during deposition. Au/mica slide have to be annealed in the oxidising part of a Bunsen burner first to flatten and clean the surface. Figure 2.15 shows an Au/mica slide before and after annealing.
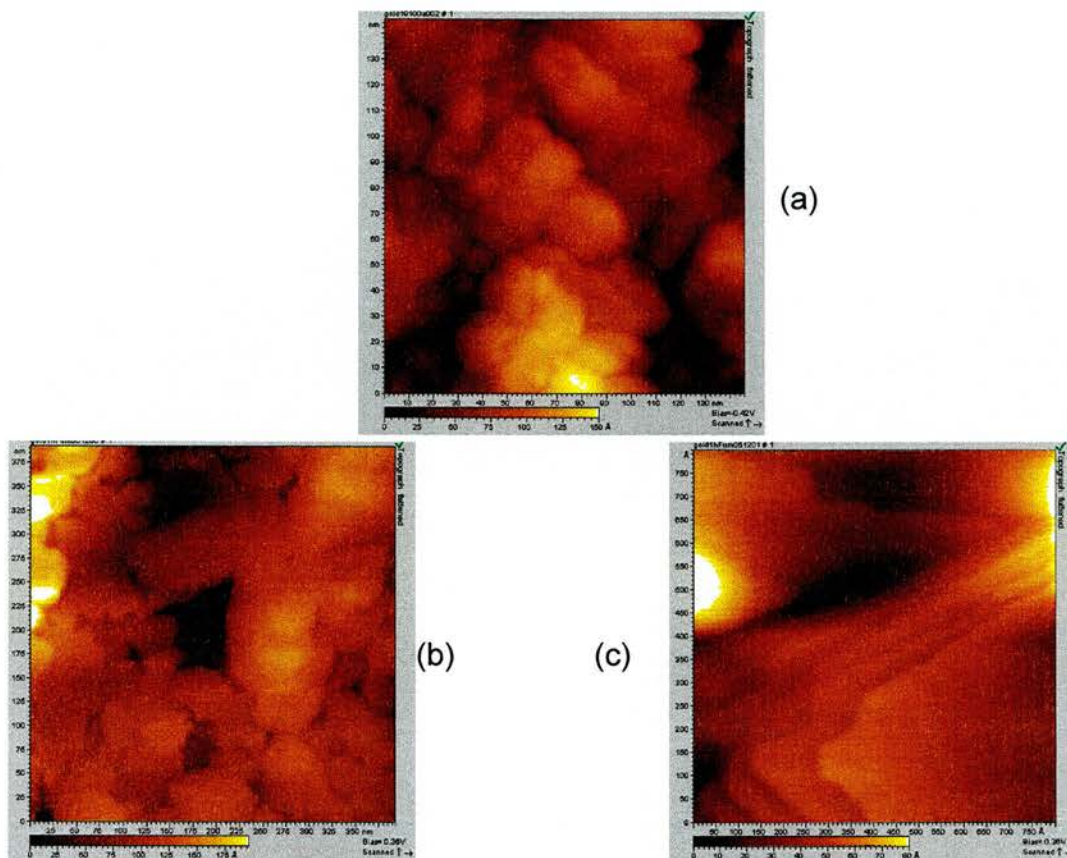
Figure 2.15 Image (a) is the gold on the mica without annealing. Images (b) and (c) is the gold annealed on the furnace the second image is at 400nm and the third image is closer in at 80nm. The steps and terraces are clear.

The Au/mica slides produced by the author were, although flat in areas, not reproducible. One of the main problems is that the equipment used in sputtering the gold onto the mica substrate was not able to measure the thickness of the gold that has been deposited. The thickness of the gold seems to be quite critical as if the gold film is thin or has thin parts flatness will not always be possible.

The Au/mica samples used in this thesis were ready made gold films from Georg Albert in Germany. The thickness of the gold on these films is measured to be 40nm. These slides still have to be annealed slightly using a blow torch to

ensure they are clean and very flat. The finished films however are very flat with lots of steps and terraces. Figure 2.16 show an STM image of these films.

Figure 2.16 This images shows that the terraces on the bought gold are significantly large. In this case they are approximately 100nm.

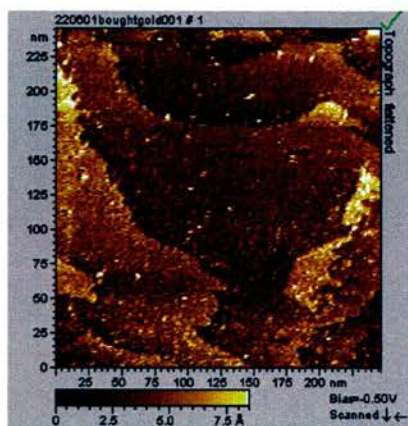# References

[1] D. P. Woodruff, T. A. Delchar. Modern Techniques of Surface Science **CSSSS (**1986) 4-8

[2] M. Kontz. Washington State University
http://www.mme.wsu.edu/reu/Matt/Matt.htm (1998)

[3] R. Weisendanger. Scanning Probe Microscopy and Spectroscopy **CUP**
 (1994) 81

[4] G. A. Attard, C. J. Barnes. Surfaces **OXP** (1998) 57

[5] G. Binnig, H. Rohrer. Surface Science **152** (1985) 17

[6] C. Codemard. Southampton http://www.orc.soton.ac.uk/~wsb/stm/stm.pdf
 1-47

[7] J.W. Niemantsverdriet Spectroscopy in Catalysis **VCH** (1993) 200

[8] M. Ellis, Texas Technical University
 http://www.phys.ttu.edu/~tlmde/thesis/TOC.html (1998)

[9] T. E. Jones, C. J. Baddeley. Surface Science **519** (2002) 237

[10] H.T. Rong, S. Frey, Y. J. Yang, M. Zharnikov, M. Buck, M. Wuhn, C. Woll,
 G. Helmchen. Langmuir **17** (2001) 1582

[11] J.M. Hollas. Modern Spectroscopy **John Wiley & Sons** (1993) 60ff

[12] R. J. H. Clark, R. E. Hester. Spectroscopy of Surfaces **16** (1988) 413

[13] R. P. Eischens, W. A. Pilskin, S. A. Francis. J. Chem. Phys. **22** (1954) 1786

[14] J. Pritchard, M. L. Sims. J. Trans Faraday Soc. **66** (1970) 427

[15] C. Walker and S. Morton   www.uksaf.org/tech/xps.html
 UK Surface Science Forum (1998)

[16] G. Ertl, J. Küppers. Surface Electrons and Surface Chemistry **VCH** (1985)

[17] R. Nix www.chem.qmw.ac.uk/surfaces/scc/scat5_3.htm
 Queen Mary University of London (2001)

[18] J.H. Scofield. Journal of Electron Spectroscopy and Related Phenomenon **8** (1976) 129.

[19] A. Ulman. Chem Rev **96** (1996) 1533

[20] U. Hopfner, H. Hehl, L. Brehmer. Applied Surface Science. **152** (1999) 259

[21] J. Hwang and M. A. Dubson. J. App. Phys. **72** (1992) 1852

[22] S. R. Snyder Journal of the Electrochemical Society **139** (1992) 5C-8C

CHAPTER 3

The adsorption of thiocresol on Au surfaces

3.1 Introduction

In contrast to the other molecules used in this thesis thiocresol was purchased from Lancaster (99% pure) and not synthesised in the St Andrews laboratories.
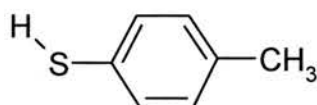
Figure 3.1 Thiocresol   Figure 3.2 Thiophenol
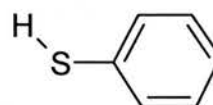
Thiocresol, shown above, was originally chosen as a model molecule as it has a similarity to the molecule synthesised to be the dendrimer precursor or Generation One (G1) dendrimer. Thiocresol on Au{111) has surprisingly not been studied before even though it is commercially available. The only previous study was carried out on Pt{111}[1]. Its p- substituent makes it an interesting model molecule for comparison with the G1 dendrimer molecule. The molecule thiophenol (TP) shown in figure 3.2 and its interactions with Au{111} have been extensively studied and there is an extensive database available for comparison with thiocresol adsorption on Au{111}[2,3,4] and on other surfaces such as Ag{111} and Cu{111}[5]. We were interested to see if the effect of the para substitution on the thiocresol makes the molecule behave any differently to TP.

3.2 Experimental

Air STM, UHV STM, RAIRS, TPD, AES, and XPS were used to investigate the
adsorption of thiocresol on Au surfaces.

3.2.1 Solution Deposition

For air STM, Au on mica substrates were used, Au/mica sheets were
purchased from Georg Alberts in Germany as thermal deposition of gold on to
mica carried out at St Andrews was unable to reproducibly give large enough
terraces due to the inability to measure the gold film thickness (see Chapter 2).
The gold thickness on the commercially available sheets is ~400nm. These
were then cut to 5mm squares and annealed using the reducing part of a
Bunsen burner flame. This gave large flat terraces on which atomic resolution
of the gold was imaged (figure 3.3).
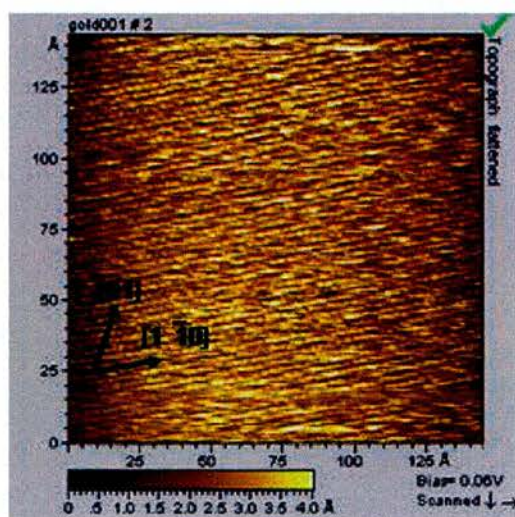
Figure 3.3 Au/mica slide showing Au{111} atomic resolution using the Molecular Imaging air STM.

The thiocresol monolayers in this situation were prepared by immersion of the Au/mica substrates in a 1mmol/L solution of thiocresol in analytical grade ethanol for 16 hours. These samples were then washed in ethanol and dried in a nitrogen stream. These types of samples were also used for XPS analysis.

The air STM used was a Molecular Imaging Picoscan SPM system. The tunnelling tips were made of 80/20% atomic weight platinum iridium wire, and were prepared by simply cutting the 0.25mm wire using extremely sharp wire cutters.

The XPS measurements were carried out on an X-ray photoelectron spectrometer in a stainless steel UHV chamber which was operated at base pressures in the low 1×10^{-9} torr range. The experiments were carried out using an Al Kα X-ray source operated at 12kV and 20mA and at a pass energy of 50eV.

3.2.2 Gas Phase Deposition

For UHV STM analysis a Au{111} single crystal (10mm diameter) was used. The crystal was attached to the backing plate by tungsten wires threaded through holes in the sample. The wires were then spot welded onto the backing plate. The single crystal was cleaned by repeated cycles of argon ion bombardment at 0.5kV and annealing to 700-800K at a crystal current of 5mA. This temperature was monitored using a thermocouple attached to the backing

plate. Thiocresol was dosed onto the Au{111} crystal using gas phase deposition at a sample temperature of 300K using a leak valve and a solid doser as thiocresol is very volatile. The thiocresol was purified prior to dosing by repeated freeze pump thaw cycles. Each dose was calculated in Langmuirs, *i.e. 1L = 1x10^{-6} torr x 1s.* Before beginning the thiocresol UHV experiments the Au{111} crystal was imaged by UHV STM to show large terraces and steps, Au herringbone reconstruction (see chapter 1) and Au{111} atomic resolution were also observed. Figure 3.4 shows the Fast Fourier Transform (FFT) plot showing the directions of the atoms in reciprocal space and figure 3.5 shows the actual STM image which enables the determination of the real directions and dimensions of atoms in ordered molecular studies. This is important information which will be used later to show the directions of the molecules as relative to the underlying Au atoms.
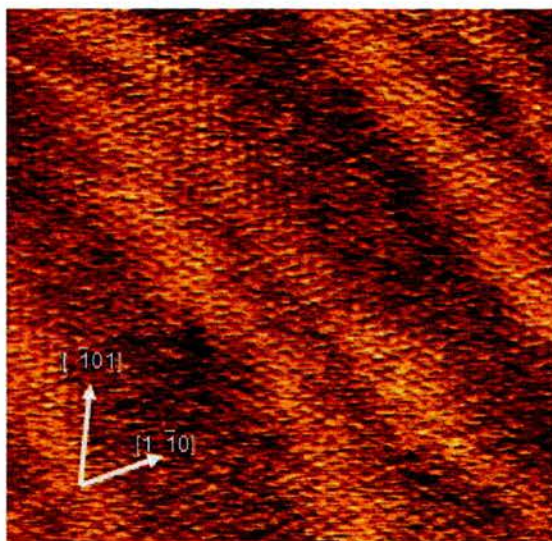

Figure 3.4 Real space STM Image of Au{111} atomic resolution and Au{111} herringbone 20nm scan.
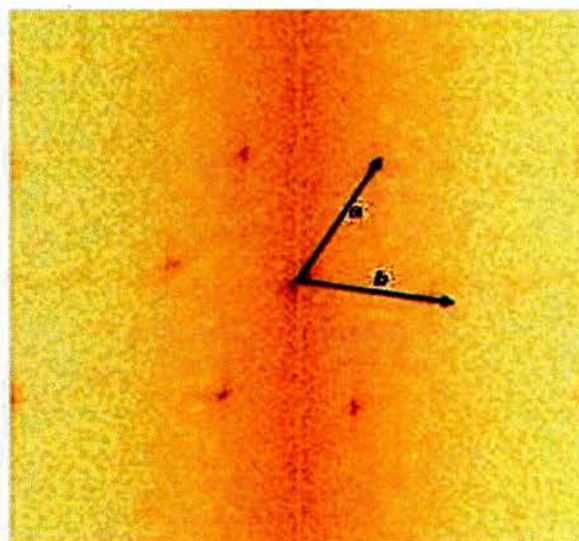
Figure 3.5 FFT of Au{111} from UHV STM .shown in real space in figure 3.4.

This type of dosing was also used for RAIRS, TPD and Auger electron spectroscopy (AES) experiments. However AES and TPD experiments are carried out in a different chamber so the actual dosing conditions may be slightly different.

UHV STM and RAIRS experiments were carried out in a stainless steel UHV chamber with a base pressure of 1×10^{-10} torr, which is also equipped with an ion gun for argon bombardment using a beam energy of 0.5kV, LEED and a facility for sample heating. STM images were taken using the constant current mode and the STM was controlled using the Scala Pro computer programme. The RAIRS was carried out using an MCT/A (mercury cadmium telluride) pyroelectric detector and data processing was achieved using the Omnic computer programme.

The TPD and AES experiments were carried out in a different stainless steel UHV chamber with a base pressure also of 1×10^{-10} torr. This chamber is equipped with LEED, an ion gun for argon bombardment, and a mass spectrometer. In this chamber the Au{111} single crystal was cleaned by repeated cycles of argon bombardment and then annealed to 700-800K until no impurities were detected by AES and the LEED showed a sharp Au($22\times\sqrt{3}$) reconstruction pattern. All experiments were carried out with the sample held at room temperature.

3.3 Results

3.3.1 Auger Electron Spectroscopy

In order to establish the saturation dose of the thiocresol on Au{111} at 300K, the crystal was exposed to doses of 0L, 25L, 50L, 100L, 200L, 800L, 1600L, and 3200L. Experimentally examining these doses using AES it is then possible to measure the peak to peak heights in counts per second of the sulphur (150eV) and carbon (270eV) peaks. When these peaks stopped growing then the surface has been totally saturated by the thiocresol molecule. Figures 3.6 and 3.7 displays the trends of these peak to peak heights differences.
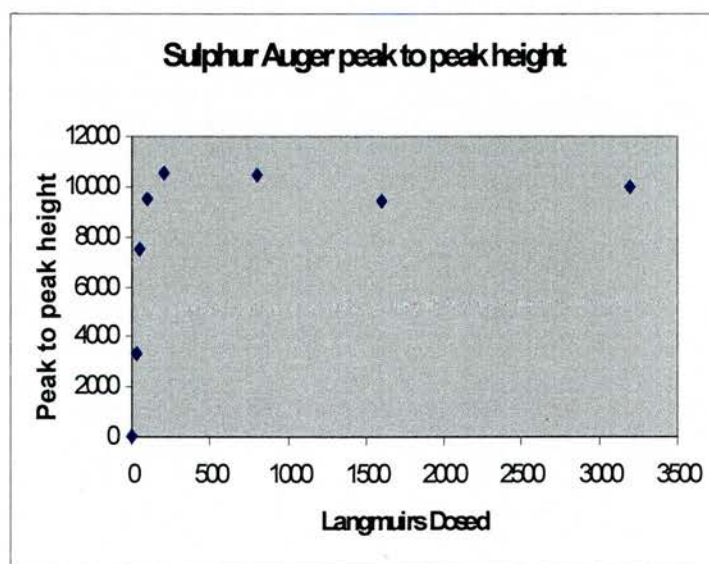
Figure 3.6 Sulphur peak height differences from AES analysis
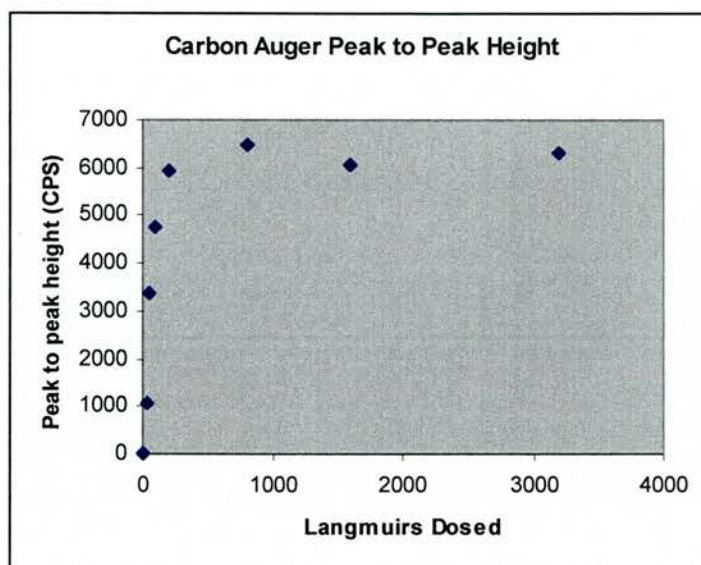
Figure 3.7 Carbon peak height differences from AES analysis

The spectra do not change throughout the experiment therefor there is no evidence of beam damage. These graphs show that saturation of the thiocresol on to the Au{111} single crystal occurs by 500-1000L and after that the peak height does not increase.

3.3.2 Temperature Programmed Desorption(TPD)

In this investigation TPD is used as one way to determine if the molecule has attached on to the surface as a whole entity. The molecular mass of the molecule is 124, Figure 3.8 shows that there are two peaks in the TPD spectra. The first has a T_{max} at ~475K and appears from a 100L dose. The second has a T_{max} at ~550K and is also visible after a 100L dose. The first peak is the largest at the 100L and 200L doses the second peak is then the largest after the 1000L dose.
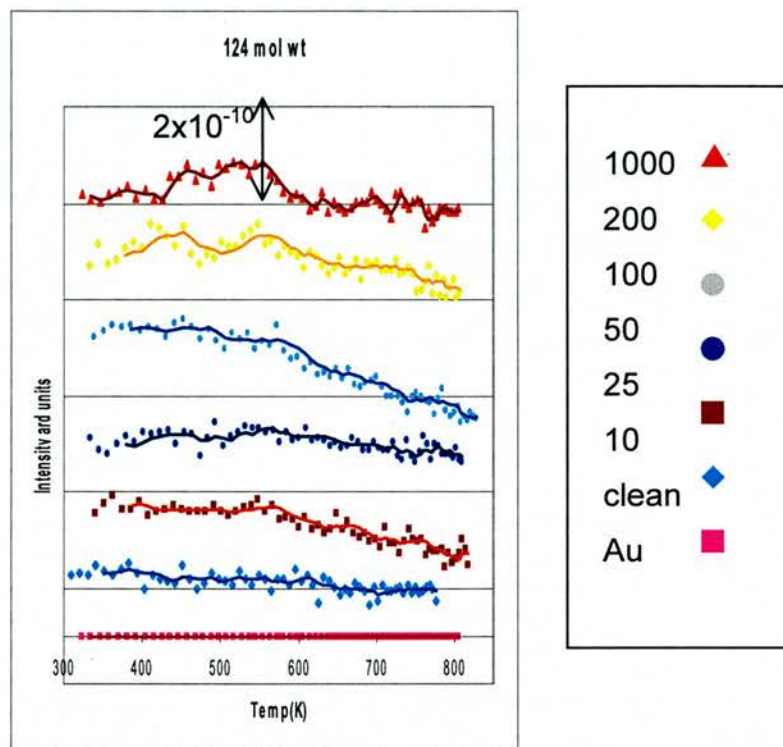
Figure 3.8 TPD showing the desorption of the thiocresol molecule (m/z124) from the Au{111} surface after different dosing amounts.

The molecular ion of complex molecules in mass spectrometry is often observed as a small peak. A mass spectrum of the molecule in the gas chamber was taken and this was show to be a small peak in comparison to m/z 33 and m/z 92 fragments the molecule would break up into. Figure 3.9 shows likely candidates for the structure of these fragments.

m/z = 33   m/z = 92
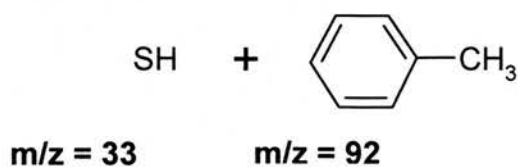
Figure 3.9 Thiocresol fractions that would be detected by Mass Spectrometry

The TPD spectra for the peaks associated with these fractions are shown in Figure 3.10.

(a)   (b)
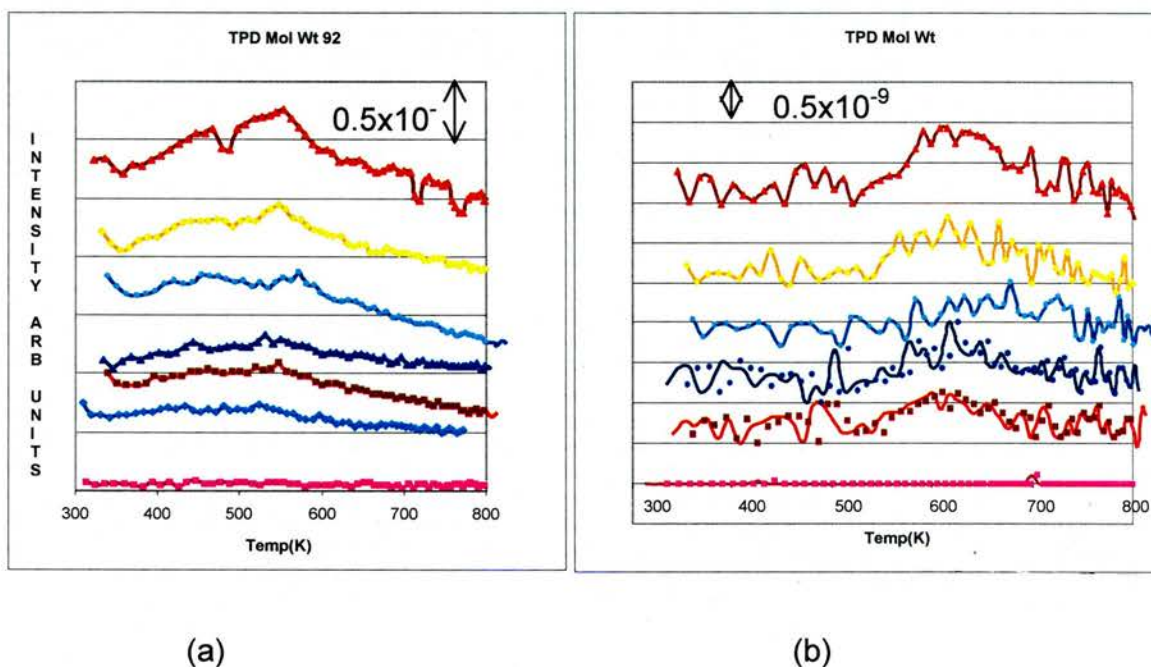
Figure 3.10 TPD showing the desorption of the toluene (m/z92) and sulphur (m/z32) from the Au{111} surface after different dosing amounts.

These spectra show that m/z 92 also has two peaks with one T_{max} at 475K and the other at 550K. The first of the peaks is always smaller than the second and both are apparent from a 10L dose. The sulphur (m/z32) desorption spectra show only one peak with a T_{max} of ~625 K up until the 1000L dose where another smaller peak with a T_{max} of ~475K is observed. Larger peaks than observed for m/z 32 were observed for H_2S (m/z 34). Again there is predominantly one peak until 1000L when another can be observed these peaks are in the same position as in m/z 32.
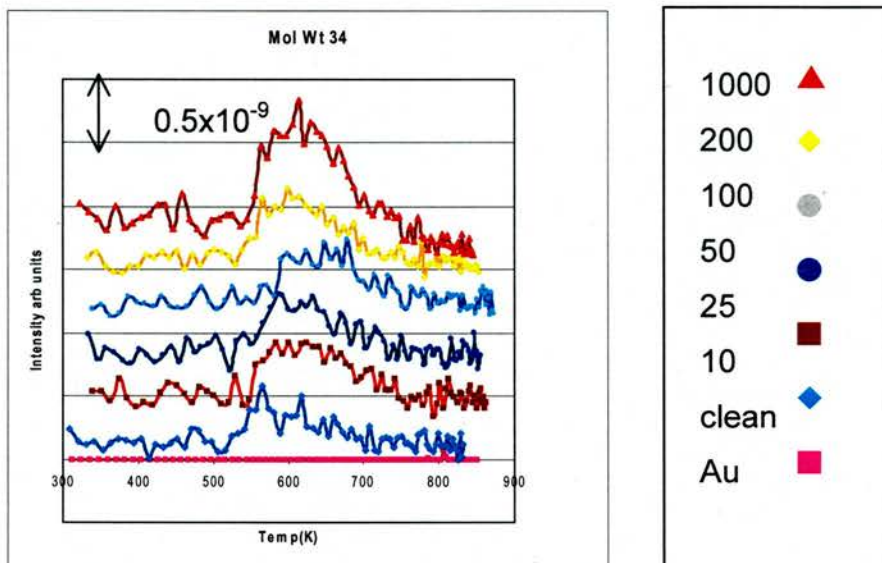
Figure 3.11 TPD showing the desorption of H_2S (m/z34) from the Au{111} surface after different dosing amounts.

3.3.3 Reflection Adsorption Infrared Spectroscopy (RAIRS)

Figure 3.12 shows the 3000cm^{-1} to 2600cm^{-1} range RAIRS spectra for the gas phase deposited thiocresol onto Au{111}.
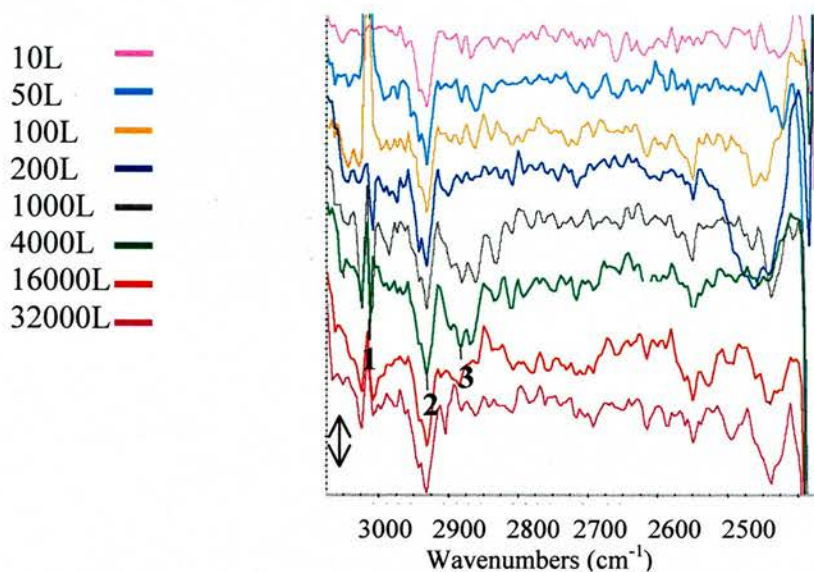
Figure 3.12 Thiocresol RAIRS spectra for 3000cm^{-1} to 2700cm^{-1} showing doses of 10L to 32000L

Figure 3.13 shows the 1300cm^{-1} to 700cm^{-1} range RAIRS spectra for the gas phase deposited thiocresol onto Au{111}.
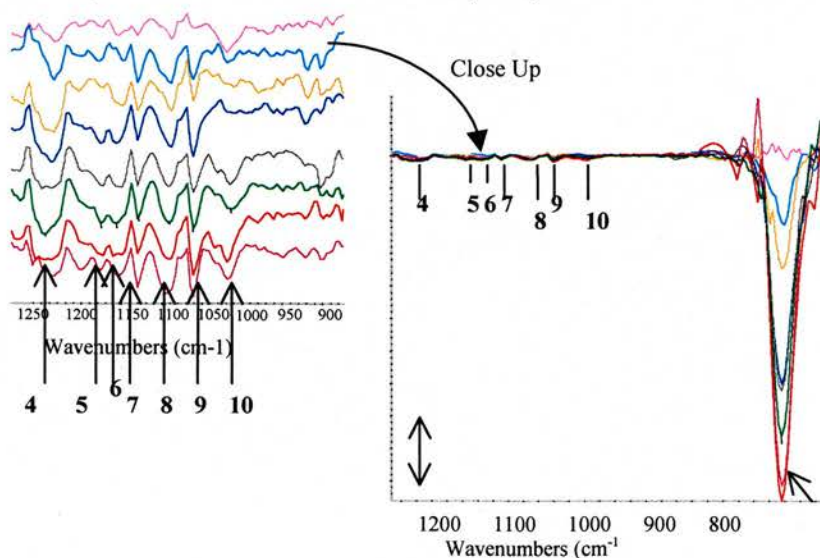
Figure 3.13 RAIRS spectra of thiocresol on Au{111} showing bands in the 1300cm^{1} to 700cm^{-1} range.

Upon looking at the spectra at first there is no evidence of the C-S stretching bond that is normally observed between $670cm^{-1}$ and $715cm^{-1}$ as this frequency is obscured by the large C-H out of plane bending peak which can be seen at $764cm^{-1}$. The bands which are present are 1. $3050cm^{-1}$, 2. $2943cm^{-1}$, 3. $2890cm^{-1}$, 4. $1245cm^{-1}$, 5. $1175cm^{-1}$, 6. $1155cm^{-1}$, 7. $1128cm^{-1}$, 8. $1091cm^{-1}$, 9. $1061cm^{-1}$ 10. $1014cm^{-1}$, 11. $764cm^{-1}$.

The peaks shown in these spectra generally increase slightly in intensity with each increasing dose. Almost all of the peaks are visible after the 50L dose however, peak 3 is not visible until the 1000L dose.

3.3.4 Ultra High Vacuum Scanning Tunneling Microscopy (UHV STM)

As mentioned in part 3.2, UHV STM of Au{111} has been imaged allowing the real space direction of the atoms to be known. This can be observed in figure 3.4. The Au{111} single crystal used had a lot of areas on its surface where there were many long steps and terraces as apparent from figure 3.14(a) which is the image of the Au{111} single crystal, after exposure to a 1000L dose.
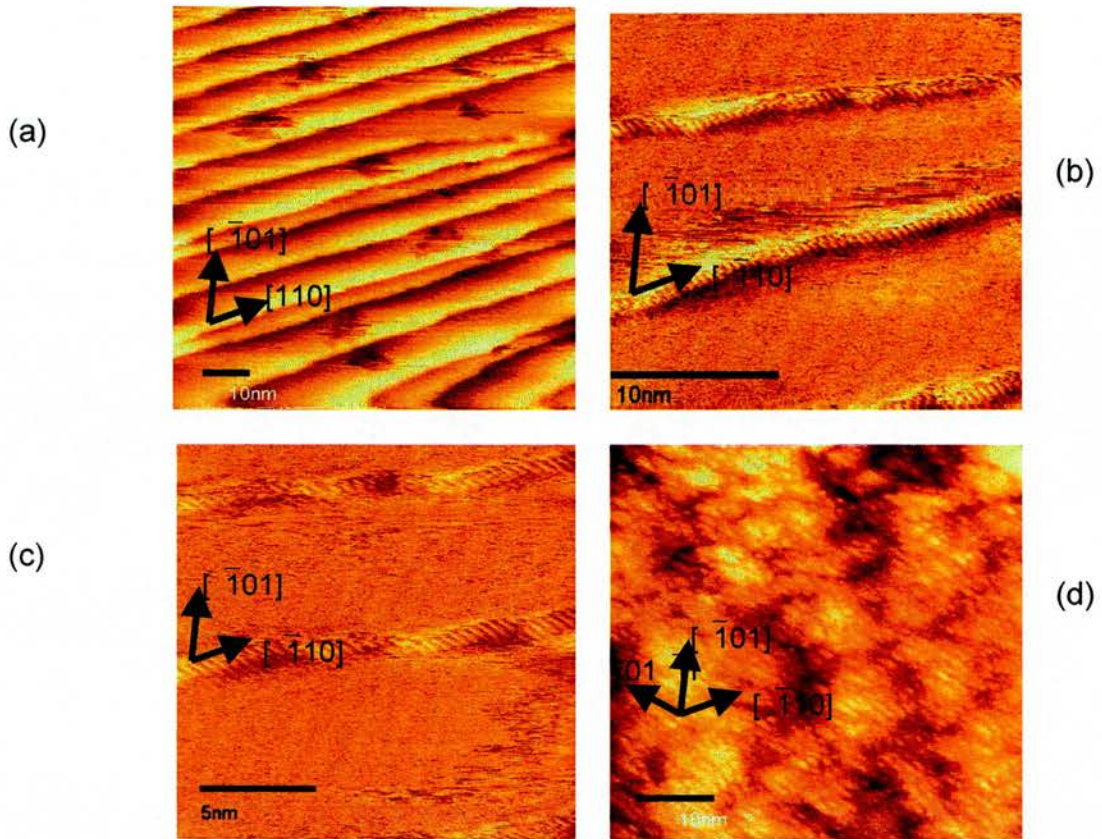
Figure 3.14 (a) 100nm by 100nm UHV STM image of Au{111} single crystal dosed with 1000L, of thiocresol, at room temperature, showing steps, terraces and etch pits. This image was acquired at a tunneling current of 0.395nA and a tip bias of -1V. (b) 30nm by 30nm UHV STM Image of Au{111} single crystal dosed with 1000L of thiocresol, at room temperature, showing steps, terraces and stripes at the step edge. This image was acquired at a tunneling current of 0.395nA and at a tip bias of -0.385V. (c) 18.2nm by 18.2nm UHV STM Image of Au{111} single crystal dosed with 1000L of thiocresol, at room temperature, showing steps, terraces and stripes at the step edge. This image was acquired at a tunneling current of 0.395nA and at a tip bias of -0.385V. (d) 60nm by 60nm UHV STM Image of Au{111} single crystal dosed with 32000L of thiocresol, at room temperature, showing a high density of molecular clusters on the surface. The image was acquired with a tunneling current of 0.228nA and a tip bias of -0.833V

Figure 3.14(a) shows steps and terraces (~10-15nm wide) and also some holes on the terraces. These holes are large, approximately 10 nm wide and 1-2nm deep and although quite deep are maybe etch pits (see chapter 2).

In figures 3.14(b) and (c) ordering can clearly be observed at the step edges.. This image is very representative of the surface of the Au{111} crystal after a 1000L dose. The steps observed are along the [$\bar{1}$10] direction with the stripes pointing in the [01$\bar{1}$] direction. The periodicity of these stripes is measured to be 4.5±0.5Å. How these stripes relate to the Au{111} surface will be discussed later in this chapter. The steps observed in this image have a height of one atomic Au layer (~2.6Å). No etch pits are apparent in either of these images.

Figure 3.14(d) above shows a typical image at a higher thiocresol dose. No obvious long range order is observed, but molecular features do appear to align along a particular direction. This image is from a Au{111} single crystal that has been subjected to a 32000L dose in UHV at room temperature. In contrast to figures 3.14(b) and (c) this image shows no distinct steps and terraces and thus no step edge nucleation. However, what this image clearly shows is a high density of clusters of molecules, almost completely covering this part of the sample. These features are ~1nm in width with a separation between molecules of ~4Å. The separation is comparable with the separation of the features at the step edge from figures 3.14 (b) and (c). The molecules appear to align in the [01$\bar{1}$] direction which is also the same as the direction of the step edge molecules.

3.3.5 Air STM

As mentioned in section 3.2.1 atomic resolution of Au{111} was imaged showing that the imaging conditions were good.

(a)

(b)
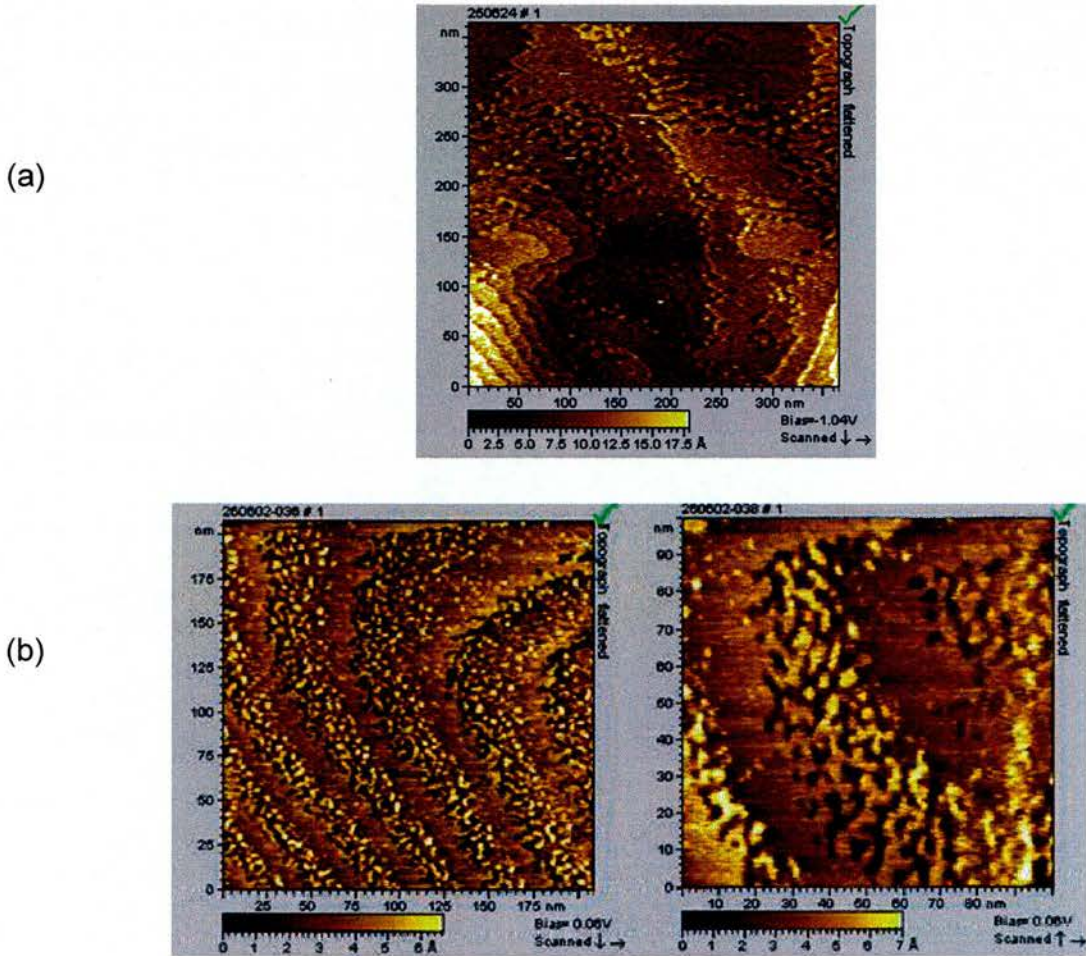
Figure 3.15 (a) Typical 400nm by 400nm image of thiocresol deposited on an Au/mica substrate from a 1mmol ethanolic solution at room temperature, for 16 hours. This image was acquired at a tunneling current of 0.096nA and a bias voltage of -1.04V. (b) Showing dramatic examples of etching and islands. These images were acquired at a tunneling current of 0.096nA and a bias voltage of -0.06V. The samples were prepared the same as for figure 3.18.

(c)
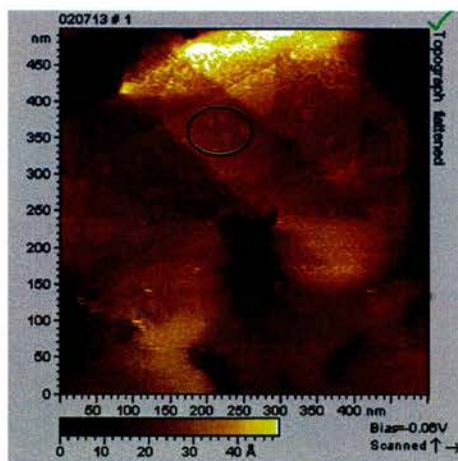
(d)
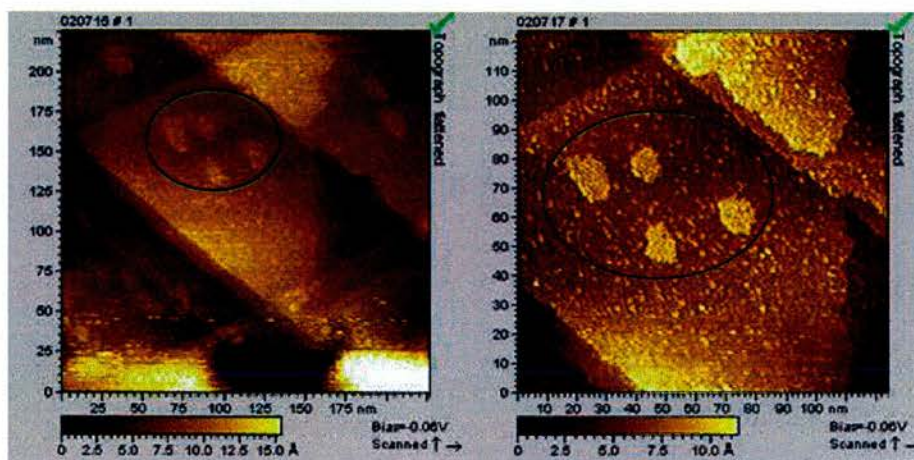
Figure 3.15 (c) 550nm wide scan of thiocresol on Au/mica substrate grown from a 1mmol heptanolic , thiocresol solution, at room temperature, These images were acquired at a 0.090nA tunneling current and a -0.060V tip bias. (d) Close up images of the islands on the Au/mica substrate that has been immersed in a 1mmol heptanolic solution, at room temperature. These images were acquired at a 0.090nA tunneling current and a -0.060V tip bias.
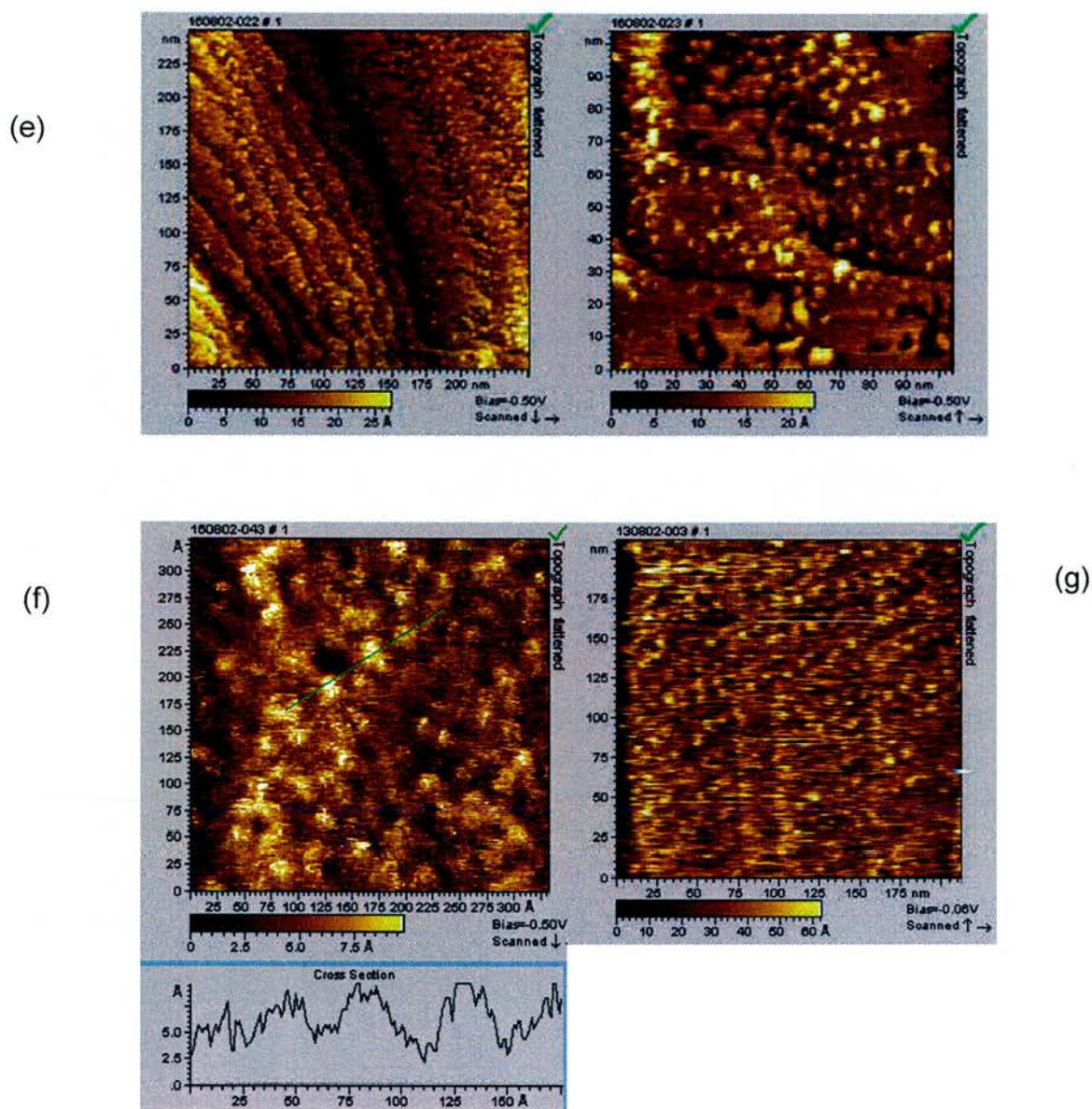
Figure 3.15 (e) Large scale (250nm by 250nm) representative image of the heated (353°C), 1mmol heptanolic thiocresol solution on Au/mica and a 100nm by 100nm scale close up image. These images were acquired at a tunnelling current of 0.370nA and a tip bias of -0.50V. (f) 300x300Å image of the flat areas (areas with no distinct islands) from figure (e). This image shows a line scan that measures the size of the islands that can be seen on the surface. This image was acquired at a tunnelling current of 0.370nA and a tip bias of -0.50V. (g) STM image of an Au/mica substrate that has been treated with a heated (80°C) 1mmol heptanolic thiocresol solution for 1 hour. These images were acquired at a 0.090nA tunneling current and a -0.060V tip bias scan 190nmx190nm.

Figure 3.15 (a) is a typical large scale constant current STM image of a Au mica slide that has been treated in a 1mmol ethanolic or heptanolic solution of thiocresol. This is a very clear example of not only etch pits but step edge etching and also islands of what could be either Au or thiocresol. The image does not appear to show any sign of long range order on the surface. This however, is best to be further investigated by looking closely at smaller areas of the sample. Figure 3.15(b) is probably the most extreme example that was produced showing these effects.

These images show that the most dramatic effect on the sample is occurring at the step edges. This image shows a high density of both pits and islands at the step edge. On measuring it was discovered that each of these islands are between 3 and 5nm wide. Other areas of the sample and other samples treated in the same way never showed islands less than 3nm wide but had some islands up to 10 nm wide. The etch pits in these images were measured to be approximately 2 or 3 gold atoms deep. It was expected that the islands would be the height of a thiocresol monolayer (lying flat or otherwise) however the measurements of these islands showed that they were approximately the same height as the depth of the etch pits. So from these images we can see that the molecule is etching at the step edge causing a high density of Au islands to congregate at the outer edge of the step while the inner part of the terrace closer to the next step is unaffected by the dosing. No evidence has been found that thiocresol forms an ordered monolayer on the Au surface.

In light of what was observed it was decided that heating the sample during monolayer growth might facilitate order on the surface as this is known to be true for many systems[6]. Attempts at this with the ethanolic solution were futile as the solution evaporated too easily. Another less volatile solvent, heptanol, was chosen. The concentration of the solution was kept the same $(1 \times 10^{-3}M)$. To be sure that changing the solvent had no difference on the monolayer growth some Au/mica substrates were immersed in the solution for 16h (same as for the ethanolic solution) and STM investigations were carried out on the resulting sample. Figures 3.15 (c) and (d) show representative images of the surface after the monolayer solution growth of thiocresol from the solution of 1mmol thiocresol in heptanol.

From these images it is shown that, in contrast to the ethanolic solution, no step edge etching or etch pits occur. Looking closely at figure 3.15(c) it is possible that that there are groups of small islands on the large terraces on the surface. The two images in figure 3.15(d) show a more detailed image of one of these terraces. The islands on these terraces are approximately the same size; they are ~25nm wide and approximately 2.5±0.2 Å in height. This height is consistent with the height of a single atomic layer of Au.

In the final close up (figure 3.15 (c) close up of 3.15 (d)) it is possible to see smaller islands (circled in figure (c) and (d)) that are about 4nm wide and 6-7Å high. These are possibly also smaller gold islands but measurements of the

height of these features reveal that they are ~3 Au atoms high. On further examination of these images it is possible to see, especially on top of the islands, that there may be some ordering occurring which would be in agreement with a previous report on aromatic thiols on Au{111}[7]. However these markings disappeared as the imaging area gets smaller, and are not detected again, hence it may have been noise or the tip conditions may have destroyed any order that may have been present. Although there is no apparent step edge etching it is observed that unlike clean Au{111} steps the step edges in these images are not straight and although not showing typical etching as before this does suggest that the solution has had some effect on the step edge.

Although the solvent used did have an effect on the growth of the monolayer and on the substrate, heating the sample was still the main priority. A new section of Au/mica substrate was immersed in a 1mmol heptanolic solution of thiocresol and heated to 353K it was left heating for 1 hour. The substrate was then removed from the solution and rinsed with ethanol and dried in a stream of nitrogen. Figure 3.15(e) is representative of the whole surface of the treated sample.

Figure 3.15(e) shows that, as with the ethanolic thiocresol solution, the surface is a mass of step edge etching, etch pits and islands in high density around the step edge. As with the ethanolic solution deposition at 300K, the islands are between 5 – 10nm wide and ~1 atomic layer of Au high. On first observation of

these images the islands appear similar to those observed in figure 3.15(a). However, it is evident that although the highest density of islands and etching is at the step edge there are in fact small islands covering the whole surface of the substrate. Figure 3.15(f) is the image of a 300Å section of the sample from figure 3.15(e) where the image focuses on a larger flat terrace area. From this image the islands can be observed more clearly. From the line scan over the islands it is possible to see the dimensions of the islands. They are approximately 25-50Å wide and 2-5Å high, and there does seems to be some periodicity between the islands of ~40Å. They seem to exhibit some short range order which is diagonally from the bottom left corner to the top right hand corner of the image. Another sample treated in the same way which is shown in figure 3.15(g) also shows some short range order.

Figure 3.15(g) shows small islands on the gold surface. These are observed to be in small rows pointing in the same direction as figure 3.23 thus showing short range directional order. Each row consists of 3 or more islands that are 5nm apart, it is possible that they are small groups of the molecule, or like the islands before, are the height of a monolayer of Au atoms.

3.3.6 X-ray Photoelectron Spectroscopy (XPS)

XPS was carried out on an Au/mica slide that had been exposed to the thiocresol solution for 16 hours. This analysis was carried out to confirm that the molecule has chemisorbed to the Au{111} surface and formed a monolayer. Figure 3.25 shows the XPS spectra of the sulphur (2p) core levels from the thiolate monolayer on Au{111}.
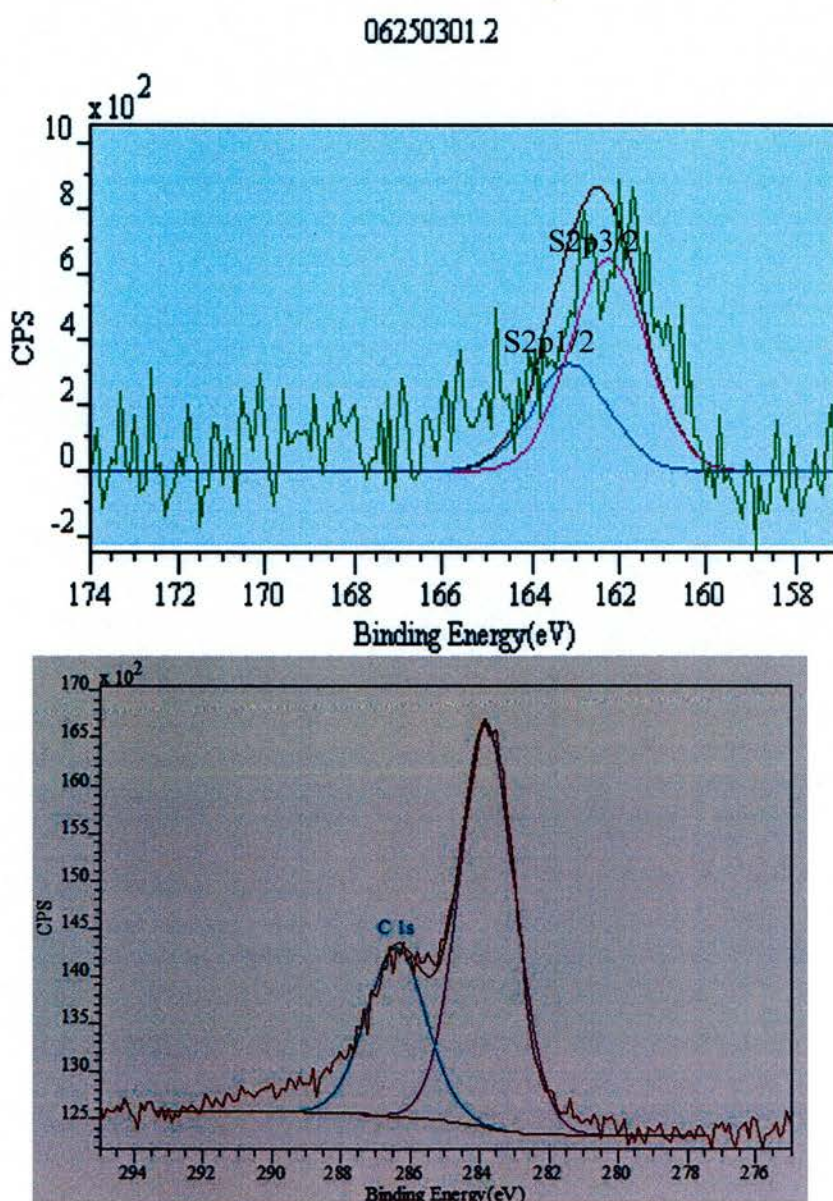
Figure 3.16 Sulphur 2p core level XPS spectra and Carbon 1s core level XPS spectra

The sulphur 2p XPS spectrum, in figure 3.16, has been subjected to a Shirley background subtraction. On investigation of this spectra the sulphur (2p) core level spectrum shows only one broad peak which can be assigned to a combination of $2p_{3/2}$ and $2p_{1/2}$ as they have the binding energies 162.1eV and 163.3eV respectively (relative to Au $4f_{7/2}$)[2,3,5,8]. Comparison of previous reports showing the sulphur (2p) binding energies of TP on Au{111} as 162.1eV and 163.3eV signifies the presence of a Au-thiolate bond consistent with the expected chemisorbed thiocresol. As the two peaks do not exist without one another the resolution of the instrument must be inhibiting the individual peaks from being seen hence a broad peak is observed.

The C1s XPS spectrum shown in figure 3.16, shows two photoemission peaks, one at 286.5eV and the other at 283.8eV. The main carbon (1s) peak can be attributed to the benzene carbon atoms while the smaller peak can be attributed to the electron deficient carbon that is bonded to the sulphur atom. This compares to work by Whelan et al.[8] on TP an Au{111} which shows carbon on Au{111} has binding energies of 284.3eV and 285.8eV. These data show that these peaks have approximately a 1:2 ratio. The expected ratio for the TP molecule is 1:5 as this is the ratio for a flat lying molecule[2]. However this does not take into account the p-substitution of the benzene ring and also the extra carbon present in the thiocresol molecule and both of these factors may increase the size of the smaller carbon peak.

3.4 Discussion

3.4.1 TPD

The TPD data are used to investigate whether, during gas phase deposition, the whole thiocresol molecule is attaching to the surface or whether only a fragment of the molecule is, *i.e. to probe whether the molecule adsorbs dissociatively.* It also shows how the molecule interacts with the surface. For example, it may indicate how strongly molecules are attached to the steps and terraces of the Au{111} surface. It is observed from the TPD data that the whole molecule has attached to the surface before desorption. This was proven because the whole molecule m/z 124 is desorbed off the surface at T_{max} 475K and T_{max} 550K. The T_{max} value for its fraction m/z 92 is the same strongly indicating that this is from the same desorption and hence is definitely a fraction of the molecule observed by the mass spectrometer. The mass spectra for the molecule show peaks at m/z 92 (biggest peak) so this observation was expected. The fact that this molecule desorbs whole from the surface is consistent with other reports of thiols on Au available[9] *e.g. ethanethiol on Au{111}.*

The main observation from these data is that the m/z 92 and m/z124 graphs shows two distinct T_{max} peaks one at 475K and the other at 550K. This shows that the molecule is desorbing from the surface at two different temperatures which in turn means that some of the molecules are more strongly bonded onto

the surface than the others. The smaller peak T_{max} = 475K is most likely to be from the thiocresol molecules that are attached to the Au terraces and the T_{max} = 550K peak may be due to the molecules attached to the step edges. This is predicted because the molecules that adsorbed onto the flat terraces are more likely to have weaker Au-S bonds in comparison to the molecules attached to the step edge. This is supported by the observation of molecular features at the step edge with STM.

The other TPD graphs for H_2S (m/z 34) and S (m/z 32) have T_{max} at 475K and 625K. Firstly it is apparent that the H_2S has the larger peak. The T_{max} of the first peak is in agreement with that of the first molecular deposition peak which means that this is likely to be due to a fragment of the molecular species. However the T_{max} of the other peak is very different, indicating that there is another desorption from the surface. This desorption is primarily of H_2S of which S is shown as a fraction.

During the desorption process some m/z 92 will be desorbed off the surface and some sulphur atoms (especially ones adsorbed strongly to the step edges) will remain attached to the Au. H_2S appears to be desorbed from the surface due to the reconstruction of S with H presumably derived from decomposition of other thiocresol species. The desorption of H_2S at 475K from a thiolated surface has been reported before[10,11] for ethane thiol on Au{100}. However, it

does not always occur for example in the case of butane thiol[12] a H_2S peak was not observed.

So from the TPD data we can confirm that during gas phase deposition of 20L or more thiocresol forms a toluenethiolate on the Au{111} surface.

3.4.2 AES and RAIRS

The AES data show clearly that after a gas phase dose of 1000L the sulphur and carbon peak heights do not increase thus showing that the Au{111} surface is completely saturated with the thiocresol molecule. However the RAIRS data in figure 3.13 show that shows that the surface is saturated with the thiocresol molecule after a 16000L dose. This difference is most likely to be due to the measurements being carried out in two different UHV chambers as this means that the dosing conditions are different because the ion gauges are in different positions. This can cause a discrepancy in the doses between the chambers of even as much as two orders of magnitude. Also the leak valve in the RAIRS chamber does not have a line of sight with the sample.

It is clear that the broad band at $763cm^{-1}$ gets larger with each increasing dose suggesting that the larger the dose the more thiocresol is chemisorbed onto the surface. [8]It has been reported before for TP on Au{322}, that at low exposures the phenyl ring of the thiocresol is tilted away from the {111} part of the surface while at saturation a more flat lying orientation is preferred it

was suggested that this was due to the existence of inequivalent adsorption sites on Au(322) which, populate simultaneously but with preferential occupation of step sites. This is the opposite of what is normally reported for aromatic thiols on Au{111}[8]. The two most prominent peaks observed are at 763cm^{-1} and 2942.9cm^{-1}. The Gaussian simulations, shown in table 1, show that the molecular vibrations causing these bands have a dynamic dipole moment perpendicular to the benzene ring.

The Gaussian calculations were carried out for a single isolated molecule. These calculate the theoretical molecular vibrations of the thiocresol molecule and the toluene thiolate. These calculations were optimised with the B3LYP method using a 6-31G basis set. Table 3.1 shows wavenumbers of the molecular vibrational modes and the predicted direction of their dipole moments. Some schematic diagrams of the molecular vibrations are also shown, the blue arrows show the direction of the stretching or bending of the molecules and the red arrows show the direction of the dipole moment. The Gaussian wavenumbers need to be corrected to give accurate band positions. The Gaussian numbers in table 3.2 need to be multiplied by 0.97 to allow comparison with the actual spectra (figure 3.17).
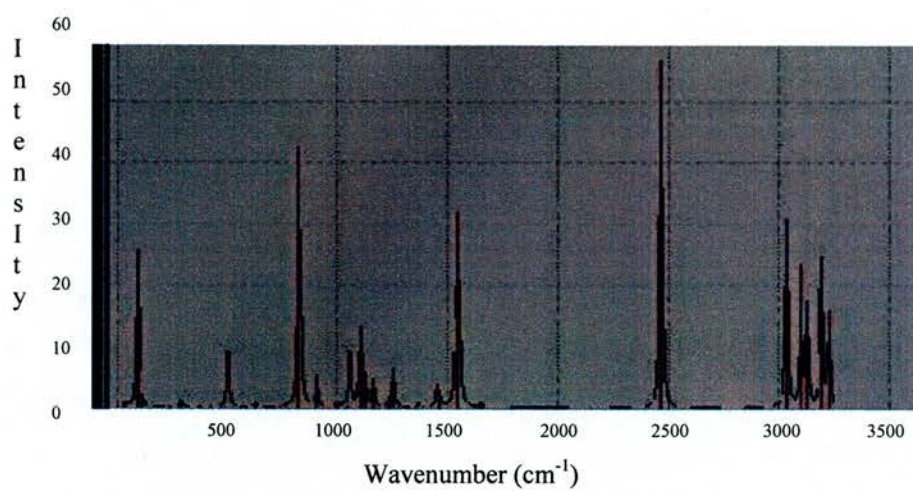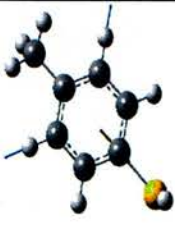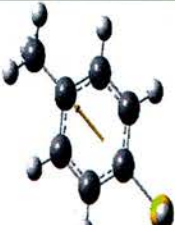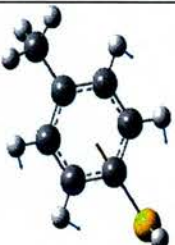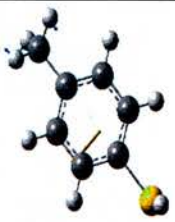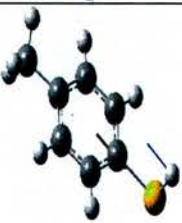
Figure 3.17 The Gaussian calculated vibrational spectrum for thiocresol

Band Number from spectra	Position of Bands (cm^{-1})	Gaussian Vibration Image	Thiocresol Transmission (cm^{-1}) (literature)	Gaussian simulation thiolate (cm^{-1}	Gaussian simulation thiocresol (cm^{-1})	Assignment of Bands
				3229.6	3225.3	Aromatic Antisymmetric C-H Stretch (parallel dipole)
1	3049.5		3030-3050	3198	3193	Aromatic Symmetric C-H Stretch (parallel dipole
			3010	3196.5	3192	Aromatic Antisymmetric C-H Stretch (parallel dipole)
				3133.5	3129.7	Antisymmetric C-H stretch from CH_3 (parallel dipole)
2	2942.9		2940-2960	3100.7	3101.1	Antisymmetric C-H stretch from CH_3 (perpendicular dipole)
3	2980		2850-2870	3035	3038	Symmetric C-H stretch from CH_3 (parallel dipole)

Band Number from spectra	Position of Bands (cm^{-1})	Gaussian Vibration Image	Thiocresol Transmission (cm^{-1}) (literature)	Gaussian simulation thiolate $(cm^{-1}$	Gaussian simulation thiocresol (cm^{-1})	Assignment of Bands
			2580-2600		2472	SH stretch (perpendicular dipole)
				1630.8		Aromatic Ring C-C stretching (parallel dipole)
			1505		1551.6	In plane aromatic CH bends and ring vibrations (parallel dipole)
				1526.5	1535.7	CH wag of P substituted CH_3 (parallel dipole)
			1480	1534.89	1534.97	CH bend of p substituted CH_3 (perpendicular dipole)
				1456.13		CH_3 umbrella CH bending (parallel dipole)

Band Number from spectra	Position of Bands (cm^{-1})	Gaussian Vibration Image	Thiocresol Transmission (cm^{-1}) (literature)	Gaussian simulation thiolate (cm^{-1}	Gaussian simulation thiocresol (cm^{-1})	Assignment of Bands
4	1244.5		1205-1215 and 1230-1240	1254	1252	Out of plane aromatic CH bend

(parallel dipole) |
5	1175		1170-1180			In plane CH bend
6	1155.4					
7	1128					C-H out of plane and in plane bends
8	1091		1091-1095 and 1112		1116.3	Semi-circle stretching and aromatic C-H in plane bending mixture

(parallel dipole) |
| 9 | 1060.5 | | | 1096 | 1101.2 | C-H in plane bending

(perpendicular dipole) |

Band Number from spectra	Position of Bands (cm^{-1})	Gaussian Vibration Image	Thiocresol Transmission (cm^{-1}) (literature)	Gaussian simulation thiolate (cm^{-1}	Gaussian simulation thiocresol (cm^{-1})	Assignment of Bands
10	1013.5		1015 and 1034	1078.7	1053	Aromatic in plane C-H deformations (parallel dipole)
			910		904.5	SH wag (parallel dipole)
11	763.5		800-795	845 (very strong)	827 (V. strong and a smaller sharp peak at 817)	Aromatic C-H out of plane bending 817 also includes ring breathing (perpendicular dipole)

The clearest observation from this table on comparing it to the spectra is that the largest peaks are the vibrations with the perpendicular dipole moments *i.e. dipole moments out of plane with the benzene ring.* The largest peak (peak 11) is assigned to the out of plane C-H bending mode. This mode is observed if the molecule is parallel or tilted towards the Au{111} surface, *i.e. 0-20°*, this is due to the surface dipole selection rule (see chapter 2). Other reports of TP[2] mercaptobiphenyls[13] and tertphenylthiols[14] show that aromatic thiols with the SH directly attached to the aromatic ring can have tilt angles of anywhere between 28° and 0°. If the molecule was upright then the dynamic dipole moment of the CH bending vibration would be parallel to the surface and therefore image dipole would cancel out the actual dipole and no vibration will be observed. This also explains why the stronger vibrations are the ones with the perpendicular dipole moment suggesting that the molecule is either flat lying or close to flat lying.

Some of the stronger vibrations with dipole moments parallel to the plane of the aromatic ring are observed (peaks 2 and 9). This occurs as the molecular plane is tilted at an angle towards the surface rather than being completely parallel to it.

The molecules may be at a 10±10° angle as was calculated by Whelan et al who used polar angle dependence to calculate this value. For TP[2] from the surface and this is usually what is reported for TP[2,4] on Au{111}. This

orientation occurs because thiocresol bonds to the substrate through its π orbitals even though the Au-S bond is the principle interaction. This molecular geometry however is expected more at low coverage than at saturation coverage, because it assists bonding between the aromatic ring π system and the metal substrate but it is not expected for high coverage. However an upright geometry never occurs for the thiocresol, and this is also reported for the TP on Au{111}[2,8] from UHV gas deposition onto Au{111}. It does however occur for benzyl thiol where a CH_2 group separates the benzene ring and the sulphur atom. This allows the molecular angle to change as the molecule is not as rigid as TP or thiocresol[15].

3.4.3 UHV STM

The STM images figures 3.14 (a-d) for gas phase deposition show that the packing of the molecule on the surface is different from the packing of the molecule from solution deposition this will be discussed in section 3.4.5. It has been established from the RAIRS data that the molecule is either flat lying or more likely tilted with the phenyl ring parallel to the surface.

The STM images show that at low depositions there is some step edge nucleation of the molecule. There will be molecules attached to the terraces but as with TP they will not be ordered[2,3,4]. The molecules on the step edges can be observed because these molecules adsorb more strongly onto the step edges. The separation between the molecules is measured to be $4.5\pm0.5\text{Å}$.

This is most likely to be 5Å in reality as this corresponds to the √3 separation which is often seen for thiols[7]. The difference between these can be assigned to drift. A common structure for thiol monolayer formation is a (√3x√3)R30° structure[7,16] this is commonly known as hexagonal coverage and is shown schematically in figure 3.18.
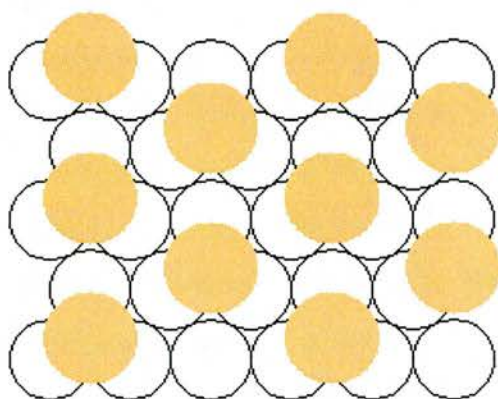
Figure 3.18 (√3x√3)R30° surface structure where the white circles are Au{111} atoms and yellow circles are the S atoms.

In this configuration the molecular separation is ~5Å. The molecules that are gathered at the step edges may possibly not be forming this configuration as the separation is measured to be 4.5Å. It is possible though that the sulphur atoms form this pattern along the step edges of the gold, and due to the thiocresol molecules strong intermolecular interactions, *e.g. π-π stacking between aromatic molecules,* they might tend to align into chains which would fit well with the step edge striping. Figure 3.19 is a proposed idea of how the thiocresol molecule has packed along the step edge. This however may mean that the molecules have a separation of 5Å between the sulphur atoms and the separation between the main bodies of the molecule will be less than 5Å.
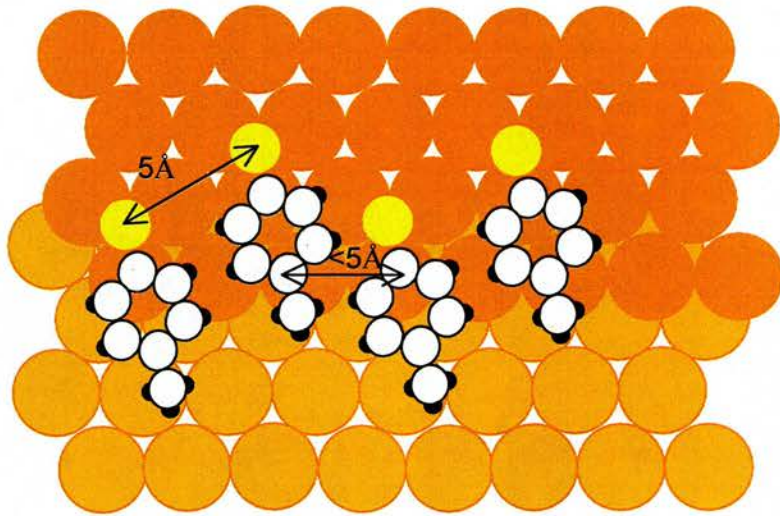
Figure 3.19 Proposed packing of thiocresol along the Au{111} step edge where the sulphur group has adsorbed in the $(\sqrt{3}\times\sqrt{3})R30°$.

Another proposed mechanism sees the sulphur group attaching to the Au{111} surface every third vacant site. Figure 3.20 shows this. The separation between the sulphur molecules which is ~ 4.5Å
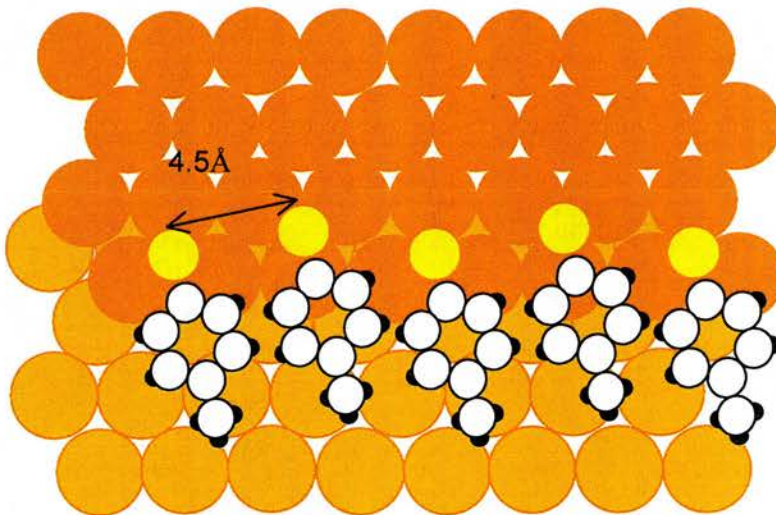
Figure 3.20 Proposed packing of thiocresol along the Au{111} step edge.

It is not unusual for benzene molecules to nucleate along the step edges of surfaces. It has been reported before that benzene favours step edges of Cu{111}, Rh{111} and Ag{110} surfaces[17,18]. For Rh{111} it is especially prevalent as it is the individual molecules that attach to the step edges and the molecules at the step edges are less mobile than on the terraces and so are much stronger bound at these sites. It is suggested that benzene, and benzene derivative molecules adsorb to the step edge sites as benzene favours adsorption sites of lower electron density. However in all of these situations the molecules do not order along the step edge they are just attached randomly.

As was mentioned before even with π-π stacking it is unusual for these types of molecules to have a separation of 4.5Å. Benzene alone chemisorbed onto surfaces and π-π stacked has a molecular separation of 3.7Å[18] which is smaller than the expected periodicity from solid benzene. This periodicity (3.5±0.2Å) however is the normal benzene containing molecule separation where π-π stacking interactions occur and this is well reported[17,18,19]. However π-π stacking is less important than the Au-S bond strength. The π-π stacking still may direct the orientation of the molecule but the distance will still be dictated by the Au-S bond, π-π stacking plays a large part in most natural aromatic self assembly.

3.4.4 XPS

XPS was used to investigate the adsorption via solution phase deposition at 300K. The data showing the formation of the carbon 1s and the sulphur 2p peaks at the expected binding energy for a TP molecule[2] confirms that this molecule has attached to the surface as a thiolate. The C1s is observed at 285eV due to the different types of carbon in this molecule for example for example a C_6H_5X and/or C_6H_6 peak and a CH_3 peak[20,21]. The amount of carbon and sulphur on the surface was calculated using the XPS data. This data showed that ~90% of the substance adsorbed onto the Au{111} surface was carbon and ~10% was sulphur. The expected ratio of carbon sulphur for thiocresol is ~73:27 taking in to account the relative sensitivity factors, *i.e.1.677 for S*, and using equation 2.11. This may mean that some sulphur was lost during deposition or that the sample was affected by some outside contamination, *i.e.* C contamination.

3.3.5 Air STM

Although it has been reported that TP molecules are expected to be upright on the surface when dosed from solution[2] the air STM images did not show whether the molecules were upright or not. They also did not show any order was present until the solution was used to dose onto the surface at a higher temperature. This is not unusual as it has been recorded many times that TP on Au does not order on the surface from solution deposition[3,7]. There has only been one instance where ordering was reported and in that situation the solvent

used was water and the molecule only ordered when the substrate was immersed for less than 2 minutes[4]. The high resolution STM images showed that the molecules formed a ($\sqrt{13}$x$\sqrt{13}$)R13.9° ordered phase structure.

This was not the case for any other solution phase deposited TP films. This lack of order may well be influenced by aromatic chain length. It has been recorded that an increase in chain length shows the molecular orientation becoming less tilted[3]. This can be explained if it is assumed that the intermolecular forces, responsible for self assembly get stronger the more aromatic rings there are. This means that the weak intermolecular forces may be the reason why TP and hence thiocresol monolayers are poorly defined on Au.

It is not only the increase in aromatic chain length that influences the packing order of the aromatic molecules on Au but also aliphatic chain length. For example it is documented that benzyl thiol $(C_6H_6)CH_2SH$ readily forms an ordered monolayer on Au{111} and always displays a highly ordered hexagonal pattern[6]. This shows the importance of the methylene group inserted between the aromatic ring and the sulphur. When benzyl thiol is adsorbed onto Au the phenyl ring sits perpendicular to the surface which is opposite to TP and thiocresol. This would then show that the angle of the molecule to the surface is important to its packing orientation on the surface. Figure 3.21 shows proposed

orientation for the thiocresol on the Au{111} surface in comparison to the reported geometry of the benzyl thiol molecule on Au{111}.
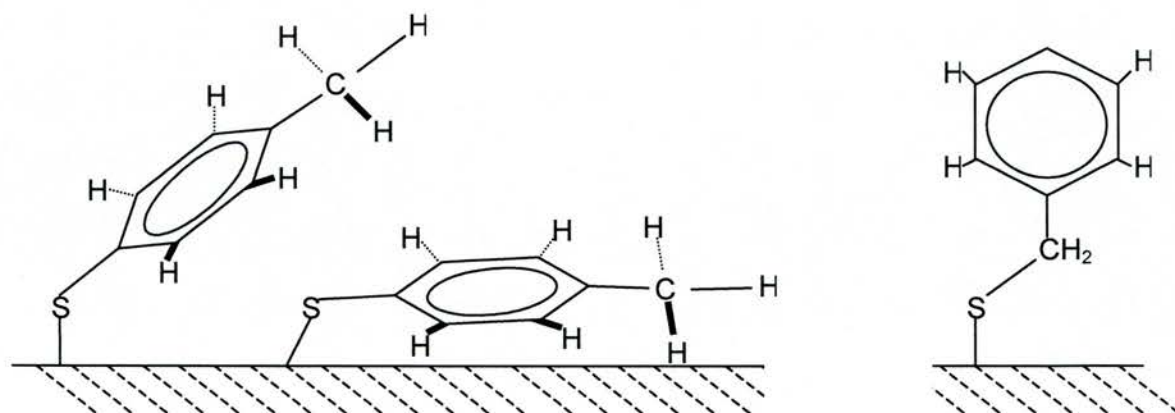
Figure 3.21 The possible molecular geometry for thiocresol on Au(a) in comparison with the reported molecular upright geometry for benzyl thiol on Au(b)

The effect of the molecules at the step edge after gas phase deposition is again apparent but after solution deposition the effect is much more dramatic. Although no ordering was observed from the solution deposition the most striking observation from air STM images was the step edge etching and the formation of islands on the surface as this happened for both solvents and at both room temperature and 353K. This at first seemed unusual as although some etching was expected (see chapter 2) the step edge etching and the formation of Au islands was not.

The formation of Au{111} islands has been recorded before from aromatic thiol deposition[7] and also from aromatic selenium molecules and their deposition onto Au{111}[22] (selenium attaches to the surface of Au in a very similar manner to sulphur as the atoms are very closely related chemically). In the aromatic

thiol research[7] 4-mercaptopyridine (4MPY) and 4-hydroxythiophenol (4HTP) were investigated, only the 4HTP will be compared with the thiocresol as it is the most similar molecule, both are p-substituted thiophenols. In this situation as for thiocresol, small islands of Au appear on the surface of the Au/mica substrate after it has been immersed in the 1mmol aqueous 4HTP solution for 12 hours. The conditions for this are different than for the thiocresol but the outcome is mostly the same, namely the formation of islands.

The dimensions of the islands from the 4HTP solution deposition are between 5-10nm which is similar to the islands that were observed after thiocresol deposition. They are approximately the height of a monolayer of Au 2.6 ± 0.2Å which again is the same as the islands formed in the thiocresol experiments. The molecular features in this research[9] are shown to preferentially adsorb along the 22x√3 reconstruction stripes however for thiocresol they preferentially adsorb along the step edges. This may be because reconstruction does not occur on the Au/mica substrate as it is kept at atmospheric pressure[22] where it is assumed molecules will have adsorbed onto the surface.

What is witnessed for thiocresol seems to be step edge etching. This may not actually be the case though as the step edges may be expanding as nearby Au islands are being incorporated into the step. This is thought to occur because for 4HTP time trials were carried out to see if different immersion times had an

effect on the amount of islands on the Au surface and during this investigation STM images showed islands disappearing into step edges.

The shape of the thiocresol Au step edges is consistent with the behaviour observed for Au/HTP. On examining figures 3.13 (e) and (f) it is evident that these islands take up at least 50% of the Au surface. It is suggested by *Jin et al*[7]. that the islands are formed in a similar way to etch pits are when an aliphatic thiol is chemisorbed onto a surface, *i.e. it is due to the increased mobility of the surface Au atoms.* This is possible because there are changes on the surface over time with the islands disappearing into the surface and this is also very likely for thiocresol.

The increased mobility on the surface occurs because the strong S-Au bond weakens the linkage between the Au atoms within the top layer and also between the top and second layers of the substrate[4]. The mobile atoms then combine to form small islands. The reason that this might occur for aromatic thiols and not aliphatic ones, is maybe due to the interaction between the aromatic thiols being stronger than for the alkanethiols because their π-π stacking interactions are stronger than the aliphatic thiols van der Waals interactions[4]. In contrast however to the thiocresol images the 4HTP molecule clearly forms ordered adlayers on top of the Au islands whereas on examining the islands on the thiocresol air STM images no order is observed. This may be

due to the molecule having a flat lying geometry or bring tilted towards the Au surface as in the gas phase deposition.

Air STM images clearly show that the molecule has attached onto the surface through solution deposition and that no order is present. Air STM also shows the tendency of the molecules to directly affect the step edges. This contrasts to the UHV STM measurements where the interaction between molecules and step edges involve alignment of molecules along step edges but no apparent step edge corrosion.

3.5 Conclusion

After adsorbing thiocresol onto Au{111} by gas phase deposition, the RAIRS data show that the molecule is either flat-lying or, most likely, tilted towards the Au surface. The STM data show that molecules do not order on the Au{111} surface, on the large terraces, at any amount of exposure, from both the solution and gas phase deposition. This from all of the reports on thiophenol on Au{111} was expected. However at lower doses (1000L) a high density of step edge striping is observed by UHV STM and even on some areas on the surface after a 32000L dose. This could be due to π-π stacking and some predicted packing orientations are shown on figures 3.28 and 3.29. The molecules most likely adopt the ($\sqrt{3}$x$\sqrt{3}$)R30° type structure[7] in the vicinity of the step edges..

The TPD, Auger, RAIRS and XPS data all suggest that the molecule has attached whole onto the surface and air STM data shows Au islands common to aromatic thiol adsorption on Au due to the mobility of the top layer of Au atoms on the substrate. Also the lack of order of aromatic thiols where the phenyl ring is attached directly to the S atom is expected.

The major difference between the solution deposition and the gas phase deposition is that the molecules order at the step edges after gas phase deposition. By contrast, solution deposition has a dramatic effect on the step edge.

References

[1] Z.Mekhalif, P.Lang, F. Garnier. J. Electroan. Chem. **399** (1995) 61

[2] C. M. Whelan, C. J. Barnes, C. J. H. Walker, N. M. D. Brown. Surface Science **425** (1999) 195

[3] S. Frey, V. Stadler, K. Heister, W. Eck, M. Zharnikov, M. Grunze. Langmuir **17** (2001) 2408

[4] L-J. Wan, M. Terashima, H. Noda, M. Osawa. J. Phys. Chem. B. **104** (2000) 3563

[5] L-J. Wan, K. Itaya. Langmuir **13** (1997) 7173

[6] P. Cyganik, M. Buck, W, Azzam, C. Woll. J. Phys. Chem. B **108** (2004) 4989

[7] Q. Jin, J.A. Rodriguez, C.Z. Li, Y. Darici, N.J. Tao. Surface Science **425** (1999) 101

[8] C.M. Whelan, C.J. Barnes, C.Grégoire, J.-J. Pireaux. Surface Science **454-456** (2000) 67

[9] J. Libuda, G. Scoles. J. Phys. Chem **103** (1999) 9933

[10] D. M. Jaffey, R. J. Madix. Surface Science **311** (1994) 159

[11] R. Valiokas, M. Ostblom, S. Svedhem, SCT. Svensson, B. Liedberg. J. Phys. Chem. B **106** (2002) 10401

[12] V. Bondzie, St. J. Dixon-Warren, Y. Yu, L. Zhang. Surface Science **431** (1999) 174

[13] J. F. Kang, A. Ulman, S. Liao, R. Jordan, g. Yang, G-Y. Liu. Langmuir **17** (2001) 95

[14] C. Fuxen, W. Azzam, R. Arnold, G. Witte, A. Terfort, C. Wöll. Langmuir **17** (2001) 3689

[15] P. Borchart, E.J. Sturrock, N.V. Richardson In Preparation.

[16] A. Ulman. Chem. Rev. **96** (1996) 1533

[17] J.I. Pascual, J.J. Jackiw, K.F. Kelly, H. Conrad, H.P. Rust, P.S. Weiss.

Phys.Rev.B **62** (2000) 12632

[18] H.A. Yoon, M. Salmeron, G.A. Somorja. Surface Science **373** (1997) 300

[19] G.B. McGaughey, M. Gagné, A.K. Rappé J.Bio.Chem **273** (1998) 15458

[20] P. Sundberg, R. Larsson, B. Folkesson
Journal of Electron Spectroscopy and Related Phenomena. **46** (1988) 19.

[21] D. Briggs, M.P. Seah. **1** (1993) second edition, Pratical surface analysis,
John Willey & Sons.

[22] M.H. Dishner, J.C. Hemminger, F.J. Feher. Langmuir **13** (1997) 4788

CHAPTER 4

The synthesis of vinyldimethyl-p-thiophenylsilane and the investigation of its adsorption on Au{111}

4.1 Introduction

Vinyldimethyl-p-thiophenylsilane is dendrimer G1. This molecule was not commercially available and so was synthesised at St Andrews University. There is no record of this molecule being synthesised before. Figure 4.1 below shows a model of the G1 molecule.
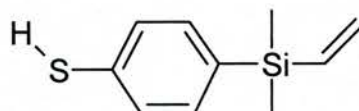
Figure 4.1 A schematic drawing of the G1 molecule Vinyldimethyl-p-thiophenylsilane.

This molecule was chosen to see how it would bind to the Au surface and how it orientated on the surface and interacts with its neighbours. It was also chosen since the presence of the vinyl end group makes it possible to use this molecule as a building block from which to synthesise further generations of dendrimer. The binding of the molecule to the surface is important as future work may include the attachment of this or larger generation thiolated dendrimer molecules to gold colloids. The vinyl groups in this molecule are also very important as this would eventually be used to attach the active catalyst to the molecule.

It has been reported that the bromine version of this molecule shown in Figure 4.2 was easily synthesised[1] and that bromine terminated ring molecules could be thiolated[2].
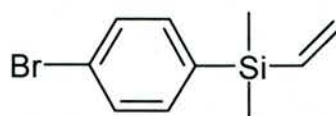
Figure 4.2 A schematic drawing of vinyldimethyl-p-bromophenylsilane.

The G1 molecule will be investigated to see if the behaviour of the vinyldimethyl silane head group compares with the CH_3 head group of the thiocresol molecule on Au{111}. In addition it was also interesting to observe how the adsorption of G1 compares to thiophenol (TP) on Au{111}[3,4,5]. s

4.1.1. Preparation of vinyldimethyl-p-bromophenylsilane

The synthesis described as the novel sequential divergent and convergent synthesis of carbosilane dendrimers by [6]Casado et al was the starting point for the synthesis described in this work. This was the synthesis of a dendrimer using consecutive divergent and convergent synthetic steps. Their synthesis was carried out using para-substituted bromobenzene, $BrC_6H_4(CH_2)_3SiMe_xCl_{3-x}$ (where x=1 or 2), to synthesise the precursor $BrC_6H_4(CH_2)_3SiMe(CH_2CH:CH_2)_2$ thus allowing convergent C-C coupling onto the periphery of a dendric carbosilane or to the silane $BrC_6H_4(CH_2)_3SiHMe_2$. This was then incorporated as a peripheral group by hydrosilation of a per(allyl-terminated) dendric carbosilane and then used in divergent aryl-aryl coupling. Repetition of this synthesis establishes a reiterative sequence and this builds the complex system of the dendrimer. Figure 4.3 shows the synthetic organic scheme.
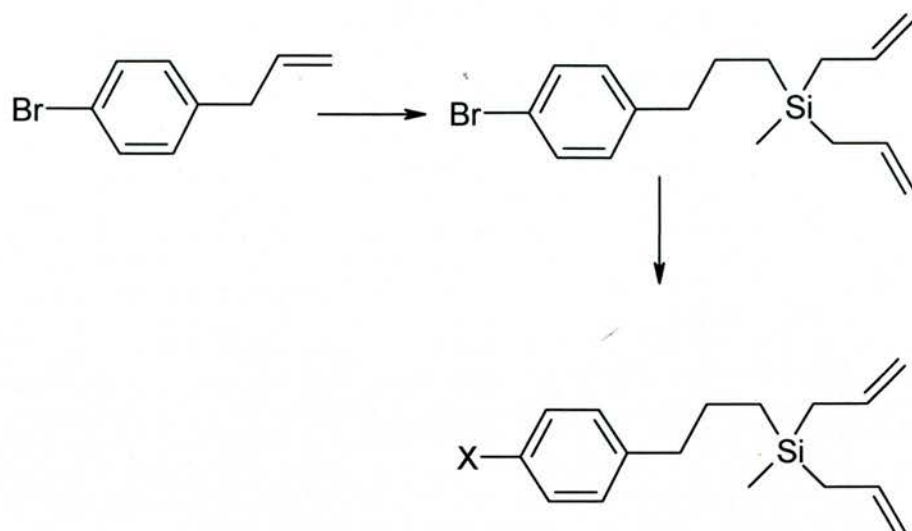
It is not possible to purchase the starting material for this reaction and it is a very complicated molecule to synthesize so this actual synthetic procedure was not used but the synthesis used to make the dendrimer after the precursor (new starting molecule) is synthesised will basically follow the same type of scheme.

The precursor is synthesised using dibromobenzene and chlorodimethylvinylsilane to make vinyldimethyl-p-bromophenylsilane. This reaction was reported in 1961 by Murphy et al[1] and was only partly successful as they only achieved a 21.6% yield. The reaction was originally carried out using a Grignard reagent. In this synthesis instead of using a Grignard reagent Butyl Lithium reagent (BuLi) was used. This was more successful and gave a yield of approximately 70%. Figure 4.4 shows the synthetic scheme involved.
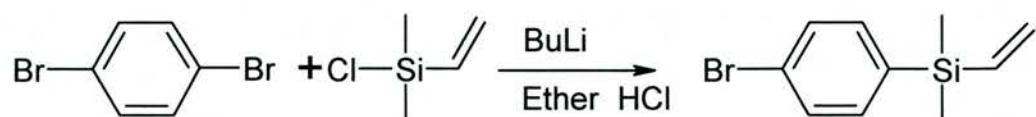
Figure 4.4. The synthetic reaction used for the synthesis of the dendrimer precursor vinyldimethyl-p-bromophenylsilane.

To attach this dendrimer precursor or G1 dendrimer to the Au {111} surface it will need a thiol head group and so become vinyldimethyl-p-thiophenylsilane. This molecule (see figure 4.1) has not been synthesised before and so a new synthetic route had to be taken. However the substitution of a bromine p-substituent with thiol functionality is well established[7]. BuLi was used once more to lithiate the vinyldimethyl-p-bromophenylsilane. This was then reacted in solution with sulphur powder at −95°C and then 6M hydrochloric acid was used to incur protonation; figure 4.5 below shows this reaction scheme.
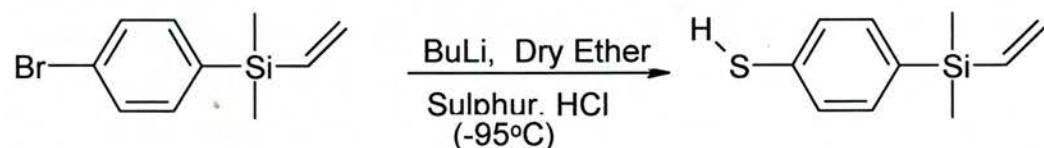
Figure 4.5 This scheme shows the desired synthetic reaction for turning vinyldimethyl-p-bromophenylsilane into vinyldimethyl-p-thiophenylsilane.

This reaction produced a number of different products. Only a very small amount of the desired product was produced. The reaction also produced a small amount of the disulphide. The main product synthesised is shown in figure 4.6

124
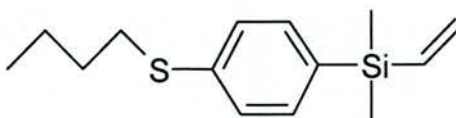
Figure 4.6 The main product of the reaction shown in figure 4.5.

It is believed that this product was synthesised because the 10ml HCl in 5ml Et$_2$OH was added to the sulphonated solution at the end of the reaction, after it had been heated to room temperature, rather than adding immediately after all of the sulphur in the reaction had dissolved. This meant that the sulphur was not protonated. In this case the sulphur had reacted with the lithiated reactant and was allowed to warm to room temperature where the unprotonated p-substituted sulphur group then reacted with the butyl bromine present in the reaction mixture from the lithiation. This occurred due to a lack of free hydrogen molecules and when the acid was added to the reaction there were very few sulphur sites left for the free hydrogens to protonate. This is displayed in figure 4.7.
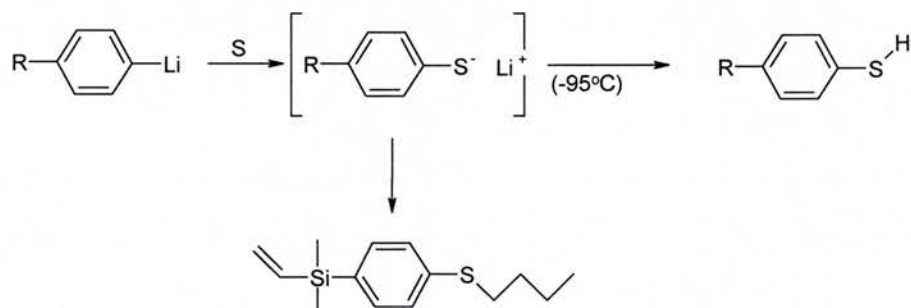
Figure 4.7. The above reaction shows what happens when the synthesis described in figure 4.5 did not work.

This part of the synthesis, although only a small part, was very difficult to carry out correctly. If the acid solution was added too quickly then the reaction would not work as was the case if it was added too slowly. The addition of the acid was very time dependent. There is a narrow time

window, once the sulphur powder is dissolved, when the HCl can be successfully added. To perfect this part of the reaction was difficult. A measurable amount of the G1 molecule was only made once in the early stages. As this was so difficult many different reaction processes were used to try to substitute the bromine for the thiol group, for example using lithium instead of butyl lithium. However when persevering with the original method, the ideal conditions were found (see section 4.2.2). The products were analysed using NMR and Gas Chromatography (GC-MS) to show that the desired molecule had been synthesised. It was discovered after the spectroscopic analysis that the disulphide had also been produced. This makes no difference because the S-S bond in the disulphide should break during dosing allowing the molecule to attach in the same way as the thiol as the Au-S bond is stronger than the S-S bond and it is well established that disulphide adsorption is similar to thiol adsorption[8].

4.2 Experimental

4.2.1 Preparation of vinyldimethyl-p-bromophenylsilane

Dibromobenzene (15.263g) was weighed into a round bottomed Schlenk flask (250ml). This was sealed and placed under vacuum for 1 hour. It was then purged with nitrogen until all that remained in the flask was a positive pressure of nitrogen. The dibromobenzene was then dissolved in dry isopropyl ether (100ml). BuLi (24ml) was then added with constant stirring from a magnetic stirrer. This mixture was left stirring for one hour to ensure lithiation. Chlorodimethylvinylsilane (8.7ml) was then added to the reaction, this was then left stirring at room temperature for 16 hours under a constant stream of nitrogen.

After 16 hours the sealed flask was opened to atmosphere, and a 1:5 solution of HCl (2M, 10ml) in H_2O (40ml) was added to the flask. This liquid then separated into two phases and more water was added. The reaction mixture was then extracted using diethyl ether and the aqueous layer was discarded. The organic layer was washed with ammonium chloride (50ml, 2M) and then with aqueous saturated sodium chloride solution (50ml). The remaining product was filtered through a sinter funnel filled with talc, dried over anhydrous $MgSO_4$ for 1 hour and then filtered through glass wool and evaporated in a rotary evaporator. The product was then purified by distillation in a Kugelröhr distillator and 8.98g of the product was produced. This is approximately 58.2% yield. NMR and GC-MS analysis were carried out on this product.

4.2.2 Preparation of vinyldimethyl-p-thiophenylsilane

Vinyldimethyl-p-bromophenylsilane (4.9g) was weighed into a round-bottomed Schlenk flask (100ml). This was sealed and put under vacuum for 1 hour, it was then purged with nitrogen until all that remained in the flask was a positive pressure of nitrogen. Dry Diethyl ether (20ml) was then added to the solution and stirred. Next the BuLi (8ml) was added and this was left stirring for 1.5 hours under a constant stream of nitrogen.

Sulphur powder (0.768g) was then weighed into a round-bottomed flask (100ml) and dry diethyl ether (20ml) was then added. Both the lithiated reaction mixture and the sulphur in ether were cooled to $-95^{\circ}C$ using a bath of acetone and liquid nitrogen. The lithiated reaction mixture was then decanted into the sulphur solution while maintaining the temperature at $-95^{\circ}C$. This flask was then removed from the freezing bath and the sulphur was watched as it slowly dissolved. As soon as this had occurred a mixture of HCl (10ml) and ethanol (5ml) was injected by syringe into the reaction mixture. The mixture at this point was a bright yellow suspension and then after approximately 30 seconds it instantly turned colourless. This mixture was then left stirring under a constant stream of nitrogen for 3 hours.

The sealed flask was then opened to atmosphere and HCl (2M, 20ml) was added to the reaction. The reaction solution was extracted by diethyl ether (20ml) and the aqueous layer was discarded. The organic layer was then dried over anhydrous $MgSO_4$ for an hour then filtered and the solvent

evaporated off using a rotary evaporator. The product obtained was a yellow liquid, and this was then analysed for purity using the GC-MS and the NMR. The product was then purified by column chromatography with hexane used as the solvent. The adsorption of G1 on an Au surface was investigated using air STM, UHV STM, RAIRS, and XPS.

4.2.3 Solution Deposition

For the air STM Au on mica substrates were used, (see Chapter 2) and for UHV STM a Au{111} single crystal was used. The G1 monolayers were prepared by the immersion of the Au/mica substrates in a 1×10^{-3}M solution of the thiol in analytical grade ethanol for 16 hours or for timed intervals of 15 minutes, 30 minutes, 1 hour, 2 hours, 4 hours, and 8 hours. These samples were washed in ethanol and dried in a nitrogen stream. An Au/mica substrate was immersed in 1mmol/L solution for 16 hours for the XPS analysis. For air STM and XPS conditions see Chapter 2.

4.2.4 Gas Phase Deposition

For the UHV STM analysis, an Au{111} single crystal was used (see Chapter 3). The conditions for gas phase deposition of G1 are similar to those described for thiocresol deposition in Chapter 3.

4.3 Results

4.3.1 Synthesis

4.3.1.1 Spectroscopic Analysis of vinyldimethyl-p-bromophenylsilane

^{1}H NMR was used to verify the purity of vinyldimethyl-p-bromophenylsilane using a Varian Gemini 2000 with a resonant frequency of 300MHz for ^{1}H machine (see appendix 1). The results of the ^{1}H NMR (CDCl$_3$) were: a doublet of doublets for the aromatic region δ 7.611, 7.585, 7. 499 and 7.471ppm$_{(1,2,7,8)}$. The CDCl$_3$ reference peak at 7.367ppm 6.5-6.2$_{(5)}$ppm CH, 6.2-5.8$_{(4)}$ppm CH$_2$, 0.448$_{(3,6)}$ppm SiCH$_3$. Next GC-Mass spectrometry (see appendix 2) was carried out on the product. This spectrum showed only one very large major peak. The mass spectroscopy of this showed an m/e of 241, 241 is the molecular weight of vinyldimethyl-p-bromophenylsilane. See figure 4.8 for schematic diagram showing correlation between molecule and nmr peak positions.
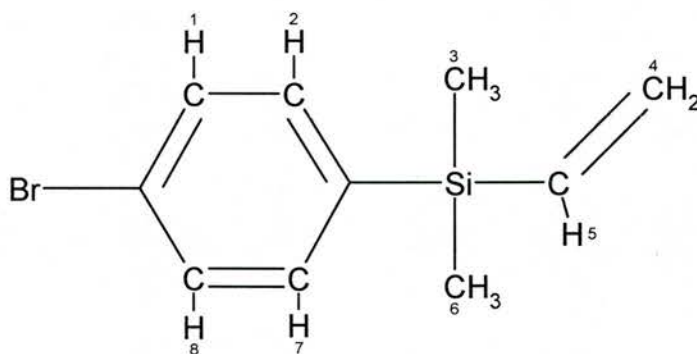
Figure 4.8 Schematic diagram of vinyldimethyl-p-bromophenylsilane with H's numbered to correlate with nmr peaks in results section above.

<u>4.3.1.2 Spectroscopic Analysis of vinyldimethyl-p-thiophenylsilane</u>

^{1}H NMR was used to verify the purity of vinyldimethyl-p-thiophenylsilane using a Varian Gemini 2000 with a resonant frequency of 300MHz for ^{1}H machine (see appendix 3). The results of the ^{1}H NMR (CDCl$_3$) were: for the aromatic region δ 7.6-7.3$_{(2,3,8,9)}$ppm. The CDCl$_3$ reference peak at 7.27ppm, 6.4-6.2$_{(6)}$ppm CH, 6.1-5.7$_{(5)}$ppm CH$_2$, 3.405$_{(1)}$ppm for SH and 0.335$_{(4,7)}$ppm for SiCH$_3$. Next GC-Mass spectrometry (see appendix 4) was carried out. Initially there were four main peaks the largest one has an m/e of 194 thus showing that it was the desired product. After purification another peak appeared that had not been in the initial spectrum this other compound was present in the separated fraction containing the product it had an m/e of 386. This showed that the new peak was due to the presence of the disulphide (see figure 4.9(b)) however not in a large quantity only about 10%. After two months this product was analysed again by GC- mass spectroscopy and this time it showed that there was now about 90% disulphide and 10% thiol. See figure 4.9(a) for schematic diagram showing correlation between molecule and nmr peak positions.

(a)
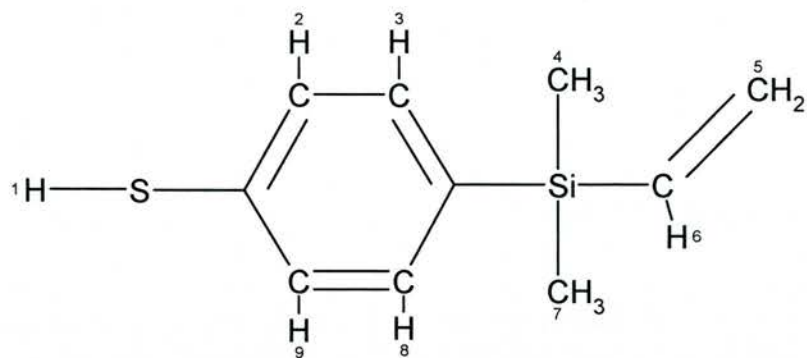
(b)
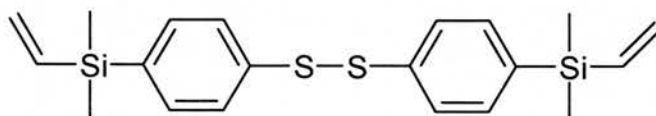
Figure 4.9 (a) Schematic diagram of vinyldimethyl-p-bromophenylsilane with H's numbered to correlate with nmr peaks in results section above. (b) Schematic diagram of disulphide.

4.3.2 Solution Deposition

4.3.2.1 Reflection Adsorption Infrared Spectroscopy (RAIRS)

Figure 4.10 shows the $3500cm^{-1}$ to $2400cm^{-1}$ range RAIRS spectra for the solution deposited G1 onto an Au{111} single crystal.
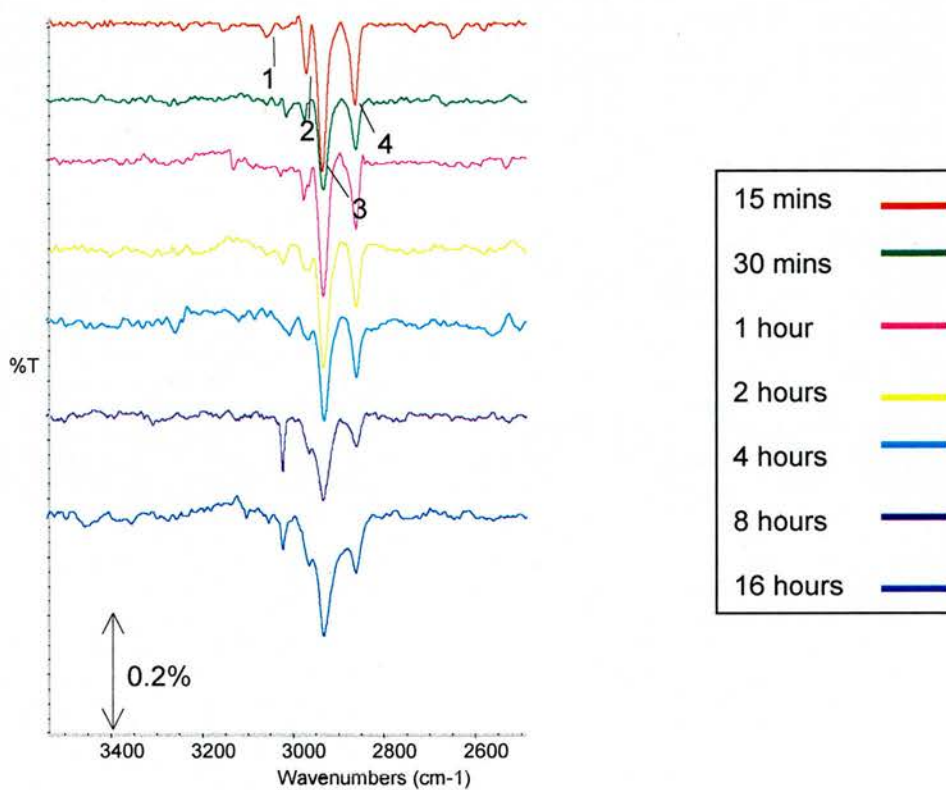
Figure 4.10 RAIRS spectra $3500cm^{-1}$- $2400cm^{-1}$ for solution deposition showing doses from 15 minutes to 16 hours in a 1mmol solution of the G1 dendrimer in ethanol.

Figure 4.11 shows the 1300cm^{-1} to 700cm^{-1} range RAIRS spectra for the gas phase deposited G1 dendrimer thiol onto Au{111}.
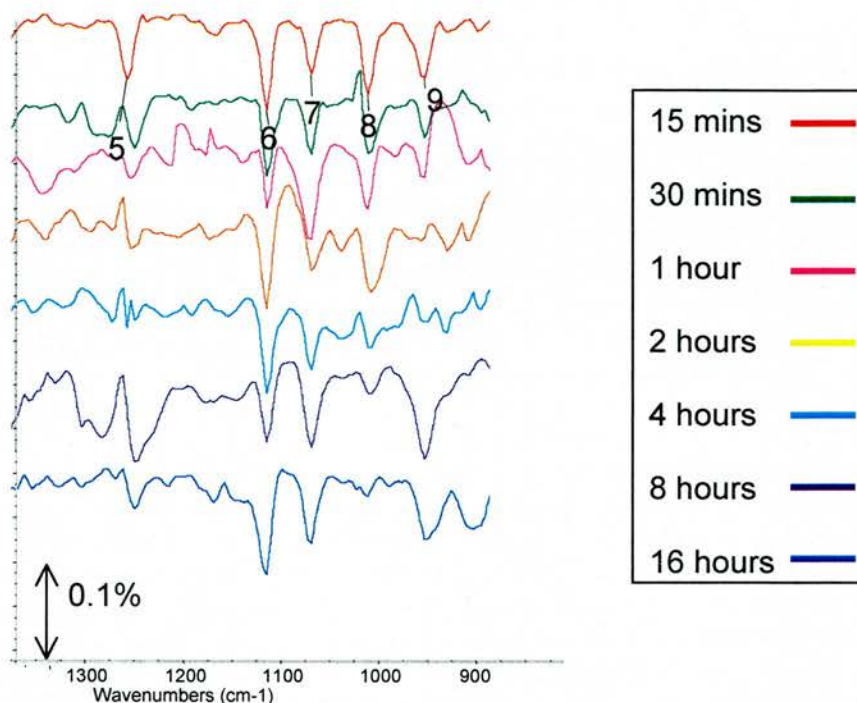
Figure 4.11 RAIRS spectra 1400cm^{-1}- 800cm^{-1} for solution deposition showing doses from 15 minutes to 16 hours in a 1mmol solution of the G1 dendrimer in ethanol.

For the thiocresol molecule there was a large C-H out of plane bending peak at 763cm^{-1} however for the G1 if this peak is present it will be obscured due to the detector cut off. This is because at the time of this analysis a different MCT detector was being used. The range of this detector was such that it was unable to detect bands below 800cm^{-1}. The bands which are present are 1. 3041cm^{-1}, 2. 3003cm^{-1}, 3. 2960cm^{-1}, 4. 2922cm^{-1}, 5. 1257cm^{-1}, 6. 1115cm^{-1}, 7. 1069cm^{-1}, 8. 1011cm^{-1}, 9. 953cm^{-1}.

The peaks shown in these spectra generally increase slightly in size with each increasing dose. There is only one peak which does not follow this trend, peak 9 which decreases in size with each subsequent dose. Peak 8 is not observed after the 8 hour dose.

4.3.2.2 X-ray Photoelectron Spectroscopy (XPS)

(a) Carbon

(b) Sulphur

(c) Silicon
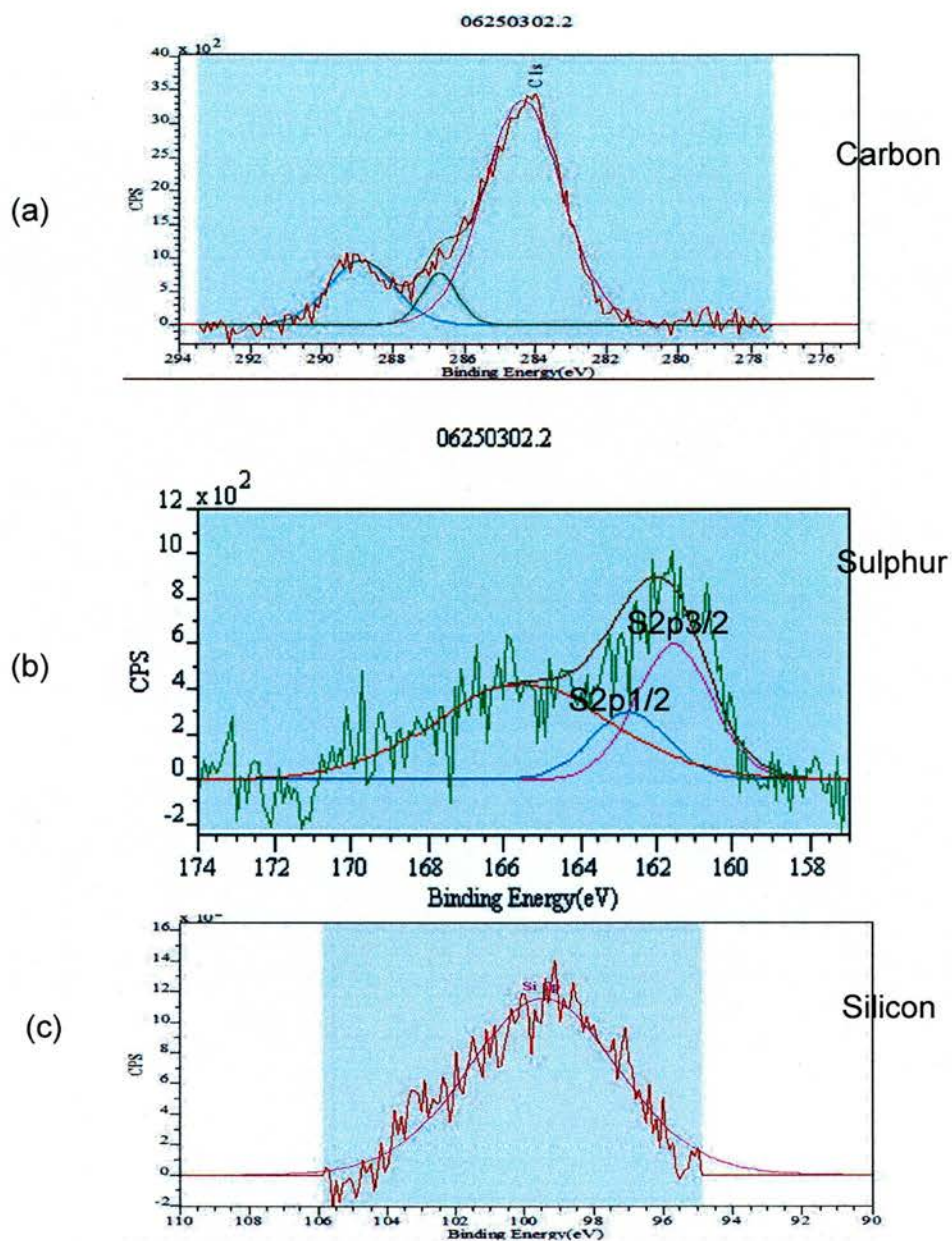
Figure 4.12 Spectra (a) Carbon 1s core level XPS spectra from and Au/mica substrate that was immersed in the 1mmol ethanolic G1 dendrimer thiol solution for 16 hours. Spectra (b) shows Sulphur 2p core level XPS spectra from and Au/mica substrate that was immersed in the 1mmol ethanolic G1 dendrimer thiol solution for 16 hours. Spectra (c) Silicon 2p core level XPS spectra from and Au/mica substrate that was immersed in the 1mmol ethanolic G1 dendrimer thiol solution for 16 hours. A pass energy of 20eV was used.

XPS was carried out on the Au/mica slide that had been exposed to a 1mmol ethanolic G1 solution, to investigate the nature of the adsorbed species produced by G1 adsorption on a Au{111} surface. Figure 4.12 (a) shows the carbon (1s) XPS spectrum which shows that there are three photoemission peaks, at 289.0eV, 286.7 and 284.5eV. Figure 4.12 (b) shows the XPS spectra of the sulphur (2p) core levels from the thiolate monolayer on Au{111}. This XPS spectrum has been subjected to a Shirley background subtraction. On investigation of this spectra the sulphur (2p) core level spectrum shows two peaks with the binding energies 161.8eV and 165.5eV respectively (relative to Au $4f_{7/2}$ with the binding energy 83.5eV)[3,4,9]. Figure 4.12 (c) shows the core level XPS spectra for Si 2p. This XPS spectrum has been subjected to a Shirley background subtraction. On investigation of this spectrum it is clear that the silicon 2p core level spectrum shows one peak which has a binding energy of ~99.5eV.

4.3.2.3 Ultra High Vacuum Scanning Tunneling Microscopy (UHV STM)

(a)

(b)

(c)

Figure 4.13 (a) 30nm by 30nm UHV STM image of Au{111} single crystal that has been immersed in an ethanolic G1 thiols solution for 1 hour molecular features are evident on the surface and also some periodical striping along the [110] direction. (b) 30nm by 30nm UHV STM image of Au{111} single crystal that has been immersed in an ethanolic G1 thiols solution for 1 hour molecular features are evident on the surface and also some periodical striping along the [110] direction. (c) 100nm by 100nm UHV STM image of Au{111} single crystal that has been immersed in an ethanolic G1 thiols solution for 1 hour showing a cris-cross effect. The smaller image to the right is the auto-correlation image which show an average direction of the features on the surface. These images were acquired at a tunneling current of 0.514nA and a tip bias of -1V.
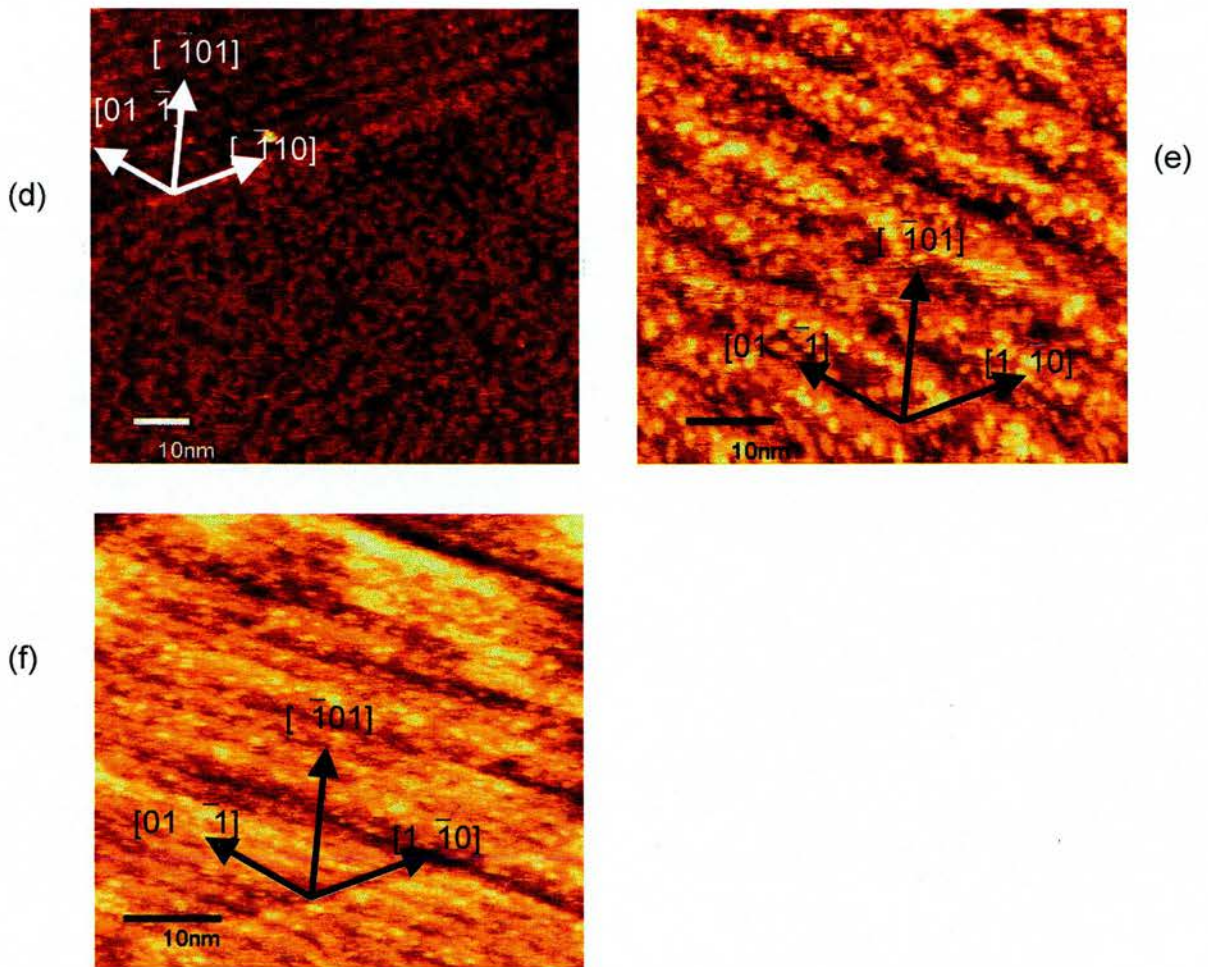
Figure 4.13 (d) 100nm by 100nm UHV STM image of Au{111} single crystal that has been immersed in an ethanolic G1 thiols solution for 2 hours showing a large terrace and some steps covered in small molecular features. (e) A 63nm by 63nm UHV STM image of Au{111} single crystal that has been immersed in an ethanolic G1 thiols solution for 2 hours showing steps and small terraces covered in small molecular features. (f) 55nm by 55nm UHV STM image of Au{111} single crystal that has been immersed in an ethanolic G1 thiol solution for 4 hours. It show what looks like steps and small terraces covered in molecular features.

(g)

(h)

(i)
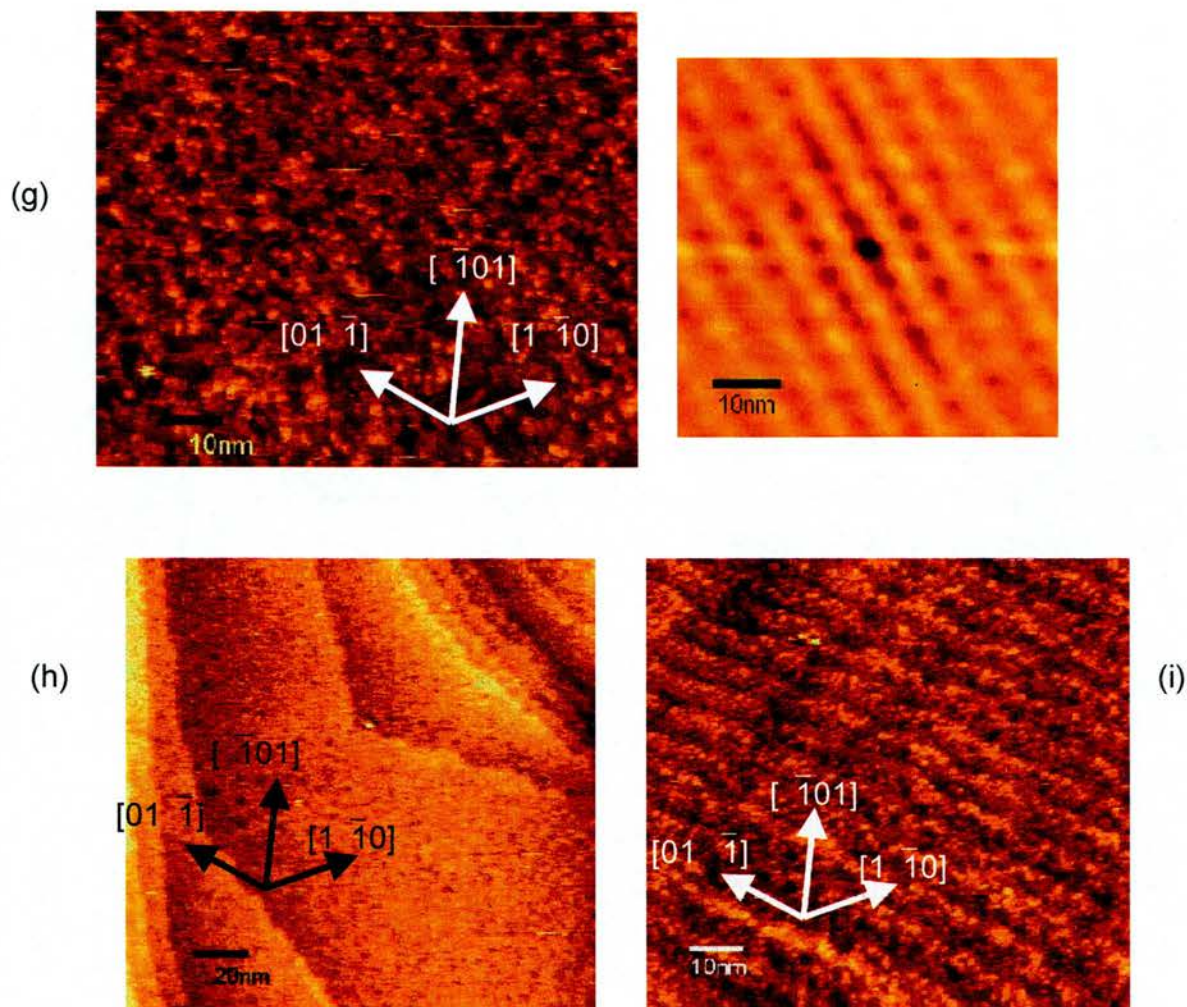
Figure 4.13 (g) 100nm by 100nm UHV STM image of Au{111} single crystal that has been immersed in an ethanolic G1 thiols solution for 4 hour showing a cris-cross effect. The smaller image to the right is the auto-correlation image which shows an average direction of the features on the surface. (h) 200nm by 200nm UHV STM image of an Au{111} single crystal that has been immersed in an ethanolic G1 thiol solution for 4 hours. It shows steps large terraces with small etch pits. This image was acquired at a tunneling current of 0.268nA and a tip bias of -0.393V. (i) 100nm by 100nm UHV STM image of Au{111} single crystal that has been immersed in an ethanolic G1 thiol solution for 8 hours. It shows steps and small terraces with molecular features on them. These images (except image (h)) were acquired at a tunneling current of 0.514nA and a tip bias of -1V.
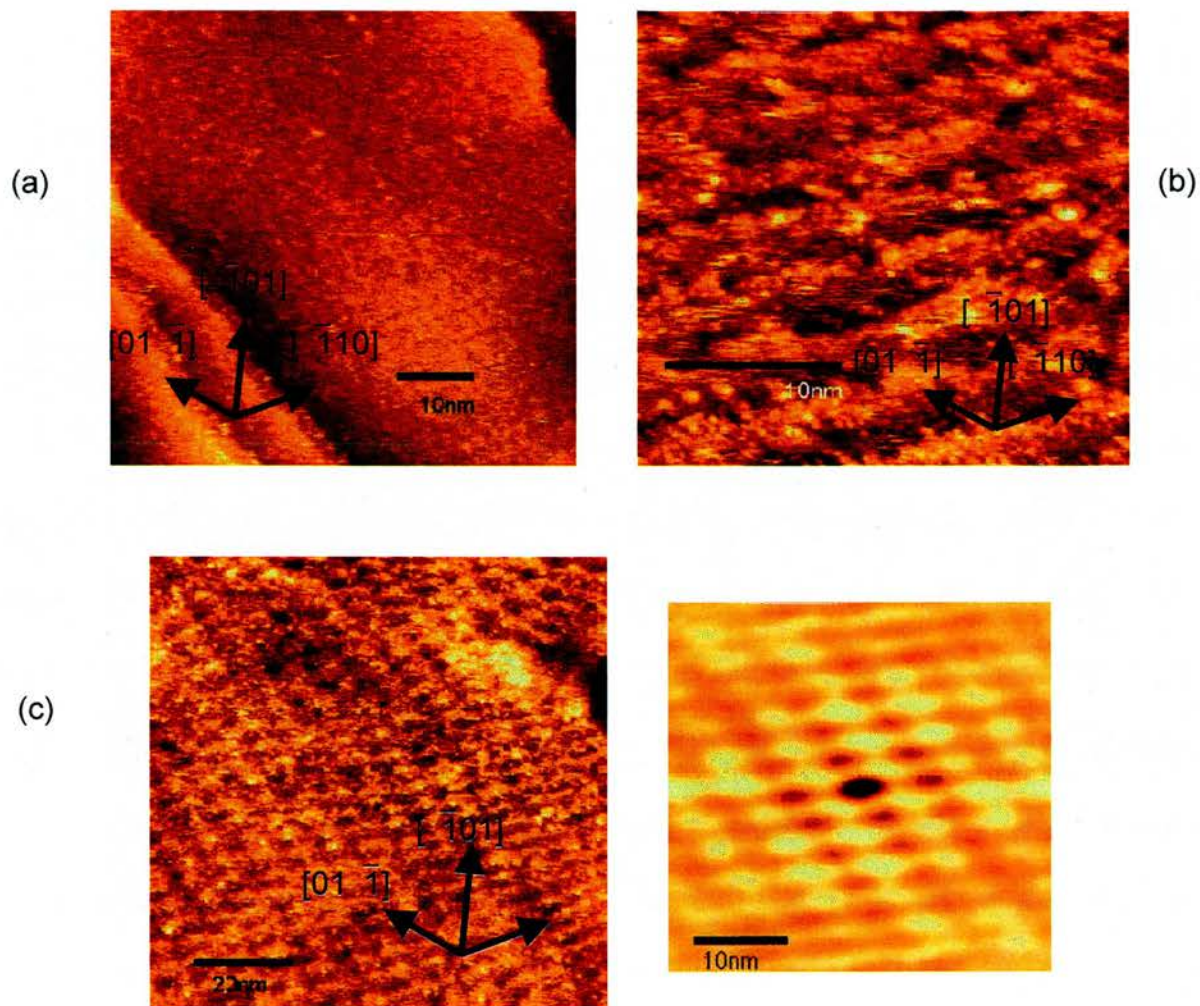
140
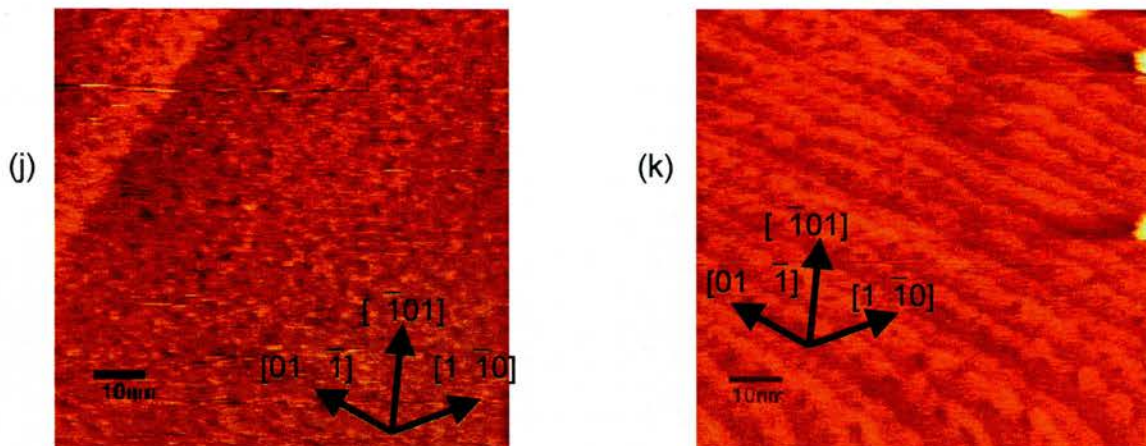
Figure 4.13 (j) 100nm by 100nm UHV STM image of an Au{111} single crystal that has been immersed in an ethanolic G1 thiol solution for 8 hours. It shows a step and large terraces and etch pits. (k) 100nm by 100nm UHV STM Image of an AU{111} single crystal that has been immersed in an ethanolic G1 thiol solution for 16 hours. It shows many steps and small terraces and etch pits on these terraces. These images were acquired at a tunneling current of 0.712nA and a tip bias of -0.341V.

As mentioned in part 3.2 the UHV STM of Au{111} has been imaged allowing the real space direction of the atoms to be determined, as can be observed in figure 3.4. Figures 4.13(a-k) show images from the UHV STM after an Au{111} single crystal had been exposed to G1 for different lengths of time. The crystal was observed after a 15 minute dose however noise prevented any usable images from being recorded.

The images show that after the 1 hour dose (figure 4.13 (b)) molecular features and clusters of molecular features are observed. Each molecular feature is ~1.5nm wide and ~1.5Å in height. The separation between these features is between 0.6nm and 1 nm. In figure 4.13(b) and (e) and (f) and (i) periodical striping is observed in the [$\overline{1}$10] direction. These stripes are approximately 2±0.2Å high, the periodicity between them is ~4nm. This image is representative of most of the surface of the Au{111} crystal after

141

being immersed in the G1 ethanolic solution. Similar to this is the lattice effect or pseudo hexagonal pattern which is observed in figures 4.13(c) and (f). This is further supported by the auto-correlation pattern which gives an average separation of the features and more clearly shows the real space directions of close packed features in the images. Auto-correlation is a computer programme that finds any repetitive periodicity in the image scanned and then filters off any features that do not belong to this periodicity. These features are not noise as their separation is constant even when the scan size and speed is changed. The periodicity between each bright feature in figure 4.13(c) in the [$\bar{1}$10] direction is ~4±0.5nm and the periodicity between the features in the direction from the top left of the image to the bottom right is ~6.7±0.5nm. However the periodic features in figure 4.13(g) does not follow either of the [1 $\bar{1}$0] and [$\bar{1}$10] directions unlike in figure 4.13(c) where the [1 $\bar{1}$0] direction is obvious. The periodicity between the large lattice features are 7.2±0.5nm in the bottom left to top right direction and 5±0.5nm in the bottom right to top left direction. It is also pertinent to remember that thermal drift can affect these images. Although this pattern is observed it is unlikely due to molecular features as these are much smaller and can be observed on top of this lattice structure. The dimensions of the molecular features are the similar to those in figure 4.13 (c).

In Figure 4.13(h) and figure 4.13(i) and (j) no molecular features are observed. However the G1 molecule has had an effect on the surface as it is covered in ~2.6Å deep holes which can identified as etch pits[10]. The step

edges have also been affected and the original direction of the steps can barely be identified. This etching is only observed for long dosing times *i.e. after 4 hour doses* and is not observed before this.

4.3.3.4 In Air Scanning Tunneling Microscopy (STM)
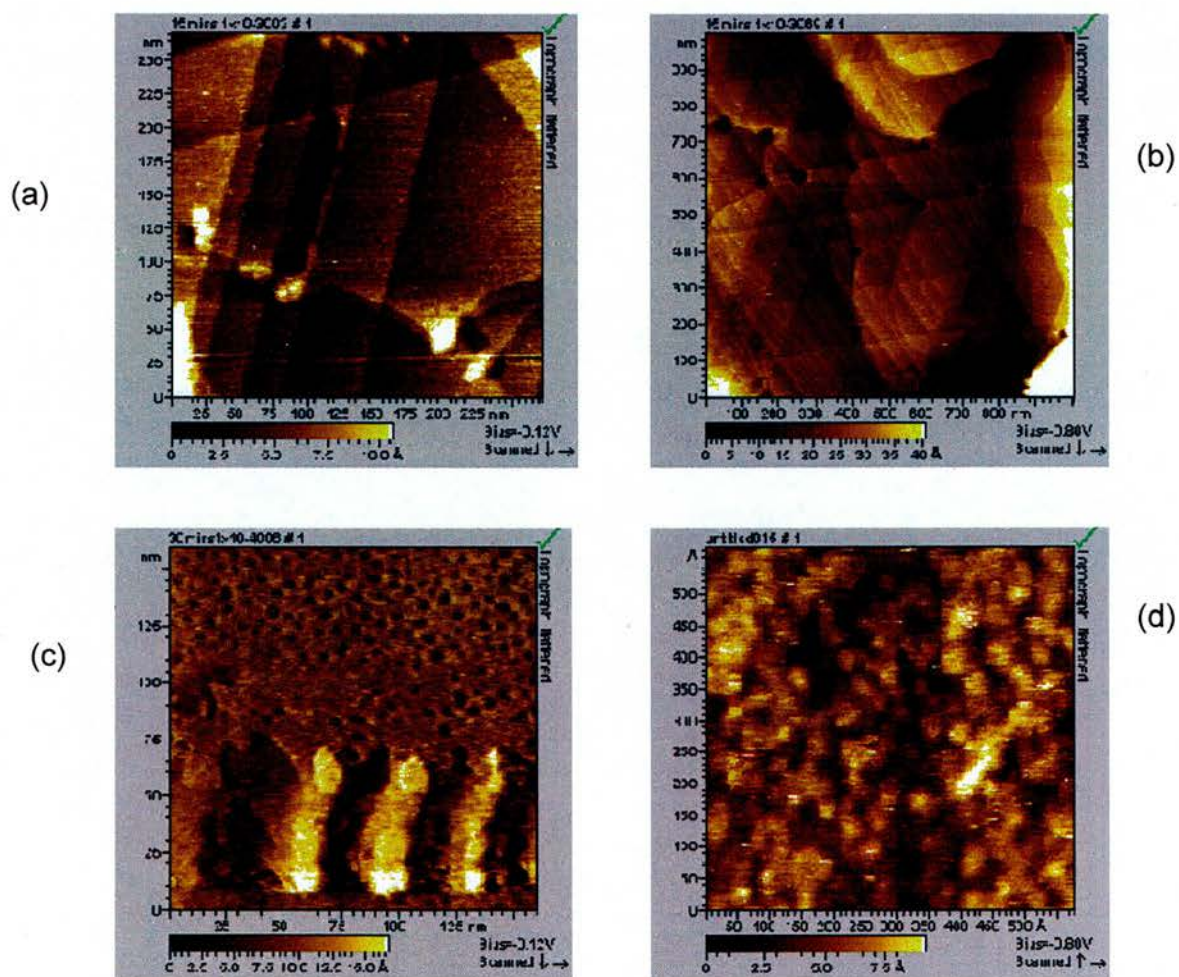
Figure 4.14(a) 275nm by 275nm image of G1 dendrimer deposited on an Au/mica substrate from a 1mmol ethanolic solution for 15 minutes. This image was acquired at a tunneling current of 0.189nA and a bias voltage of -0.12V. (b) 1000nm by 1000nm image of the G1 dendrimer deposited on an Au/mica substrate from a 1mmol ethanolic solution for 30 minutes. This image was acquired at a tunneling current of 1.057nA and a bias voltage of -0.12V. (c) 150nm by 150nm image of the G1 dendrimer deposited on an Au/mica substrate from a 1mmol ethanolic solution for 30 minutes. This image was acquired at a tunneling current of 0.474nA and a bias voltage of -0.12V. (d) 500Å by 500Å image of the G1 dendrimer deposited on an Au/mica substrate from a 1mmol ethanolic solution for 1 hour. This image was acquired at a tunneling current of 0.474nA and a bias voltage of -0.80V.

143

(e) (f) (g) (h)
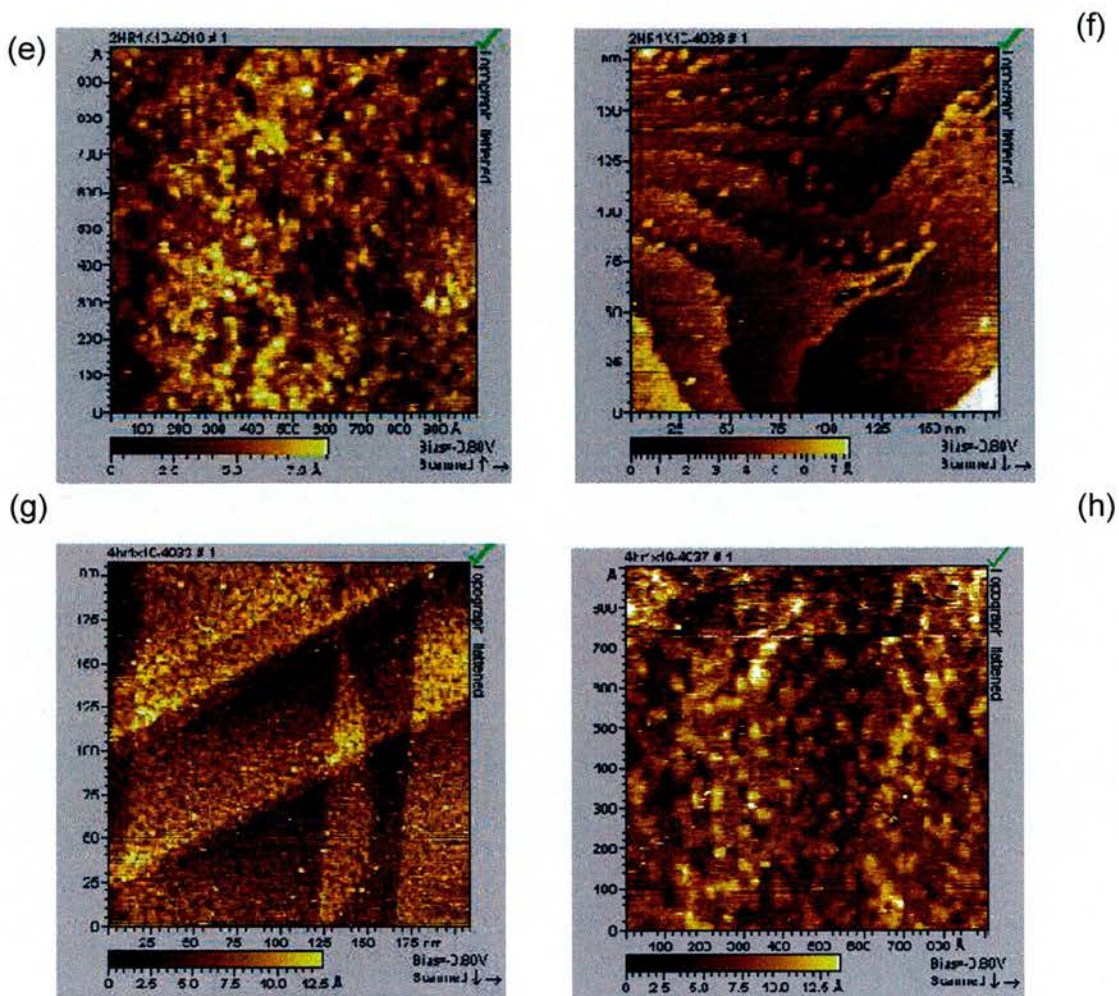
Figure 4.14 (e) 1000Å by 1000Å image of the G1 dendrimer deposited on an Au/mica substrate from a 1mmol ethanolic solution for 2. This image was acquired at a tunneling current of 0.474nA and a bias voltage of -0.80V. (f) 175nm by 175nm image of the G1 dendrimer deposited on an Au/mica substrate from a 1mmol ethanolic solution for 2 hours. This image was acquired at a tunneling current of 0.474nA and a bias voltage of -0.80V. (g) 200nm by 200nm image of the G1 dendrimer deposited on an Au/mica substrate from a 1mmol ethanolic solution for 4 hours, this shows etching and possibly molecular features. This image was acquired at a tunneling current of 0.474nA and a bias voltage of -0.80V. (h) 900Å by 900Å image of the G1 dendrimer deposited on an Au/mica substrate from a 1mmol ethanolic solution for 4 hours, close up of (g). This image was acquired at a tunneling current of 0.474nA and a bias voltage of -0.80V.

144
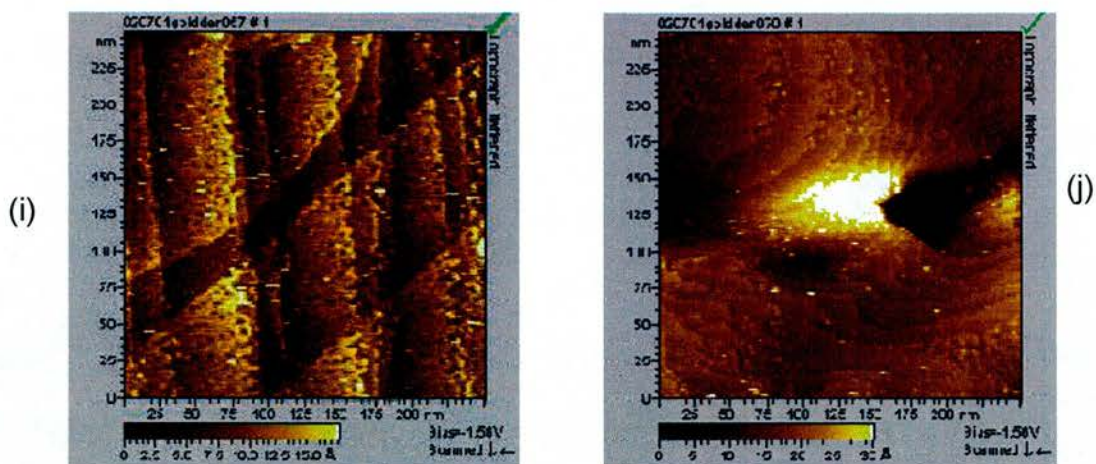
Figure 4.14(i) A 250nm by 250nm image of the G1 dendrimer deposited on an Au/mica substrate from a 1mmol ethanolic solution for 16 hours. This image shows dramatic etching. This image was acquired at a tunneling current of 0.466nA and a bias voltage of -1.56V. (j) 250nm by 250nm image of the G1 dendrimer deposited on an Au/mica substrate from a 1mmol ethanolic solution for 16 hours, This image shows lots of step edge modification and Au islands. This image was acquired at a tunneling current of 0.466nA and a bias voltage of -1.56V.

As mentioned in section 3.2.1 atomic resolution of Au{111} was imaged showing that the imaging conditions were good. Figure 4.14 (a) is a typical large scale constant current STM image of the prepared G1 molecule on a gold/mica slide.

The images in Figures 4.14 (a-j) show that there are no etch pit effects or molecular features observed before the 1 hour dose. No molecules are observed on the 15 minute and 30 minute sample. The images following a one hour dose images show etch pits have occurred and that there are molecular features on the surface. These molecular features are observed on the surface from the 1 hour dose until the 16 hour dose (although all images are not shown). These features are, on average, ~2nm wide and ~3Å high however the resolution of the image is such that it is possible that

145

2 or more molecules are being measured or that the curvature of the tip is blurring the size of the features.

Etch pits are not imaged again until the 4 hour dose time and by the 16 hour dose there are not only a lot of etch pits but also areas of step edge etching and areas that show island formation. These islands are ~2.5nm high and similar to those observed from the thiocresol solution dose onto Au/mica (chapter 3). Those were identified as Au islands. Although molecules are not observed it is assumed they are attached to the Au surface and the newly formed Au islands. In some of the 16 hour samples it is difficult to distinguish whether the features shown in the images are due to severe etching or molecular features.

4.3.3.1 Reflection Adsorption Infrared Spectroscopy (RAIRS)

Figure 4.15 shows the 3500cm^{-1} to 2400cm^{-1} range RAIRS spectra for the solution deposited G1 onto an Au{111} single crystal.
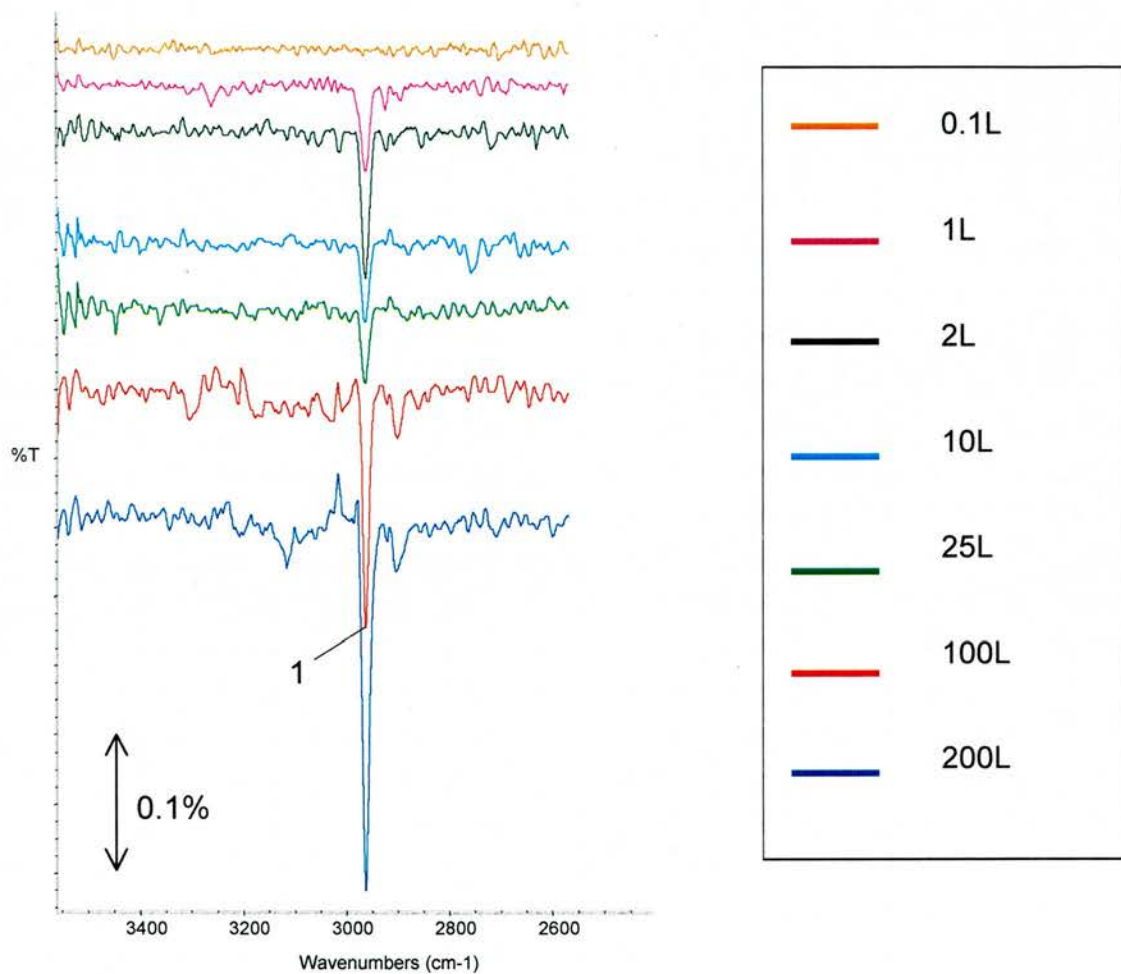
4.15 RAIRS spectra 3500cm^{-1}- 2400cm^{-1} for gas phase deposition showing doses from 0.1 langmuirs to 204.8L carried out in a UHV chamber base pressure 1x10^{-10} torr.

Figure 4.16 shows the 2200cm^{-1} to 700cm^{-1} range RAIRS spectra for the gas phase deposited G1 dendrimer molecule onto Au{111}.
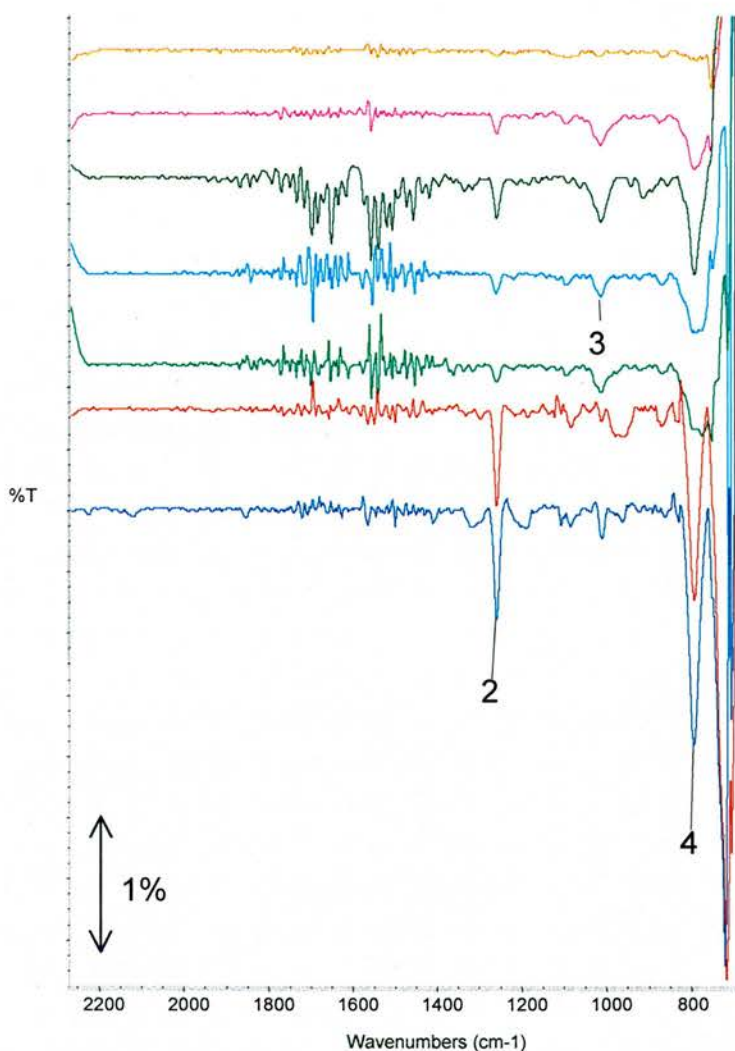
4.16 RAIRS spectra 2200cm^{-1}- 700cm^{-1} for gas phase deposition showing doses from 0.1 langmuirs to 204.8L carried out in a UHV chamber base pressure 1x10^{-10} torr.

For the thiocresol molecule there was a large C-H out of plane bending band at 763cm^{-1}. For the G1 molecule this peak is at 796cm^{-1}. The bands which are present are 1. 2962cm^{-1}, 2. 1260cm^{-1}, 3. 1010cm^{-1}, 4. 796cm^{-1}. It is possible that there is also a band at 2900cm^{-1} that appears after the 100L dose. All of these bands generally increase in intensity with increasing dose.
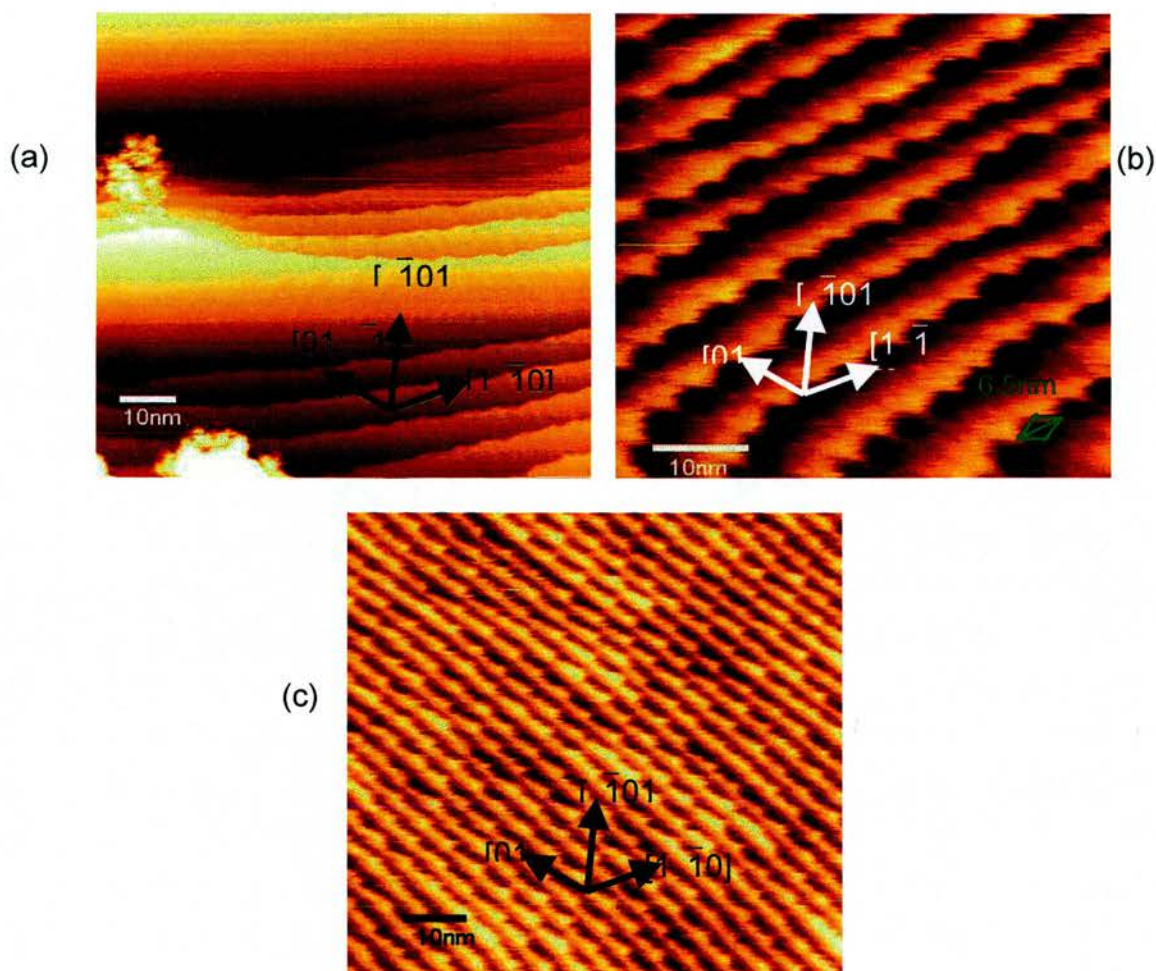
Figure 4.17(a) 100x100nm UHV STM Image of Au{111} single crystal dosed with 51.2L of G1 showing steps, terraces and reconstruction. This image was acquired at a tunneling current of 1.336nA and at a tip bias of -0.286V. (b) 55x55nm UHV STM Image of Au{111} single crystal dosed with 102.4L of G1 showing steps, terraces and etched reconstruction. This image was acquired at a tunneling current of 0.551nA and at a tip bias of -1.049V. (c) 100x100nm UHV STM Image of Au{111} single crystal dosed with 204.8L of G1 showing steps, terraces and etched reconstruction. This image was acquired at a tunneling current of 0.574nA and at a tip bias of -1.028V.

As mentioned in part 3.2 the UHV STM of Au{111} has been imaged allowing the real space direction of the atoms to be known this can be observed in figure 3.4. Figure 4.17(a) is representative of the substrate after a 50L dose. Reconstruction can still be observed. The steps seem to be etched in the fcc regions of the reconstruction (see Chapter 1). Figure

4.17(b) similar to figure (a) shows reconstruction and etching of the fcc section of the reconstruction. This effect is more dramatic after the 100L dose. The steps seem to be in the [1 $\overline{1}$0] direction. The periodicity between the peaks of the etched reconstruction (marked in green in figure (b) is 6nm. The next dose that the Au{111} single crystal was subjected to was a 200L dose. Figure 4.17(c) is similar to figure (b) apart from the steps seem to be in the [01 $\overline{1}$]. The periodicity between the features is approximately 6nm which is the same as for between the peaks in figure (b). The periodicity between the steps is ~4nm.

4.4 Discussion

4.4.1 XPS

XPS was used to investigate the nature of the adsorbed species produced following G1 adsorption onto the surface from solution phase deposition. The data show the presence of the S2p the C1s and the Si 2p peaks at the expected binding energy. Comparison to previous research by Whelan et al[3,9], shows that the binding energies of the S $2p_{3/2}$ and $2p_{1/2}$ are 162.1 and 163.1 respectively, and that the sulphur (2p) peaks are at the expected binding energies for TP on Au{111}. This signifies the presence of a Au-thiolate bond consistent with the expected chemisorbed G1 dendrimer thiol. This is consistent with the work by Whelan et al. however, unlike the case of thiocresol adsorption two peaks are observed. These cannot be assigned to be the $2p_{3/2}$ and $2p_{1/2}$ peaks as their binding energies are too far apart as they have the binding energies 161.8eV and 165.5eV, relative to Au $4f_{7/2}$ peak at binding energy 83.5eV. The broad peak at 161.8eV is a convolution of the expected $2p_{3/2}$ and $2p_{1/2}$ peaks which, due to the resolution of the XPS equipment used, are not observed as two peaks. The other smaller peak at 165.5eV is most likely due to elemental sulphur. The presence of elemental sulphur may be due to radiation damage by the XPS gun. Elemental sulphur when analysed on its own has a binding energy of 164.2eV[11]. This binding energy is affected by the Au substrate.

The main carbon (1s) peak at 284.5eV can be attributed to the benzene carbon atoms while the other smaller peak at 286.7eV can be attributed to the electron deficient carbon that is bonded to the sulphur atom[5,9]. This

compares to work by Whelan et al.[3] on TP an Au{111} which reveals C(1s) peaks at binding energies has of 284.3eV and 285.8eV. The other very small peak at 289eV which is not present in the TP data or in the thiocresol data can possibly be assigned to the vinyl group. These data show that the two largest peaks have almost got a 1:4 ratio. A 1:5 ratio for the thiophenol molecule was used to indicate that the molecule is flat lying[3]. However this does not take into account the p-substitution of the benzene ring and also the extra carbons on the CH_3 parts of the molecule. The C1s is observed at 285eV due to the different types of carbon in this molecule for example as for thiocresol a C_6H_5X and/or C_6H_6 peak, a CH_3 peak, and $Si-(C_2H_5)$ C-Si[12,13,14]. However there is a small peak at 282eV which may have be caused by an oxidised species maybe from the underlying mica.

Comparison of this work to previous reports by Long et al.[15] and Shabtai et al.[16] show the silicon (2p) binding energies of silicon containing self assembled molecules to be at 102.8eV for Si 2p and 153.8eV for Si 2s. This shows that the Si peak observed is at the expected binding energy of 153.8eV. Silicon 2s is also observed as a small peak at ~153eV. This confirms that the molecule has most likely attached to the surface. There is only one Si 2p peak expected to be observed due to the proximity of the $2p_{3/2}$ and $2p_{1/2}$. The XPS data showed that the ratio of the molecules observed are 57:18:25 for C, S and Si respectively. The expected ratio of carbon:sulphur:silicon for G1 is ~67:18:15 calculated using equation 2.11 and taking into accoun the relative response factors. The amount of sulphur is approximately the same however the amount of carbon is lower (as for

thiocresol) and the amount of silicon is larger. The increase in silicon may be due to the mica substrate. This would be observed if there was a small hole in the Au{111} surface however if this was the case a large peak for oxygen would be observed.

4.4.1.2 RAIRS

In the case of thiocresol (Chapter 3) one of the key pieces of orientational information came from the band at $764cm^{-1}$. For the G1 molecule the detector used means that we cannot ascertain this information. As mentioned this band is the out of plane C-H bending mode and would indicate whether the molecule is flat lying, close to flat lying or standing upright.

The purpose of the RAIRS experiments was three-fold. It was used to establish whether the molecule adsorbs intact onto the Au substrate, to evaluate the adsorption geometry of the adsorbed species and finally, to compare adsorption from the gas phase and adsorption from solution. To help with the analysis of the IR data, we carried out a Gaussian DFT calculation on an isolated G1 dendrimer. The output of this calculation gives the frequency of the vibrational modes of the molecule and the direction of the dynamic dipole moment associated with each vibration. The calculations were optimised with the B3LYP method using a STO-3G basis set Table 4.1 shows these vibrational wavenumbers and the predicted direction of their dipole moments and figure 4.19 shows a is a schematic diagram generated by the Gaussian calculation programme. The dynamic dipole moment is

shown by the red arrow in the centre of the image. The wavenumbers need to be corrected to give accurate band positions. It is approximately the case that the predicted wavenumbers generated by the Gaussian programme needs to be multiplied by 0.97 to allow comparison with the actual spectra.

Figure 4.18 shows the spectrum generated by the Gaussian calculation.
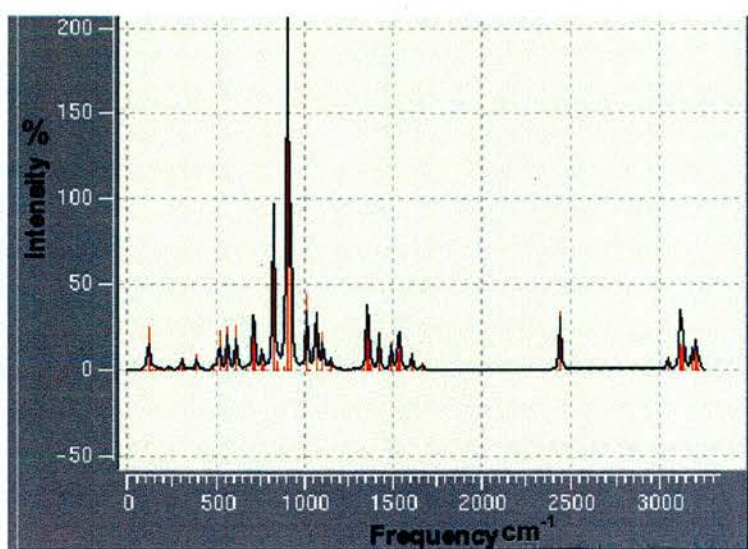
Figure 4.18 The Gaussian calculated vibrational spectrum for G1

Band No for solution deposition	Position of bands (cm⁻¹) for solution deposition	Band No for gas phase deposition	Position of bands (cm⁻¹) for gas phase deposition	Gaussian Simulation G1 (cm⁻¹)	Gaussian Band relative IR intensity	Assignment of Bands (cm⁻¹)
1	3041			3206	18.05	Antisymmetric CH stretch from vinyl (perpendicular)
2	3003			3135	16.29	Symmetric CH stretch from vinyl (almost parallel)
3	2960	1	2962	3123	13.52	Antisymmetric CH stretch from CH₃ (parallel)
4	2922			3119	14.75	Antisymmetric CH stretch from CH₃ (perpendicular)
				2439	34.52	SH stretch (parallel)
				1541	17.24	In plane CH bending from ring and CH₃ (parallel)
				1495	16.19	C=C stretch and CH bend of vinyl (perpendicular)
				1423	21.87	In plane CH ring bend (perpendicular)
				1364	20.04	CH bending from CH₃ (perpendicular)
5	1257	2	1260	1356	33.37	CH bending from CH₃ (perpendicular)
6	1115			1149	6.92	Aromatic CH in plane bending (almost parallel)

7	1069			1105	22.39	Ring vibration due to di-substitution (perpendicular)
				1073	13.01	Antisymmetric vinyl CH bend (almost perpendicular)
8	1011	3	1010	1067	34.00	CH wag/bend from vinyl and CH in plane bend (diagonal)
9	953			1016	43.93	CH bending from vinyl (perpendicular)
				924	91.41	CH bending from CH₃ (almost parallel)
				904	222.56	Small aromatic CH bend but mostly CH₃ CH bending (parallel)
4			796	828	48.33	Out of plane CH bend (perpendicular)

Table 4.1 Assignment of G1 RAIRS peaks for both gas phase and solution deposition RAIRS spectra

156
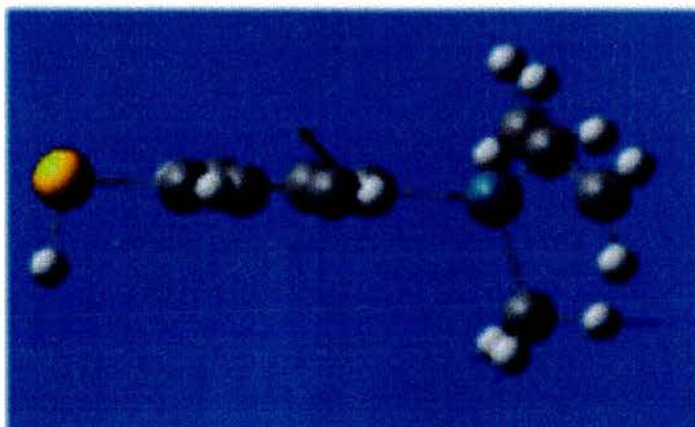
Figure 4.19 This is a schematic diagram generated by the Gaussian calculation programme B3LYP method and a STO-3G basis set. The diagonal dipole moment is shown by the red arrow in the centre of the image, i.e. a diagonal dipole is neither parallel nor perpendicular.

The first observation which may be made from examining this data is that the IR spectrum for gas phase deposited G1 data contains less vibrational modes than the spectrum for solution phase deposition. Each of the three main bands observed in the gas phase deposited case are also observed as intense bands in the solution phase deposited case. This indicates that the surface species in the two cases are likely to be closely related. The decreased number of bands observed for gas phase deposition may be related to a much more uniform adsorption geometry, where the intensity of many of the vibrations is decreased by the metal-surface selection rule.

4.4.2.2 Gas Phase Deposition RAIRS

The output of the Gaussian calculation predicts that the most intense feature should occur at 904 cm^{-1}. Allowing for the error in calculations of vibrational frequency by such calculations this should correlate with a band at ~875 cm^{-1}. This band is not observed after gas phase deposition. This band consists

157

mostly of in plane bending of the CH_3 groups (here "plane" refers to the plane of the aromatic moiety). So if the G1 molecule has adsorbed onto the substrate whole and this peak is not observed then this points to the aromatic ring being parallel or close to parallel to the surface.

Further support for this assignment comes from the most intense band in the gas phase spectrum at 796 cm^{-1} which correlates well with the predicted peak at 828 cm^{-1} (803 cm^{-1} following correction of the Gaussian wavenumbers). This corresponds to the out of plane C-H bending vibration of the aromatic H atoms which has a strong perpendicular component to the dynamic dipole moment. This is similar to TP and possibly thiocresol, which have been shown to prefer to adopt a flat lying or almost flat lying geometry, *i.e.10±10°* (this is what is reported for TP on Au by Whelan et al.[3] and Wan et al.[5]). Reports of TP on Au{111}[3] mercaptobiphenyls on Au{111}[17] and tertphenylthiols on Au{111}[18] show that aromatic thiols with the SH directly attached to the aromatic ring can have tilt angles of anywhere between 28° and 0°.

The other three bands observed in the gas phase deposition case are all more difficult to unequivocally assign. The band at 1010 cm^{-1} could be assigned to either the 1067 or 1073 cm^{-1} bands predicted by the Gaussian calculation (which following correction should appear at ~1035 cm^{-1}). These bands are both associated with vibrations of the vinyl functionality - each of which have dynamic dipole components perpendicular to the plane of the aromatic ring. If the metal surface selection rule is taken into account then

both of these bands should be observed in the RAIRS spectrum if the molecule has a flat lying or almost flat lying geometry[19]. The importance of this band is that it indicates that at least a fraction of the vinyl groups are still intact on the surface which has important implications in the design of catalysts based on this system. The band at 1260 cm^{-1} could be related to either of the 1364 or 1356 cm-1 bands which are both related to CH_3 bending vibrations. On the basis of the above arguments, it seems more likely that the band is associated with the 1356 cm^{-1} (~1315 cm^{-1} after correction) which has a component of the dynamic dipole moment perpendicular to the surface. However one band is present at 1115cm^{-1} which is due to an in plane bending mode which has a dipole moment parallel to the surface. This is the only in band observed with a parallel dipole moment but it shows that there may be some molecules or part molecules upright on the surface however the most predominant bands are the ones with a perpendicular dipole moment.

No bands were resolved in the 1400-1650 cm^{-1} range due to difficulties encountered with gas phase water miscancellation. The final band observed in the gas phase spectrum appears at 2962 cm^{-1}. It is very difficult to assign this peak unequivocally since a range of C-H stretching vibrations are predicted by the Gaussian calculation. The overcalculation of vibrational frequencies by Gaussian seems to be more dramatic at higher wavenumbers. As such, and bearing in mind the assignments of the other peaks, the 2962 cm^{-1} peak is most likely to derive from one (or a combination of e.g. the 3119 and 3114 cm^{-1} predicted bands) of the C-H

stretching modes with a perpendicular dynamic dipole moment. Therefore the gas phase deposited G1 dendrimer, can be assigned, as a species which is almost flat lying.

Although it is common for aromatic thiols such as TP and thiocresol to be parallel or close to flat lying, larger or longer molecules normally stand upright after gas phase dosing. However, this is not observed for G1, even though it is a larger molecule. This may be because Si containing molecules have been known to chemisorb onto Au{111} surfaces by the Si atom[20]. Work done by Marchenko et al. shows that there is a strong interaction between Si and Au. And in fact it shows that it is possible for a sterically compact tetra-coordinated silicon group to become penta-coordinated and adopt a bipyramidal geometry when in contact with an electron donating atom such as Au. This would mean that a "supervalent" Si may be covalently bonded to the Au making the molecule lie parallel to the surface. This however may not be possible as the vinyl group attached to the Si atom may sterically hinder the adsorption and this vinyl group is definitely observed on the RAIRS spectra. If this is occurring then the dipole moment from the silicon end of the molecule will be affected. The almost parallel dipole moments will most likely be moved upwards and become either diagonal or almost perpendicular. The Gaussian does not show this as it is calculated for a single G1 molecule in the gas phase. Figure 4.20 shows a schematic diagram of how the G1 dipole moment would attach to the substrate if the silicon is also chemically attached onto the Au substrate.
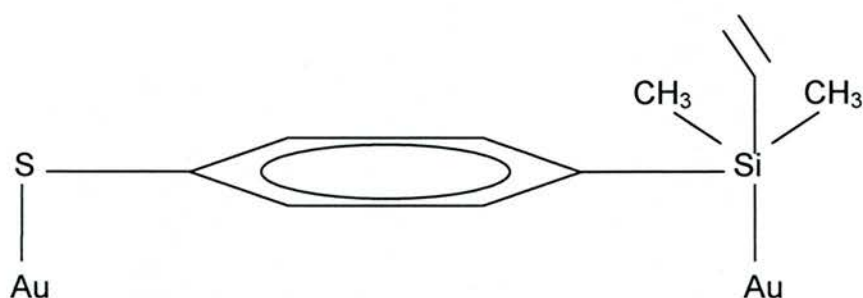
Figure 4.20 A schematic diagram of the G1 molecule if it is chemisorbed onto the gold by both the Si and S atoms creating a supervalent silicon.

This would show that a vibration from the CH_3 part of the molecule which before would have been almost parallel would either now be diagonal or almost perpendicular. This means that the vibration identified as peak 1 would be observed if the molecule was flat lying.

4.4.2.3 RAIRS following solution deposition

As discussed above more bands were observed on the solution deposited G1 RAIRS spectrum than on the gas phase deposited G1 spectrum. This could be for two reasons. Firstly the geometry of the molecules on the surface may be different for example, it is reported by Wan et al[5] for solution deposition, that molecules, after a long dosing are likely to stand upright on the surface where as after gas phase deposition it is more likely that they are parallel or close to parallel as is the case for TP[3]. This flat lying orientation occurs because the molecule bonds to the substrate principally through its π orbitals[5]. The flat lying molecular geometry is expected more at low coverage from gas deposition than from long term solution deposition, as it assists bonding between the aromatic π system and the metal substrate. The difference in geometry would mean that a difference in the intensity of RAIRS bands would be expected.

The other reason for this difference in number of bands may be that a multilayer has formed on the substrate after solution deposition rather than a monolayer. The STM data for the UHV analysis of solution deposited G1 may be used to support this theory. Figure 4.13 (c) shows a lattice structure but individual features are also present on top of this structure. This would indicate that there is an ordered monolayer and a disordered second layer. This second layer must be strongly bound to the first as washing the substrate with ethanol after dosing and placing under UHV conditions would eliminate any weakly bound molecules.

As with gas phase deposition the output of the Gaussian calculation predicts that the most intense feature should occur at 904 cm^{-1}. Allowing for the error in calculations of vibrational frequency by such calculations this should correlate with a band at ~875 cm^{-1}. This band is not observed after gas phase deposition. This band consists mostly of in plane bending of the CH_3 groups (here "plane" refers to the plane of the aromatic moiety). So if the G1 molecule has adsorbed onto the substrate whole and this peak is not observed then this points to the aromatic ring being parallel or close to parallel to the surface. Unlike for gas phase deposition there is no further support for this assignment from an intense band at 796 cm^{-1} which would correlates with the predicted peak at 828 cm^{-1} (803 cm^{-1} following correction of the Gaussian wavenumbers).

The nine bands observed from solution deposition are all more difficult to unequivocally assign. The band at 953cm^{-1} is most likely assigned to the

predicted band at 1016cm^{-1} which is consistent with vinyl group bending these bands may be observed in this case and not in the gas phase deposition is probably due to a more random orientation of the molecules as was discussed above. The two bands at 1115 and 1069cm^{-1} will also be due to the random orientation of the molecules on the Au surface. The band at 1011 cm^{-1} could be assigned to either the 1067 or 1073 cm^{-1} bands predicted by the Gaussian calculation (which following correction should appear at ~1035 cm^{-1}). These bands are both associated with vibrations of the vinyl functionality - each of which may have dynamic dipole components perpendicular to the plane of the aromatic ring due to Si bonding with Au eithr by losing CH_3x2 or by forming a supervalent silicon. If the metal surface selection rule is taken into account then both of these bands should be observed in the RAIRS spectrum if the molecule has a flat lying or almost flat lying geometry[21]. The importance of this band is that it indicates that at least a fraction of the vinyl groups are still intact on the surface which has important implications in the design of catalysts based on this system. The band at 1257 cm^{-1} could be related to either of the 1364 or 1356 cm-1 bands which are both related to CH3 bending vibrations. On the basis of the above arguments, it seems more likely that the band is associated with the 1356 cm^{-1} (~1315 cm^{-1} after correction) which has a component of the dynamic dipole moment perpendicular to the surface.

No bands were resolved in the 1400-1650 cm^{-1} range due to difficulties encountered with water miscancellation. The final bands observed in the solution deposition spectrum appear at 2922, 2960, 3003 and 3041cm^{-1}. It is

very difficult to assign these peaks unequivocally since a range of C-H stretching vibrations are predicted by the Gaussian calculation. The overcalculation of vibrational frequencies by Gaussian is more dramatic at higher wavenumbers as such and bearing in mind the assignments of the other peaks, these peaks most likely derived from a combination of bands e.g. the 3206 and 3119 cm^{-1} predicted bands of the C-H stretching modes with a perpendicular dynamic dipole moment. The solution deposited G1 dendrimer has a random orientation where the molecules seem to be mostly flat lying but there also seems to be evidence, *i.e. IR peak six and a larger amount of visible bands on comparison with gas deposition,* of some more upright molecular orientation.

4.4.3 STM of Solution Deposition

Figures 4.13 (a-i) show the solution deposition of the G1 thiol dendrimer onto a Au{111} single crystal. From these images three distinct observations can be made. These are, the formation of molecular features, the formation of etch pits and the formation what is either areas of regularly sized steps and terraces or molecular ordering. This pattering comes in the form of stripes (figure 4.13 e, f and i) or a lattice type structure (figure 4.13 c and g).

Figure 4.14 (a-i) show the solution deposition of the G1 thiol dendrimer onto a Au/mica substrate. From these images two observations can be made. These are the formation of etch pits (see Chapter 1), step edge etching and what looks like Au island formation (see Chapter 3 for thiocresol) and the formation of molecular features.

There are many similarities between the air and UHV STM data as would be expected. However there are also differences. One of the main similarities are the etch pits. As discussed in Chapter one, etch pits are a common occurrence on Au that has been exposed to a dose of a thiol molecule[10], as is step edge etching and the formation of Au islands. The G1 molecule only seems to etch the Au substrates after long dosing times. The surface begins to have large areas of etching after 2 hours of solution dosing, although there was an area of the Au/mica substrate that showed etch pits after a 30 minute dosing period however this was a small area of only one sample. For the most part no etching occurs at lower dosing times. Islands consistent with the step height of Au are observed in figures 4.14 (f) and (j). This is consistent with the effect that thiocresol had on the Au/mica substrate. As was mentioned in Chapter Three this effect has been reported before for 4-hydroxythiophenol (4HTP) on Au/mica[22].

The other similarity between the air STM and the UHV STM of the solution deposited G1 is the formation of what looks to be molecular features. In the air STM images these are measured to be between 1-2nm wide and ~1.5Å high, however in the air STM images these are measured to be ~4.2nm wide and ~3Å high. The molecular features imaged by the air STM appear to be double the size of the features measured by the UHV STM. This is unlikely to be correct; the molecular features on both substrates should be the same size. There could be at least two explanations for this discrepancy. Firstly the tip may not have been atomically sharp, or some of the G1 molecules may have attached to it as it was imaging. Tip defects would affect the

image by making the features appear rounder and possibly larger. The other parameter to be taken into account is water vapour in the air. As this is an air STM there is no guarantee that the atmospheric conditions will not affect the substrate. This means that the water in the air may settle on the substrate or on the tip causing the features imaged to appear larger. This therefore means that the molecular features imaged by both the air and UHV STM are most likely to be the same size. The height of these molecular features are much smaller than the length of the molecule (~11Å). This indicates again that after solution deposition G1 is tilted toward the surface or parallel to it.

One dramatic feature that is observed for G1 adsorbed onto the Au{111} surface and imaged under UHV, which is not observed for the Au/mica in the air STM is the appearance of apparent long range ordering. It is clear to see that although molecules are attached to the terraces there is no short range order the similar to that reported for TP on Au as reported by the Frey[3], Whelan[4] and Wan[5] research groups. The same was concluded for thiocresol in Chapter 3. However what is observed in many of the figures is the occurrence of lines, similar to steps, in the [01 $\bar{1}$] or [1 $\bar{1}$0] directions. In certain cases striping is observed in two directions (see figures 4.13(c) and (g)) this would appear to form a lattice or honeycomb type structure. These stripes which look like steps are between 2Å and 1Å in height they have a regular periodicity of ~4nm between steps, *i.e. the terraces are 4nm wide.*

There are two possibilities as to what is causing this long range order. The first of these is that it is a molecular unit cell. This type of long range order has been reported before by Dong et al.[23,24] when adsorbing large dendron molecules onto a Au{111} surface. These lines had a periodicity of 3.1±0.3nm. The explanation for these features is that the long range order is due to the chemisorption between the thiol group and the Au surface and also due to π-π stacking between benzene rings. Although these molecules are much larger than the G1 dendrimer thiol they have similar properties *e.g.* *both are large thiols and both have aromatic functionalities.* However it is doubtful that π-π stacking and Au-S interactions would cause this periodicity as it is well known that the distance between molecules that exhibit π-π stacking is 3.7Å[23,24]. The molecules used by Dong et al. are much bigger than those normally associated with π-π stacking and this is likely to increase the periodicity. However the G1 molecule is not as large and therefore if π-π stacking were involves a much smaller periodicity might be expected. It is unlikely that the order observed for the G1 molecule is a molecular unit cell as molecular features can clearly be observed on top of these features. This then points to the order being due to the Au substrate rather than the molecule.

As it seems possible that the Au substrate is itself responsible the long range periodicity the stability of the Au{111} surface has to be investigated. Because the periodicity between the terraces is so regular it is very similar to a Au{111} vicinal surface. Surfaces that are vicinal to the {111} plane are normally prepared by the mis-cut of a Au{111} surface plane by a specific

angle, for example 3.5° for a {788} surface, with respect to the {111} orientation towards the [$\bar{2}$11] azimuthal direction. Many different Au vicinal surfaces are possible for example {233}, {322}, {455}, {788}, {11,12,12} and {11,9,9} are just a few types, there are other less stable ones. Every vicinal surface exhibits a regular array of steps and terraces of a specific size for example the above vicinal surfaces have terrace sizes of 1.4±0.5nm, 1.3±0.5nm, 3.5±0.5nm, 3.9±0.5nm and 5.6±0.5nm respectively with the {11,9,9} surface having a periodicity of 7nm which is made up of 1x4.2nm terrace and 2x1.4nm terraces. These periodicities lie along the [$\bar{2}$11] direction. Each of these vicinal surfaces apart from {11,9,9} exhibits Au reconstruction with a periodicity of 7.2±0.5nm along the [01$\bar{1}$] direction. The stripes in figure 4.13 (a-i) which look like steps are between 2Å and 1Å in height they have a regular periodicity of ~4nm between steps, *i.e. the terraces are 4nm wide.* The step heights would suggest that these features are molecular rather than from the Au substrate however the terrace sizes are consistent with a Au{788} surface[25].

There could be two reasons why vicinal surface are being observed. The first is that the Au substrate may be cut off the horizontal plane (3.5° off the plane for a {788} surface) in certain areas. This could mean that the surface is a mixture of large {111} step and terrace areas and also large areas of Au{788} where the periodicity of the steps is 3.9±0.5nm and the periodicity between the reconstruction on these small terraces is 7.2±0.5nm[26]. It thought to be unlikely that the Au surface has extensive {788} facets before dosing as when the clean gold surface was imaged small terraces such as

the ones in figure 4.14 were not observed. However a large number of steps on the surface of this Au{111} single crystal were observed and in the large part the terrace sizes are small, not however as small as 4nm. This means that the stripes on the surface are likely to have been caused by the adsorption of the G1 molecule.

The most probable cause for this is molecularly induced faceting of the Au surface by the G1 molecule. Similar faceting of metal substrates has been observed before and is discussed in detail in a review by Chen et al[27] for example, lysine faceting of Cu{001}[24]. As discussed above the Au substrate is {111} even though after dosing it looks to be {788}. This may mean that when the molecules are adsorbed onto the surface either by gas phase deposition, or from solvent they are somehow creating {788} facets. This theory is supported by the fact that there is a common periodicity in the [$\bar{2}$11] direction that arises after dosing. This periodicity or terrace width is ~4±0.5nm. Faceting is not an unusual phenomena, molecules have been known to create facets in directions different from the original substrate. For example lysine on Cu{001} induces faceting as reported by Zhao et al.[24] as does glycine on Cu{110} also reported by Zhao et al.[28] So it is possible that the molecules are inducing Au faceting resulting in an Au{788} surface.

If a {788} surface is being produced it would be assumed that the molecules would preferentially adsorb onto nucleation sites (herring bone reconstruction elbows) which in this case are ~7nm apart at the step edges as occurs when Co is adsorbed onto Au{788}[23,29] however it is clear from

figures 4.9 – 4.19 that the molecules randomly attach to the small terraces and to the step edges and no clear ordering is present. This lack of order, as discussed in Chapter three, is common for aromatic thiols on Au[3,4,5].

Another explanation for the formation of these steps is the phenomenon called "step bunching". According to Jeong et al.[30] highly stepped areas are often rearranged into flat reconstructed terraces with much more sharply inclined regions with closely bunched steps. Experiments on systems such as GaAs{100}, Pt{111} and Au{111} have shown the that there is a regularity in the size and spacing of these steps and terraces. This is quite similar to what is occurring for the G1 molecule on the Au{111} single crystal, however the array of large terraces and small terraces is very uniform in step bunching whereas in this case the occurrence of larger terraces on the Au{111} surface after dosing is minimal. As the images recorded by Dong et al. are similar to figures 4.13(a-i) it is quite likely that they to have encountered some molecularly induced faceting of the Au{111} surface.

The main question after this is why do the molecules induce a {788} vicinal surface and not any of the others? This is most likely due to the size of the G1 molecule and the stability of the {788} surface. Vicinal Au{788} is a very stable vicinal surface and is the most used vicinal Au surface. The length of the G1 molecule is ~11Å this would then mean (bearing in mind that it is flat lying or close to flat lying) that it would take up most of the terrace on a {233} or {322} surface. Thus it would be energetically more stable for the molecule to pack on a {788} as it would leave a large area of the metal substrate free.

Of the larger sized vicinal surfaces {455} is generally unstable[31] and {11,12,12} surface may be too large. Larger terraced vicinal surfaces however, do seem to be more favourable for the G2 molecule (see Chapter 5) so the size of the molecule may make a difference.

4.4.4 UHV STM Gas Phase Deposition

Reconstruction is observed on figure 4.17(a). This is unusual as Dishner et al.[32] reports that normally when a molecule is adsorbed onto a surface the reconstruction is destroyed, however in this case it has not. This may be due to the molecule having a low sticking probability which would mean that it has not chemisorbed onto the area being imaged. Looking closely at this image it is possible that the molecule is adsorbing onto the step as they seem to have been altered (perhaps etched see Chapter one) by the G1 dendrimer thiol. It is the reconstruction at the step edges that appears to be mostly affected. It appears that the fcc regions[32] of the reconstruction that are altered. This shows that the G1 molecule has most likely, preferentially adsorbed onto step edges of the Au{111} surface.

The effect of the molecule on the Au{111} reconstruction is further observed in figures 4.17(b) and 4.17(c). These images all show this effect in a more dramatic way. The images show that the etching in the fcc areas has increased. No island formation was observed for gas phase deposition.

In figure 4.17(b) there is a high density of steps with a periodicity in the [$\bar{2}$11] direction of ~4nm and the periodicity between the reconstruction peaks is 6.5±0.5nm. Again as with the solution deposited G1 molecule this looks as if the molecule has created facets on certain parts of the surface which have a {788} orientation. This same periodicity is shown in figure 4.17(c). Unlike from solution deposition shown in figures 4.13-4.15 the step heights are measured to be 2.4±0.5Å which conclusively shows that these are Au microterraces. More support that the surface is now {788} is shown particularly in figure 4.17(c). This image is very similar to images produced by Baudot et al. for Co deposited on Au{788}[26,29] at 130K and then imaged at room temperature. It shows that at the end of each reconstruction fcc nucleation site that there is a brighter area where the G1 molecule has most likely preferentially adsorbed there. Co preferentially adsorbs to these Au sites forming nanodots. Figure 4.17(c) also shows a pattern very similar to figures 4.13(c) and 4.14(b). The large areas of reconstruction visible in figure 4.17(a) show that the molecule preferentially adsorbs to the {788} sites or it may show that after a 51L dose the molecule has not yet caused any faceting.

It is very likely considering the periodicity of these features from both solution deposition and gas phase deposition that the reconstruction has some influence in the way that the molecules induce the facets causing the substrate to be {788}. This would explain why the Au/mica substrate does not show this effect. However what is unusual is that it is assumed that once the Au single crystal is no longer in UHV that the reconstruction is

destroyed[26]. However the reconstruction is still visible after deposition and the periodicity along the vicinal steps is consistent with reconstruction on vicinal Au{788} (~6.5±0.5nm). On investigation there are many reports which show that the reconstruction is not easily destroyed and that it is even present after some thiols have been dosed onto it[33,34]. Therefore it is likely that the reconstruction survived being in atmosphere for a short period of time. Although the STM images in this chapter seem to be representative of the surface they may not be as the images are only of a small area. However, these images were taken from different areas of the substrate so it is assumed that they are representative of the whole surface.

4.5 Conclusion

Although the synthesis was problematic the analytical studies (nmr, GC) showed that the molecule was successfully synthesised. After adsorption onto the surface by both gas phase and solution phase deposition the RAIRS and XPS data show that the molecule has adsorbed onto the Au surface intact. These studies show that the molecule may be more disordered on the Au{111} surface after solution deposition than after gas phase deposition. It also may show that the molecule chemisorbs onto the Au preferentially through solution deposition.

Once adsorbed onto the surface from solution deposition some long range order can be observed in the form of striped or pseudo hexagonal patterns. Although it has not been proven conclusively this is likely due to molecular induced faceting. This is the most likely explanation as the formation of Au{788} areas is also observed after gas phase deposition. This vicinal surface was not observed before dosing and it was not observed in the thiocresol study. The formation of a {788} surface rather than any other surface could be due to the stability of this vicinal surface however, there is no conclusive proof as to why this surface is preferentially induced.

The occurrence of these stepped areas, the survival of the reconstruction after the gas phase deposition and what looks like step edge nucleation of the molecule after both gas phase and solution deposition, points to the

likelihood that the molecule has low sticking probability and it preferentially adsorbs to the step edges.

References

[1] C. J. Murphy and H. W. Post Journal of Organic Chemistry (1961) 1486

[2] P. J. Thomas M. A. Gonzalez, R. G. Pews. Synth Commun **25** (1995) 2813.

[3] C. M. Whelan, C. J. Barnes, C. J. H. Walker, N. M. D. Brown. Surface Science **425** (1999) 195

[4] S. Frey, V. Stadler, K. Heister, W. Eck, M. Zharnikov, M. Grunze. Langmuir **17** (2001) 2408

[5] L-J. Wan, M. Terashima, H. Noda, M. Osawa. J. Phys. Chem. B. **104** (2000) 3563

[6] M. A. Casado and S. R. Stobart   Organic Letters Vol.2   2000 Pg. 1549-1552

[7] J Morrison personal communication

[8] F. Schreiber. Progression in Surface Science **65** (2000) 151

[9] C.M. Whelan, C.J. Barnes, C.Grégoire, J.-J. Pireaux. Surface Science **454-456** (2000) 67

[10] G. E. Poirier. Chem. Rev. **97** (1997) 1117

[11] http://www.lasurface.com/Data_base/Aw_xps_consult_gen.htm

[12] S. Contarini, S.P. Howlett, C. Rizzo, B.A. De Angelis. Applied Surface Science, **51** (1991) 177

[13] D. Briggs, M.P. Seah. **1** (1993) second edition, John Willey & Sons.

[14] M.H. Dishner, J.C. Hemminger, F.J. Feher. Langmuir **13** (1997) 4788

[15] Y-T. Long, S. Herrwerth, W. Eck, M. Grunze. Phys. Chem. Chem. Phys. **4** (2002) 522

[16] K. Shabtai, S. R. Cohen, H. Cohen, I. Rubinstein. J. Phys. Chem. B. **107** (2003) 5540

[17] J. F. Kang, A. Ulman, S. Liao, R. Jordan, g. Yang, G-Y. Liu. Langmuir **17** (2001) 95

[18] C. Fuxen, W. Azzam, R. Arnold, G. Witte, A. Terfort, C. Wöll. Langmuir **17** (2001) 3689

[19] J.W. Niemantsverdriet Spectroscopy in Catalysis **VCH** (1993) 200

[20] A. Marchenko, N. Katsonis, D. Fichou, C. Aubert, M. Malacria.
J. Am. Chem. Soc. **124** (2002) 9998

[21] J.W. Niemantsverdriet Spectroscopy in Catalysis **VCH** (1993) 200

[22] Q. Jin, J.A. Rodriguez, C.Z. Li, Y. Darici, N.J. Tao. Surface Science **425** (1999) 101

[23] B. Dong, F. Huo, L. Zhang, X. Yang, Z. Wang, X. Zhang, S. Gong, J.Li.
Chem. Eur. J. **9** (2003) 2331

[24] X. Zhao. J. Am. Chem. Soc. **122** (2000) 12584

[25] J. E. Ortega, A. Mugarza, V. Repain, S. Rousset, V. Perez-Dieste,
A. Mascaraque. Phys. Rev. B **65** (2002) 165413

[26] V. Repain, G. Baudot, H. Ellmer, S. Rousset Mat. Sci. Eng. B. **96** (2002) 178

[27] Q. Chen, N. V. Richardson. Progress in Surface Science (article in press)

[28] X. Y. Zhao, R. G. Zhao, W. S. Yang, T. Sakurai. *Surf. Sci.* **424** (1999) L347.

[29] G. Baudot, S. Rohart, V. Repain, H. Ellmer, Y. Girard, S. Rousset
App. Surf. Sci. **212-213** (2003) 360

[30] H-Y. Jeong, J. D. Weeks. Phys. Rev. B. **57** (1998) 3939

[31] S. Rousset, F. Pourmir, J.M. Berroir, J. Klein, J. Lecoeur, P. Hecquet,
B. Salanon. Surface Science **422** (1999) 33

[32] M. H. Dishner, J. C. Hemminger, F. J. Feher Langmuir **13** (1997) 2318

[33] Z. X. Xie, X. Xu, J. Tang, B. W. Mao. J. Phys. Chem. B. **104** (2000) 17719

[34] Q. Wu, W. H. Shang, J. W. Yan, Z. X. Xie, B. W. Mao.
J. Phys. Chem. B **107** (2003) 4065

CHAPTER 5

The adsorption of Generation 2 dendrimer thiol on Au surfaces

5.1 Introduction

Figure 5.1 below is a schematic diagram of the G2 dendrimer thiol. This molecule was not commercially available and so was synthesised by the author. There is no record of this molecule being synthesised before.
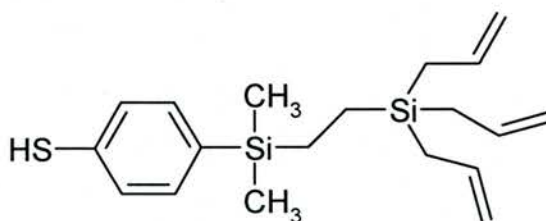
Figure 5.1 A schematic drawing of the G2 dendrimer thiol molecule.

This molecule was synthesised from the vinyldimethyl-p-bromophenylsilane (see chapter 4 for G1 dendrimer). This chapter will show how G2 binds to the surface and how it interacts with its neighbours and also how it behaves in comparison to G1 and thiocresol. The final aim was possibly use this molecule to synthesise dendrimers G3, G4...etc.
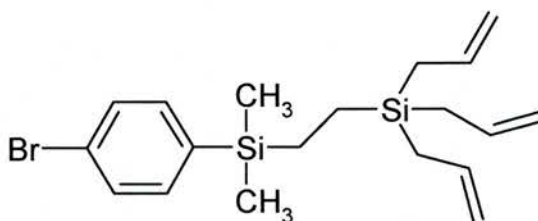
Figure 5.2 A schematic drawing of the G2 dendrimer thiol molecule.

This chapter shows how the G2 molecule has been investigated to see how the behaviour of the larger allyl silane head group compares with the vinyldimethyl silane head group of the G1 molecule, the CH_3 head group of the thiocresol molecule on Au{111} and also how it compares to thiophenol (TP) on Au{111}[1,2,3].

5.1.2. Preparation of vinyldimethyl-p-bromophenylsilane

The precursor is synthesised using dibromobenzene and chlorodimethylvinylsilane to make vinyldimethyl-p-bromophenylsilane. This reaction was reported in 1961 by Murphy et al[4] and was only partly successful as they only achieved a 21.6% yield. The reaction was originally carried out using a Grignard reagent. In this synthesis instead of using a Grignard reagent butyl lithium reagent (BuLi) was used. This was more successful and gave a yield of approximately 70%. Figure 5.3 shows the synthetic scheme involved.
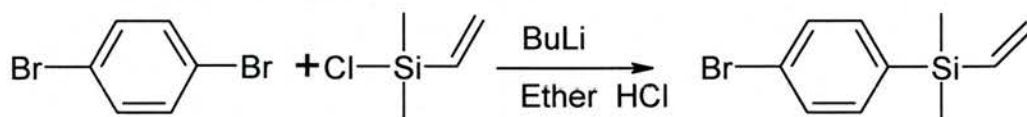
Figure 5.3. The synthetic reaction used for the synthesis of the dendrimer precursor vinyldimethyl-p-bromophenylsilane.

5.1.3 Preparation of brominated G2 dendrimer

[5]A well documented and well used synthetic procedure was used to produce the G2 molecule in figure 5.2 from the brominated G1 precursor shown in figure 5.3. This was a fairly straightforward procedure where the vinyl group of the vinyldimethyl-p-bromophenylsilane is substituted with trichlorosilane. This reaction was aided by Spiers catalyst (hexachloroplatinic acid 0.399g in 10ml). Figure 5.4 shows this reaction scheme. This is a synthetic step that would be used repetitively in the synthesis of larger dendrimers of this kind.
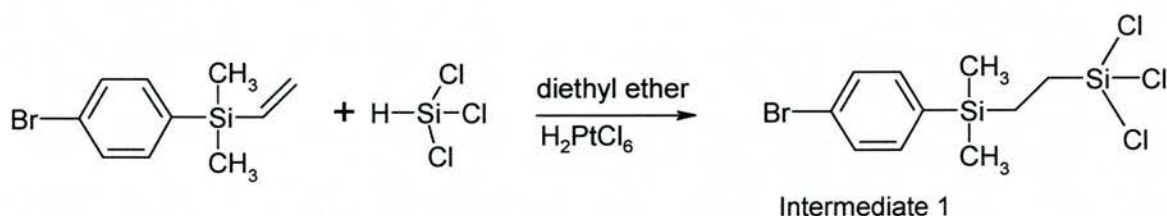
Figure 5.4 This is the first synthetic step used in the synthesis of larger dendrimers of this kind. The reagents used in this reaction are $HSiCl_3/H_2PtCl_6$.

Once the vinyl group was removed the next part of this reaction was also straight forward. It consisted of substituting the Cl atoms attached to the Si atom with allyl groups. This was carried out using the Grignard reagent allyl magnesium bromide. This is a synthetic step that would be used repetitively in the synthesis of larger dendrimers of this kind. The reaction for this is shown in figure 5.5.
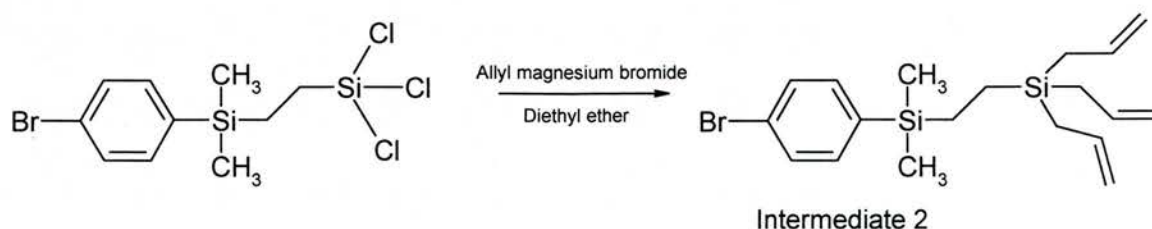
Figure 5.5 This is a synthetic steps that would be used repetitively in the synthesis of larger dendrimers of this kind. The reagent used in this reaction is allyl magnesium bromide. This is step two.

There was only one major problem that occurred during this synthesis which was that if the solvent from part one of the reactions was not removed then the excess trichlorosilane inhibited the reaction between the chlorine atoms of the molecule and the allyl bromide. It was obvious when this problem occurred as the ammonium chloride added to the reaction at the end to react off any remaining Grignard reagent caused a very violent reaction.

5.1.4 Thiolation of the G2 dendrimer

As with the G1 dendrimer, to attach this G2 molecule to the Au {111} surface a thiol head group is required. This molecule (see figure 5.1) has not been synthesised before. Synthetic approaches involving substituting a bromine p-substituted group to a p-substituted thiol group to make different thiophenols have been reported before[6]. The synthetic route used for thiolating G1 molecule was attempted first. BuLi was used again to lithiate the vinyldimethyl-p-bromophenylsilane. This was then reacted in solution with sulphur powder at −95°C and then 6M hydrochloric acid was used to incur protonation; figure 5.6 below shows the desired reaction scheme.
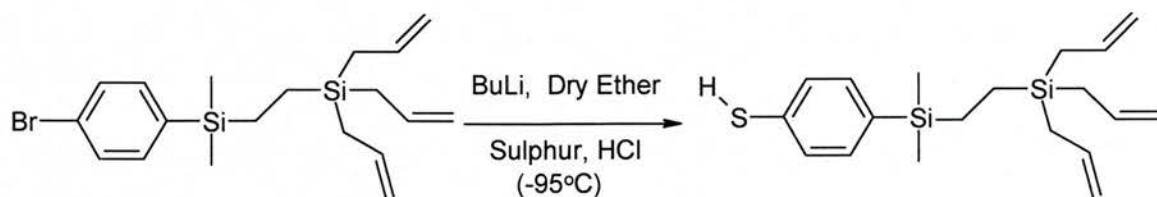
Figure 5.6 This scheme shows the desired synthetic reaction for turning G2 brominated dendrimer into G2 dendrimer thiol.

The first and second attempts at this did not yield the correct product. The same strict conditions were applied to this reaction as were for the G1 reaction. Many attempts later this did still not yield the desired product. Many other methods were then attempted, for example using lithium metal rather than BuLi, or attempting to make styrene thiol as the precursor and growing the dendrimer from it, or even making a new type of molecule all together.

Eventually the thiolation of the G1 molecule had been perfected and so it was decided that another attempt at thiolation using the synthetic scheme shown in figure 5.6 would be attempted. This time on the second attempt the thiolation according to the nmr indicated that the G2 thiol terminated dendrimer had been synthesised. It is not known why the reaction did not work on the other occasions. The nmr shows that the thiol has been made but it is not possible to see whether the disulphide has also been produced.

5.2 Experimental

5.2.1 Preparation of G2 dendrimer thiol

Vinyldimethyl-p-bromophenylsilane (7.1mmol) was weighed into a round bottomed Schlenk flask (250ml). This was sealed and put under vacuum. It was then heated with a blow torch to ensure it was completely dry and then it was left under vacuum for 2 hours. It was then purged with nitrogen gas. The vinyldimethyl-p-bromophenylsilane was then dissolved in dry diethyl ether (200ml). An excess of Spiers catalyst (20 drops) was then added with constant stirring from a magnetic stirrer and finally an excess of trichlorosilane (10ml) was added. This mixture was refluxed for eight hours and then the heat was switched off and it was left stirring with a positive pressure of nitrogen over night. NMR was carried out on a small amount of the reaction taken by syringe to ensure no vinyl groups remained.

The reaction was then put under vacuum and the solvent and remaining trichlorosilane were evaporated off using hot water, leaving only the product shown in figure 5.4. Fresh dry diethyl ether was then added to this product and excess of allyl magnesium bromide (20ml). This reaction was left stirring for 24 hours under a positive pressure of nitrogen sealed off from air.

After 24 hours ammonium chloride (50ml, 2M) was cooled in ice for 15 minutes and it was then slowly added to the reaction mixture to use up any remaining

183

allyl magnesium bromide. This solution was then and then extracted using hexane and washed with aqueous saturated sodium chloride solution (50ml). The remaining organic solution was dried over anhydrous $MgSO_4$ for 1 hour and then filtered through glass wool and evaporated in a rotary evaporator. NMR and GC-MS analysis were carried out on this product.

5.2.2 Solution Deposition

For the air STM Au on mica substrates were used, (see chapter 2) and for UHV STM a Au{111} single crystal was used. The G2 monolayers were prepared by the immersion of the Au/mica substrates in a $1 \times 10^{-3}M$ solution of the thiol in analytical grade ethanol for 16 hours. These samples were washed in ethanol and dried in a nitrogen stream. An Au/mica substrate was immersed in 1mmol/L solution for 16 hours for the XPS analysis. For air STM and XPS conditions see chapter 2.

5.2.3 Gas Phase Deposition

For the UHV STM analysis, an Au{111} single crystal was used (see chapter 3). The conditions for gas phase deposition of G2 are similar to those described for thiocresol deposition in Chapter 3.

5.3 Results

5.3.1 Synthesis

5.3.1.1 Spectroscopic Analysis of the Intermediate 1

^{1}H NMR was used to verify the absence of the vinyl group from vinyldimethyl-p-bromophenylsilane using a Varian Gemini 2000 with a resonant frequency of 300MHz for ^{1}H machine (see appendix 1). The results of the ^{1}H NMR (CDCl$_3$) were: a doublet of doublets for the aromatic region δ 7.647, 7.626, 7.479 and 7.452ppm$_{(1,2,7,8)}$. The CDCl$_3$ reference peak at 7.373ppm, 1.38-1.00$_{(4,5)}$ppm SiCH$_2$, 0.426$_{(3,6)}$ppm SiCH$_3$. See figure 5.7 for schematic diagram showing correlation between molecule and nmr peak positions.
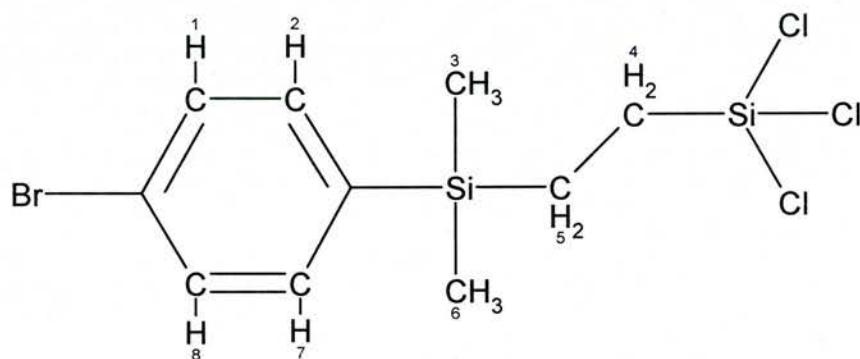
Figure 5.7 Schematic diagram of vinyldimethyl-p-bromophenylsilane after hydrosilation with H's numbered to correlate with nmr peaks in results section above.

5.3.1.2 Spectroscopic Analysis of Intermediate 2

^{1}H NMR was used to verify the purity of vinyldimethyl-p-thiophenylsilane using a Varian Gemini 2000 with a resonant frequency of 300MHz for ^{1}H machine (see appendix 3). The results of the ^{1}H NMR (CDCl$_3$) were: for the aromatic

region δ 7.62-7.44$_{(1,2,17,16)}$ppm. The $CDCl_3$ reference peak at 7.372ppm, 5.94-5.8$_{(6,9,12)}$ppm CH of $CH=CH_2$, 5.0-4.94$_{(7,10,13)}$ppm CH_2 of $CH=CH_2$, 0.7-0.56$_{(5,8,11)}$ppm $SiCH_2$, and 0.357$_{(3,15)}$ppm for $SiCH_3$. See figure 5.8 for schematic diagram showing coloration between molecule and nmr peak positions.
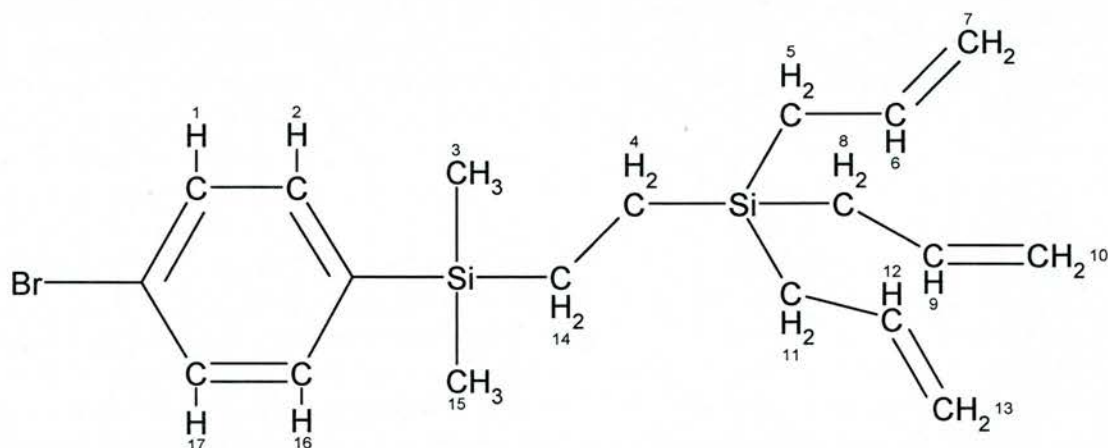
Figure 5.8 (a) Schematic diagram of brominated G1 with H's numbered to correlate with nmr peaks in results section above.

5.3.1.3 Spectroscopic Analysis of brominated G2

^{1}H NMR was used to verify the purity of vinyldimethyl-p-thiophenylsilane using a Varian Gemini 2000 with a resonant frequency of 300MHz for ^{1}H machine (see appendix 3). The results of the ^{1}H NMR ($CDCl_3$) were: for the aromatic region δ 7.5-7.26$_{(1,2,17,16)}$ppm. The $CDCl_3$ reference peak at 7.27ppm, 5.8-5.0$_{(6,9,12)}$ppm CH of $CH=CH_2$, 4.9-4.84$_{(7,10,13)}$ppm CH_2 of $CH=CH_2$, 3.502$_{(1)}$ppm for SH, 0.675-0.509$_{(5,8,11)}$ppm $SiCH_2$, and 0.250$_{(3,5)}$ppm for $SiCH_3$. Next GC-Mass spectrometry (see appendix 4) was carried out. Initially there were four main peaks the largest one has an m/e of 194 thus showing that it was the

desired product. See figure 5.9 for schematic diagram showing coloration between molecule and nmr peak positions.
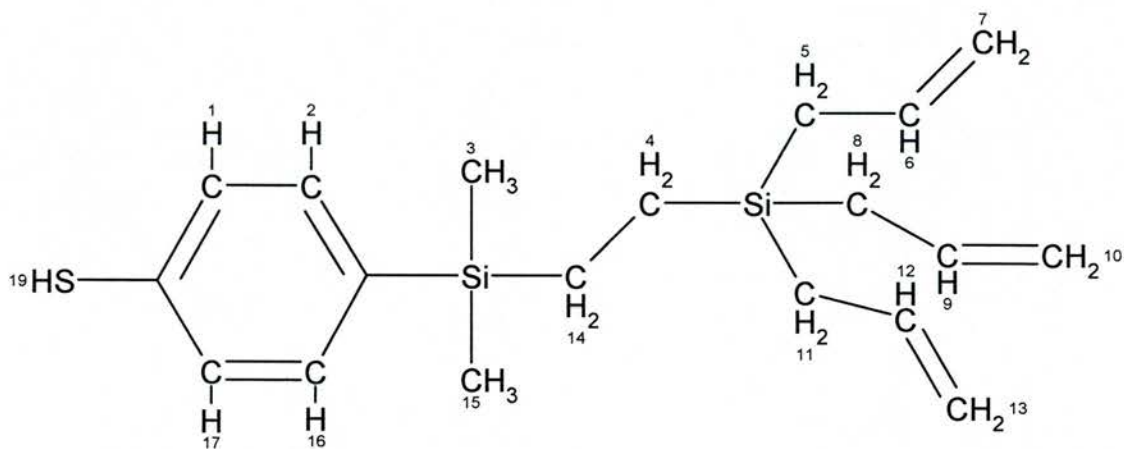
Figure 5.9 Schematic diagram of G1 thiol dendrimer with H's numbered to correlate with nmr peaks in results section above.

5.3.2 Solution Deposition

5.3.2.1 X-ray Photoelectron Spectroscopy (XPS)
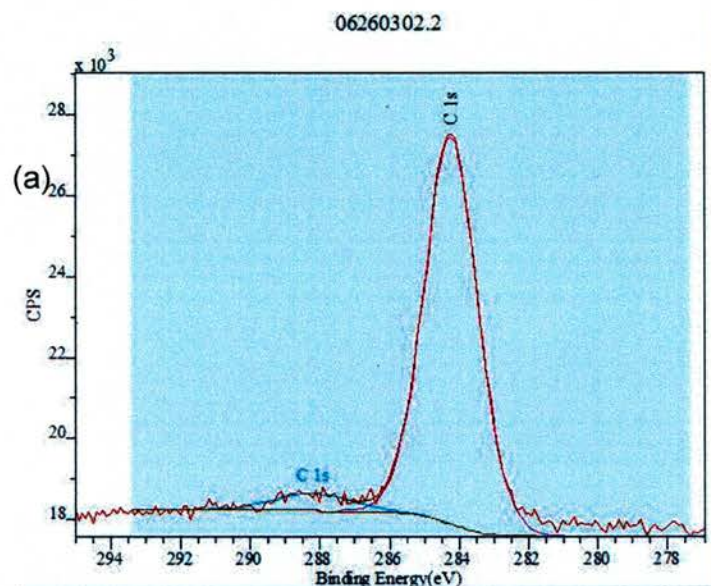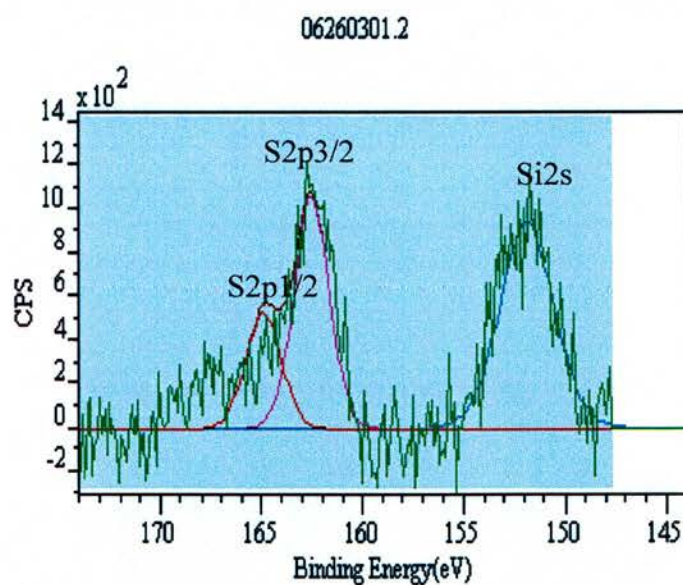
Figure 5.10 (a) Carbon 1s core level XPS spectra from and Au/mica substrate that was immersed in the 1mmol ethanolic G2 dendrimer thiol solution for 16 hours. (b) shows Sulphur 2p core level XPS spectra from and Au/mica substrate that was immersed in the 1mmol ethanolic G2 dendrimer thiol solution for 16 hours and Silicon 2s core level XPS spectra from a Au/mica substrate that was immersed in the 1mmol ethanolic G1 dendrimer thiol solution for 16 hours. All experiments were carried out a a pass energy of 20eV.

XPS was carried out on the Au/mica slide that had been exposed to a 1mmol ethanolic G2 solution, to investigate the elements present on the sample surface (other than Au) as this would in turn give some insight as to whether the molecule had adsorbed onto the surface. Figure 5.10 (a) shows the XPS spectrum of carbon (1s) after it has been subjected to a Shirley background subtraction, which shows two photoemission peaks at 289eV and one at 284.3eV. Figure 5.10 (b) shows the XPS spectra of the sulphur (2p) core levels and the silicon 2s core levels from the thiolate monolayer on Au. This XPS spectrum has been subjected to a Shirley background subtraction. On investigation of this spectrum the sulphur (2p) core level spectrum shows one peak at the binding energy which is assigned to the $2p_{3/2}$ and the $2p_{1/2}$ with the binding energy at 162.3eV (relative to Au $4f_{7/2}$ with the binding energy 83.5eV)[1,2,7]. In the same spectra a peak at 151.5eV can be assigned to Si2s(151.5eV).

5.3.2.2 Ultra High Vacuum Scanning Tunneling Microscopy (UHV STM)
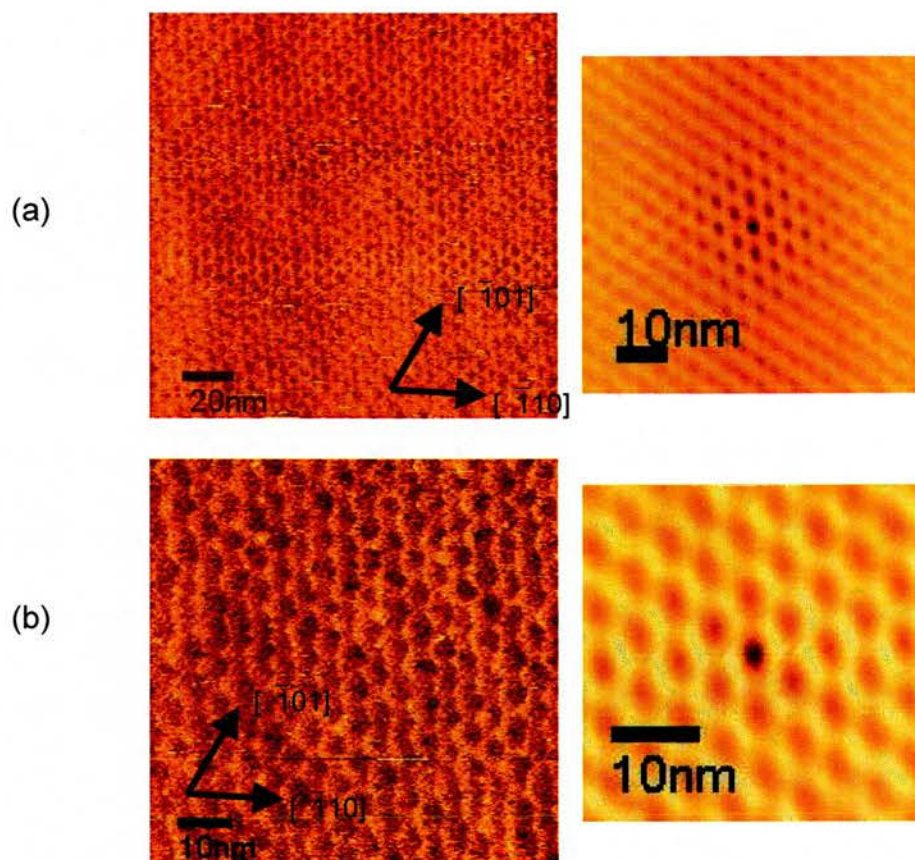
Figure 5.11 (a) 200nm by 200nm UHV STM image of Au{111} single crystal that has been immersed in an ethanolic G2 thiol solution for 16 hours. The smaller image to the right is the auto-correlation image which shows an average direction of the features on the surface. (b) 95nm by 95nm UHV STM image of an Au{111} single crystal that has been immersed in an ethanolic G2 thiol solution for 16 hours. The smaller image to the right is the auto-correlation image which shows an average direction of the features on the surface.

The UHV STM of Au{111} has been imaged allowing the real space direction of the atoms to be determined, as can be observed in figure 5.12.
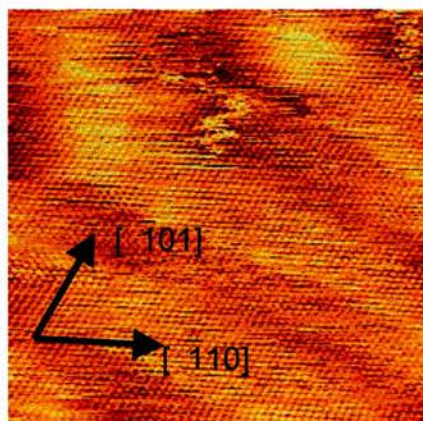
Figure 5.12 Real space STM Image of Au{111} atomic resolution

Figures 5.11(a-b) show images from the UHV STM after an Au{111} single crystal had been dosed for 16 hours. These images all show the same features but at different resolutions. The images are representative of most of the surface of the Au{111} crystal after being immersed in the G2 ethanolic solution. The images show a "loop" like pattern where the periodicity in the [$\bar{1}2\,\bar{1}$] and the [$01\,\bar{1}$] direction is ~6.4±0.5nm and the periodicity in the vertical direction is 8.2±0.5nm. This is further supported by the auto-correlation pattern which gives an average separation of the large features and more clearly shows the real space periodicity. Auto-correlation is a computer programme that finds any repetitive periodicity in the image scanned and then filters off any features that do not belong to this periodicity. These features can be discounted as being noise as their separation is constant even when the

scan size and speed is changed. It is not known whether these are ordered

etch pits or molecular features.

5.3.2.3 In Air Scanning Tunneling Microscopy (STM)
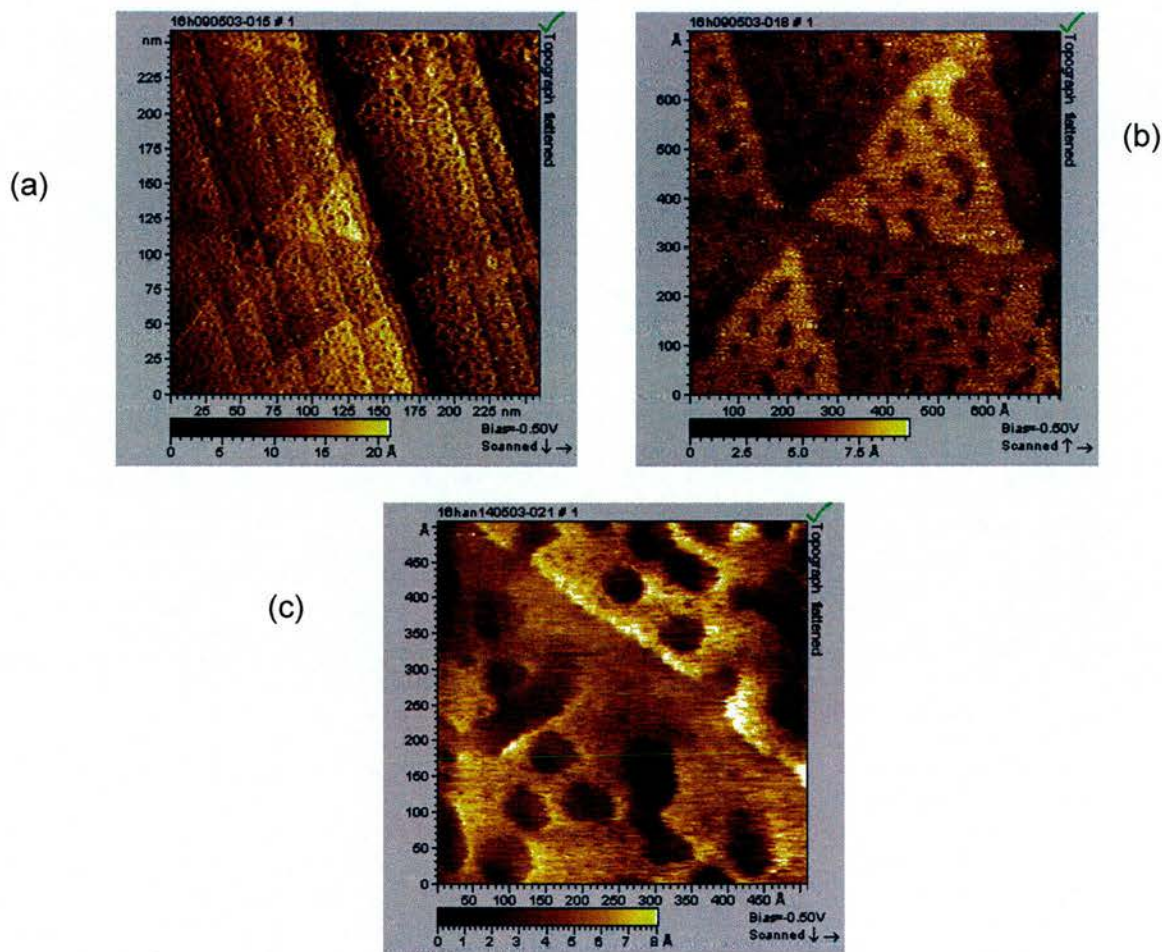
Figure 5.13 (a) 260nm by 260nm image of the G2 dendrimer deposited on an Au/mica substrate from a 1mmol ethanolic solution for 16 hours. This image was acquired at a tunneling current of 0.474nA and a bias voltage of -0.50V. (b) 750Å by 750Å image of the G2 dendrimer deposited on an Au/mica substrate from a 1mmol ethanolic solution for 16 hours. This image was acquired at a tunneling current of 0.474nA and a bias voltage of -0.50V. (c) 500Å by 500Å image of the G2 dendrimer deposited on an Au/mica substrate from a 1mmol ethanolic solution for 16 hours, close up of (c). This image was acquired at a tunneling current of 0.474nA and a bias voltage of -0.50V.

As mentioned in section 3.2.1 atomic resolution of Au{111} was imaged showing that the imaging conditions were good. Figure 5.13 (a) is a typical large scale constant current STM image of the prepared G1 molecule on a gold/mica slide.

The images in Figures 5.13 (a-c) show a large number of etch pits but also areas of step edge etching. No molecular features are imaged but the dramatic etching effects conclusively show that the molecule is adsorbed onto the surface.

5.3.3 Gas Phase Deposition

5.3.3.1 Reflection Adsorption Infrared Spectroscopy (RAIRS)

Figure 5.14 shows the $3500cm^{-1}$ to $2400cm^{-1}$ range RAIRS spectra for the gas phase deposited G2 onto an Au{111} single crystal.
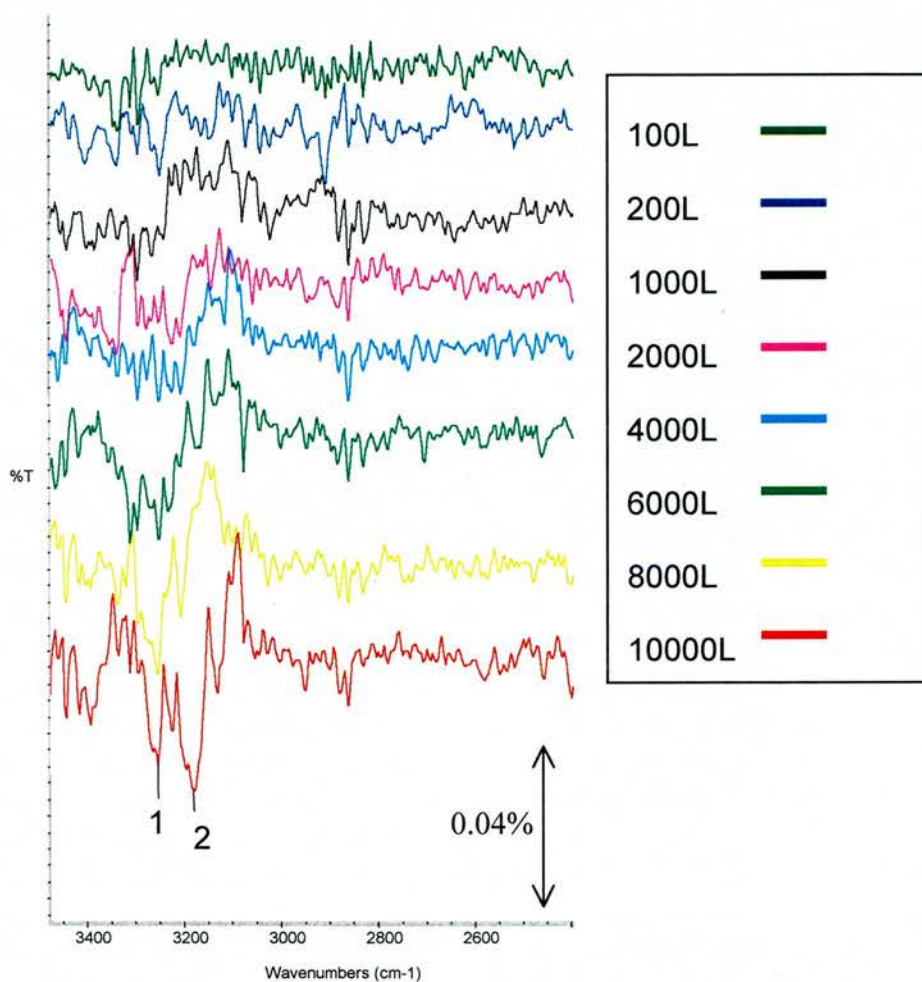
Figure 5.14 RAIRS spectra $3500cm^{-1}$- $2400cm^{-1}$ for gas phase deposition showing doses from 100 langmuirs to 10000L carried out in a UHV chamber base pressure $1x10^{-10}$ torr.

Figure 5.15 shows the 1400cm^{-1} to 800cm^{-1} range RAIRS spectra for the gas phase deposited G1 dendrimer molecule onto Au{111}.
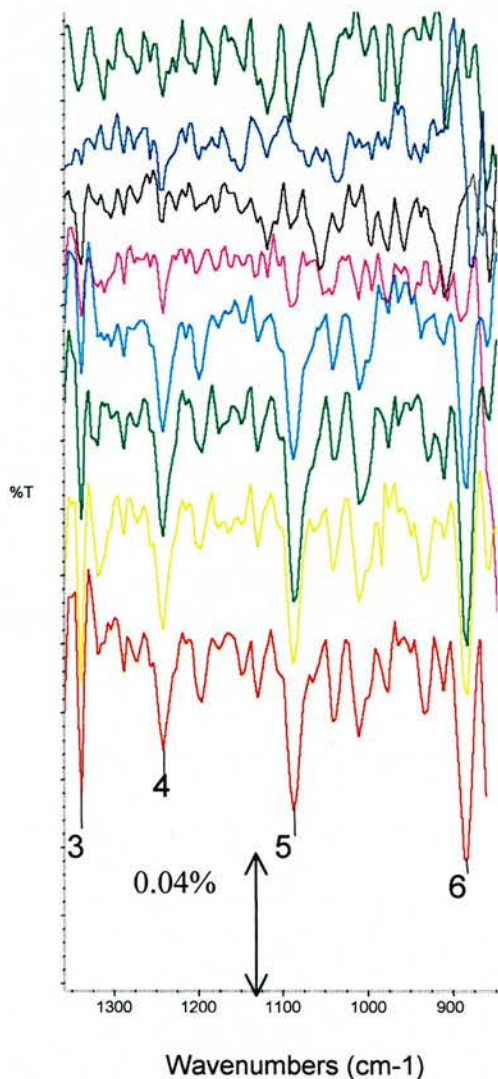
Figure 5.15 RAIRS spectra 1400cm^{-1}- 800cm^{-1} for gas phase deposition showing doses from 100 langmuirs to 10000L carried out in a UHV chamber base pressure 1x10^{-10} torr.

Figure 5.16 shows the 2200cm^{-1} to 700cm^{-1} range RAIRS spectra for the gas phase deposited G1 dendrimer molecule onto Au{111}.
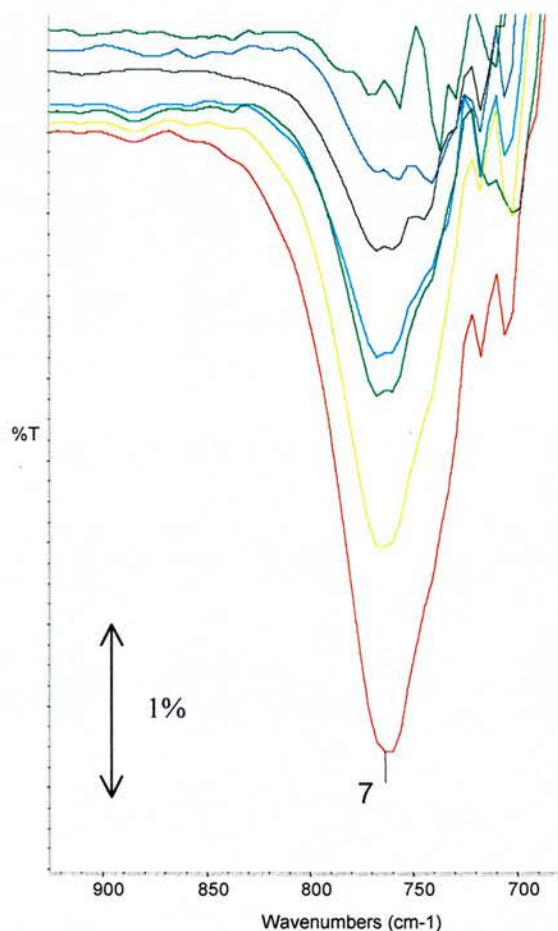
Figure 5.16 RAIRS spectra 1000cm^{-1}- 750cm^{-1} for gas phase deposition showing doses from 100 langmuirs to 10000L carried out in a UHV chamber base pressure 1x10^{-10} torr.

For the thiocresol molecule there was a large C-H out of plane bending peak at 764cm^{-1}. For the G2 molecule this peak is at 763cm^{-1}. The bands which are present are 1. 3254cm^{-1}, 2. 3180cm^{-1}, 3. 1338cm^{-1}, 4. 1241cm^{-1}, 5. 1086cm^{-1}, 6. 884cm^{-1} and 7. 763cm^{-1}. There may be two peaks around peak 7 but one looks like it increases in size more that the other and therefore one peak is lost under the signal of the other. All of these peaks generally increase in size with increasing dose.

5.3.3.2 Ultra High Vacuum Scanning Tunneling Microscopy (UHV STM)
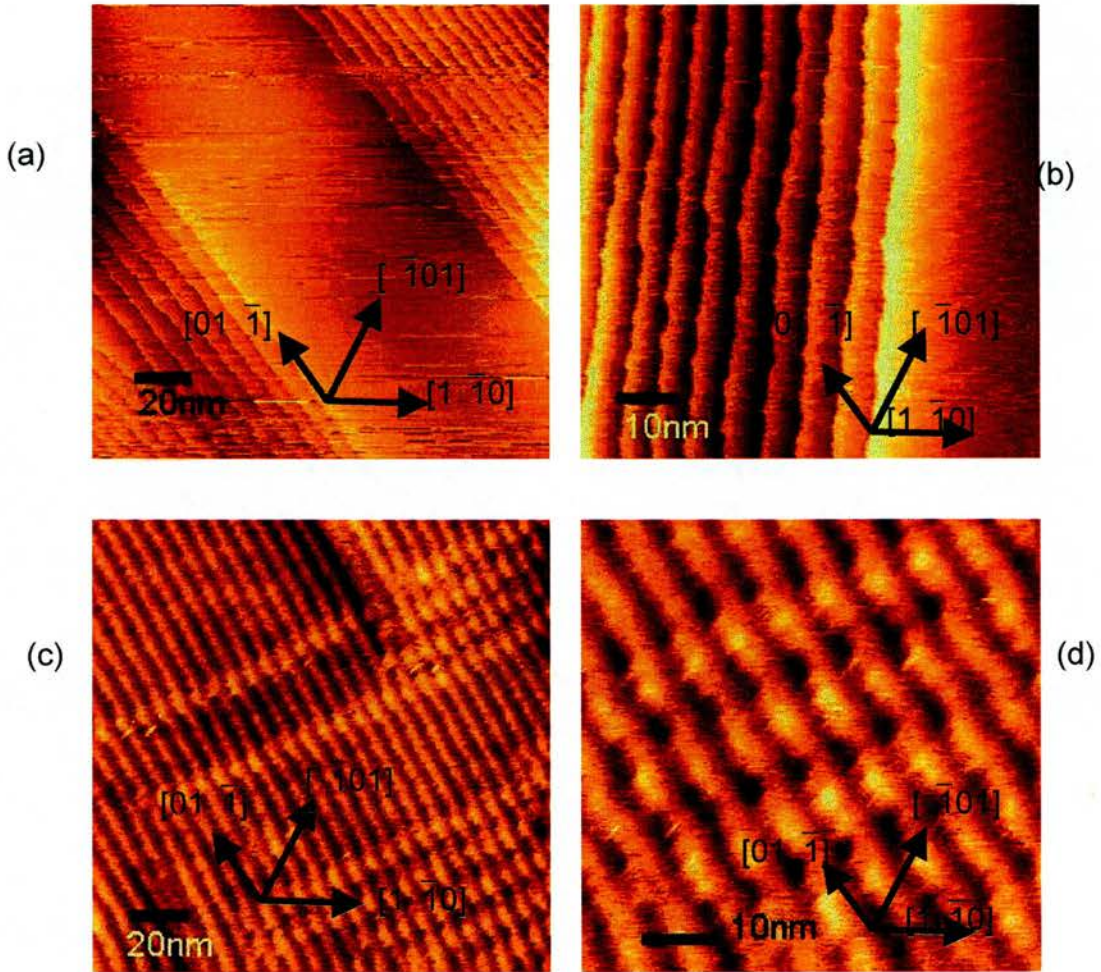
Figure 5.17 (a) 200x200nm UHV STM Image of Au{111} single crystal dosed with 500L of G2 showing steps bunching and a large terrace. This image was acquired at a tunneling current of 1.336nA and at a tip bias of -0.286V. (b) 100x100nm UHV STM Image of Au{111} single crystal dosed with 2000L of G2 showing steps and a terrace and some reconstruction is visible. This image was acquired at a tunneling current of 0.551nA and at a tip bias of -1.049V. (c) 200x200nm UHV STM Image of Au{111} single crystal dosed with 5000L of G2 showing a constant periodicity of steps and with some molecular features. This image was acquired at a tunneling current of 0.574nA and at a tip bias of -1.028V. (d) 75x75nm UHV STM Image of Au{111} single crystal dosed with 5000L of G2 showing a constant periodicity of steps and with some molecular features. This image was acquired at a tunneling current of 0.574nA and at a tip bias of -1.028V.
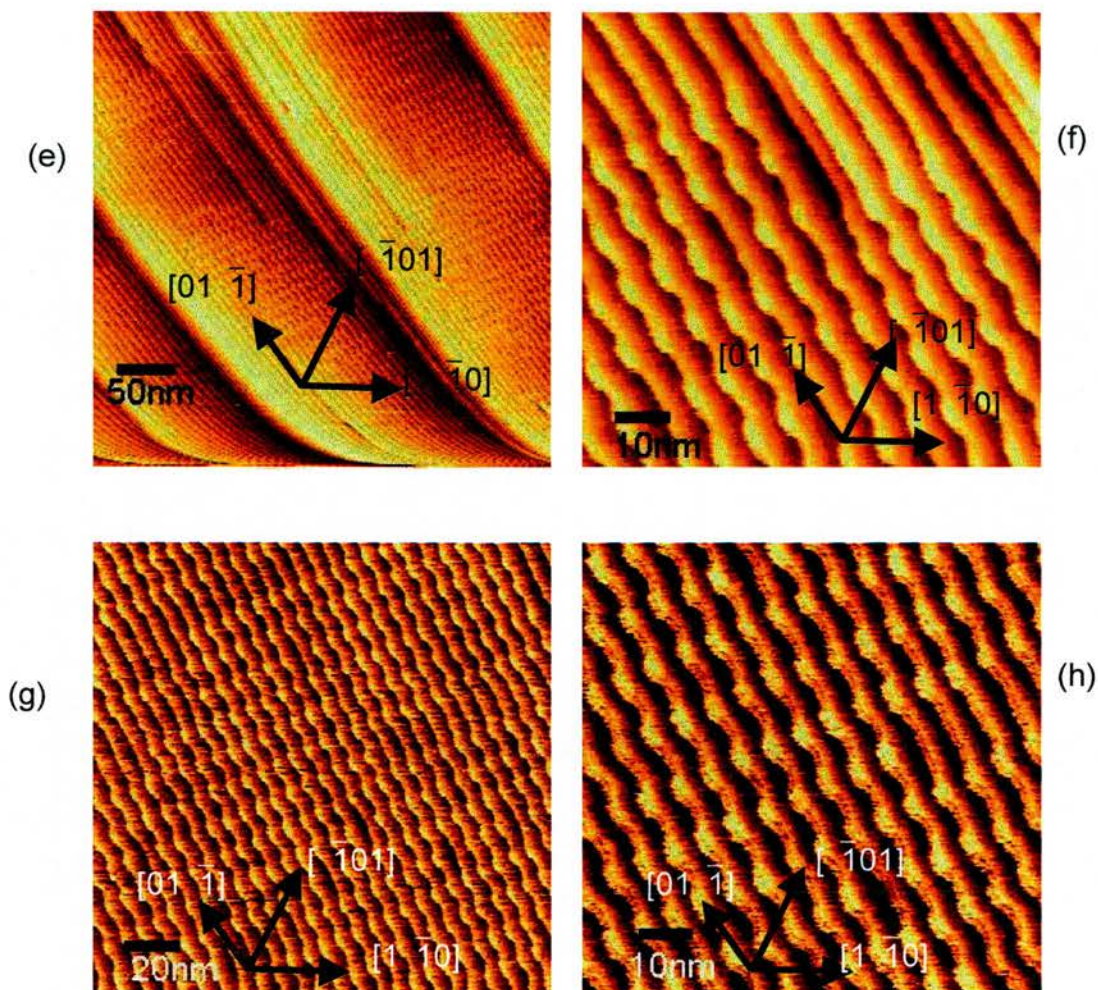
Figure 5.17 (e) 500x500nm UHV STM Image of Au{111} single crystal dosed with 10000L of G2 showing consistently periodic steps or lines with molecular features. This image was acquired at a tunneling current of 1.336nA and at a tip bias of -0.286V. (f) 100x100nm UHV STM Image of Au{111} single crystal dosed with 10000L of G2 showing consistently periodic steps or lines with molecular features. This image was acquired at a tunneling current of 0.551nA and at a tip bias of -1.049V. (g) 210x210nm UHV STM Image of Au{111} single crystal dosed with 10000L of G2 showing consistently periodic steps or lines with molecular features. This image was acquired at a tunneling current of 0.574nA and at a tip bias of -1.028V. . (h) 110x110nm UHV STM Image of Au{111} single crystal dosed with 10000L of G2 showing a constant periodicity of steps and with some molecular features. This image was acquired at a tunneling current of 0.574nA and at a tip bias of -1.028V.

As mentioned in part 5.3.2.2 the UHV STM of Au{111} has been imaged allowing the real space direction of the atoms to be known (figure 5.12). Figure 5.17(a) is representative of the substrate after a 500L dose. The image shows

198

two areas of steps (or bunches of steps) with a regular periodicity of 8.4±0.5nm and a large terrace in between them. Figure 5.17(b) is similar to figure (a) as it shows bunches of steps with a regular periodicity of 8.2±0.5nm and a large terrace. In this image herringbone reconstruction (see chapter one) is also observed. This image is from a much larger 2000L dose. Figures (c) and (d) are very different from figures (a) and (b). These images show the regular periodicity of steps (8.2±0.5nm) but however, no large terraces are observed. Also shown in these images are what look to be molecular features in rows along the step edges. Between steps these features have the same periodicity as the steps but along the step edges where the features seem to be grouped into rows of 4-6 these features have a periodicity of 15±0.5nm. This effect becomes more dramatic after the 10000L dose. The figures 5.17 (e)-(g) show the surface after a 10000L dose in all of these images the periodicity of the steps is 8.2±0.5nm and the periodicity of the molecular features along the step edges is 14.5±0.5nm. The steps appear to be in the [01 $\bar{1}$] direction.

5.4 Discussion

5.4.1 XPS

XPS was used to confirm that the elements present in the G2 molecule had chemisorbed onto the surface from solution phase deposition. The sulphur 2p, the carbon 1s and the silicon 2p peaks at the expected binding energy. Comparison to previous research by Whelan et.al[1,7], who show for TP on Au{111}, that the binding energies of the S $2p_{3/2}$ and $2p_{1/2}$ are 162.1 and 163.1 respectively. The S2p peak in the present case is in agreement with this binding energy but due to relatively poor instrumental resolution we are unable to resolve the two components of the S2p peak. The presence of the 2p peak signifies the presence of a Au-thiolate bond consistent with the expected chemisorbed G2 dendrimer thiol. These peaks are measured relative to the Au $4f_{7/2}$ peak at binding energy 83.5eV. Two peaks are observed for carbon (1s) at 289eV and 284.3eV. Two peaks are expected for TP[3,7] and TP related molecules. This compares to work by Whelan et al.[1] on TP an Au{111} which shows carbon on Au{111} has binding energies of 284.3eV and 285.8eV. the two carbon peaks observed are due to the aromatic ring, an Si-CH$_3$ peak, an Si-CH$_x$ peak and a C=C peak[8,9,10,11].

Comparison of this work to previous reports by Long et al.[12] and Shabtai et al.[13] showing the silicon (2s) binding energies of silicon containing self assembled molecules to be at 102.8eV for Si 2p and 153.8eV for Si 2s. This shows that the Si peak observed is at the expected binding energy. Silicon 2s is also observed

as a small peak at ~151.5eV. This confirms that the molecule has most likely attached to the surface.

This XPS data shows that ~79% of the substance adsorbed onto the Au{111} surface was carbon, ~8% was sulphur and ~13% was silicon. The expected ratio of carbon:sulphur:silicon for G1 is ~72:10:18 this was calculated using equation 2.11 and using the relative response factors for example 1.677 for S2p. The ratio of actual silicon, sulphur and carbon on the Au{111} surface is very close to the theoretical results. This further supports the fact that the molecule has adsorbed intact onto the surface. The ratio of C:S:Si from G2 id different to the ratio of C:S:Si from G1. This is expected and shows that the molecule is not degrading to G1 as it attaches to the molecule.

5.4.2 RAIRS

In the case of thiocresol (chapter 3) the IR data showed that the molecule was orientated with the molecular plane parallel to the surface. In G1 we believe that the gas deposited G1 is close to parallel to the surface but the solution deposited G1 is more random.

The purpose of the RAIRS experiments was three-fold. It was used to establish whether the molecule adsorbs intact onto the Au substrate, to evaluate the adsorption geometry of the adsorbed species and finally, to compare adsorption from the gas phase and adsorption from solution. To help with the

analysis of the IR data, we carried out a Gaussian DFT calculation on an isolated G2 dendrimer. The output of this calculation gives the frequency of the vibrational modes of the molecule and the direction of the dynamic dipole moment associated with each vibration. The calculations were optimised with the B3LYP method using a STO-3G basis set Table 5.1 shows these vibrational wavenumbers and the predicted direction of their dipole moments. The Gaussian wavenumbers need to be corrected to give accurate band positions. It is approximately the case that the predicted wavenumbers needs to be multiplied by 0.97 to allow comparison with the actual spectra.

Figure 5.18 shows the IR spectrum predicted by the gaussian calculation.
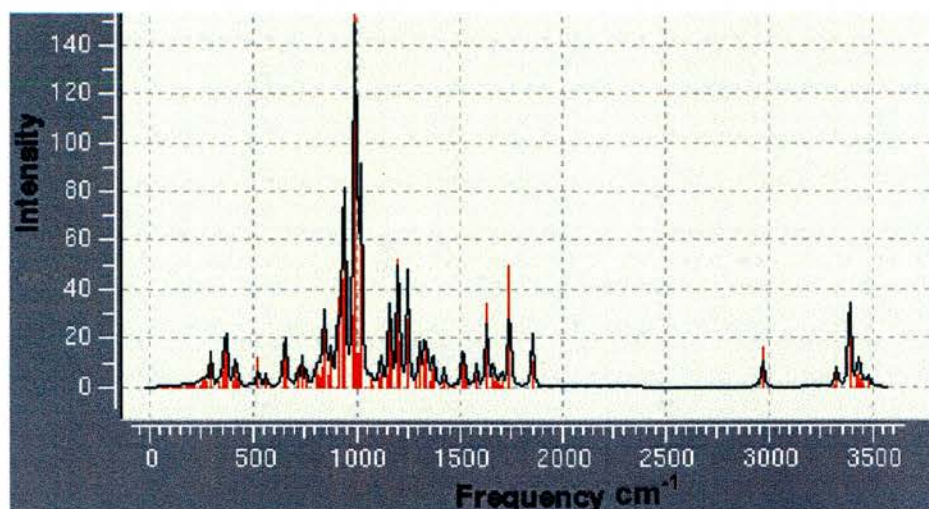
Figure 5.18 Gaussian IR spectra for the isolated G2 molecule in the gas phase. This shows the expected vibrations of the G2 molecule

Band No for gas phase deposition	Position of bands (cm⁻¹) for gas phase deposition	Gaussian Simulation G2 (cm⁻¹)	Gaussian Band relative IR intensity	Assignment of Bands (cm⁻¹)
		3390.5	20.0	Symmetric CH stretch from one vinyl group (perpendicular)
1	3254	3390	17.2	Symmetric CH stretch from another vinyl group (parallel)
		3389	20.9	Symmetric CH stretch from final vinyl group (parallel)
2	3227	3328	7.1	Symmetric C-H stretch from CH_2-CH_2 middle section of molecule
		2969	16.1	SH stretch (parallel)
		1853	10.4	C=C stretch from vinyl group (perpendicular)
		1741	50.1	Aromatic C=C antisymmetric stretch and CH bend (parallel)
		1632	34.4	Aromatic C=C symmetric stretch and CH bend (parallel)
		1510	13.4	In plane symmetric aromatic CH bend and CH wag from CH_3 (parallel)
3	1338	1372	10.9	Symmetric CH wag of CH_2 before vinyl group and bonded to Si (perpendicular)
		1340	15.9	Symmetric CH wag of CH_2 before vinyl group and bonded to Si (parallel)
		1329	10.9	Symmetric CH bend of CH_2 (parallel)
		1307	18.5	Symmetric in plane CH ring bend plus SH wag (parallel)
4	1241	1249	25.8	Symmetric in plane CH ring bend. (parallel)
		1246	27.7	Antisymmetric CH bend from CH_2-CH_2 middle section (perpendicular)
		1207	18.8	Ring breathing and antisymmetric aromatic in plane CH bend plus SH wag (parallel)

		1200	51.9	Ring breathing and antisymmetric aromatic in plane CH bend. (parallel)
5	1086	1166	14.2	Symmetric CH wag of vinyl groups (parallel)
		1159	26.8	Symmetric CH wag of vinyl groups (perpendicular)
		1029	75.3	Antisymmetric CH bend of CH_3 groups bonded to Si (perpendicular)
		1011	13.4	Out of plane antisymmetric aromatic CH bend and CH bend of vinyl CH_2 (perpendicular)
		1004	13.3	CH bend from CH_2 of vinyl and C-C stretch from CH_2=CH_2 (diagonal)
		994	167.8	Antisymmetric CH bend of CH_3 bonded to Si (parallel)
		986	29.1	CH bend from a vinyl group (parallel)
		985	24.5	CH bend from another vinyl group (parallel)
		984	13.4	CH bend from final vinyl group (parallel)
		974	58.9	Antisymmetric CH stretch from vinyl group (perpendicular)
		937	29.1	Antisymmetric CH stretch from CH_3 (parallel)
		929	43.79	Antisymmetric CH wag from vinyl groups and CH_2 (perpendicular)
6	884	909	36.45	Symmetric CH wag from vinyl groups and CH_2 (perpendicular)
		875	14.62	Symmetric CH bending from CH_3 and CH_2 groups (perpendicular)
7	763	848	30.45	Out of plane CH bend (perpendicular)

Table 5.1 Assignment of G2 RAIRS peaks for gas phase deposition RAIRS spectra

The gaussian spectrum clearly shows more peaks than there are in table 5.1. This is because all peaks of a low relative intensity were omitted. RAIRS analysis was carried out for G2 solution deposition however the spectra produced were unfortunately affected greatly by noise and hence unusable in this thesis.

The output of the Gaussian calculation predicts that the most intense feature should occur at 994 cm^{-1}. Allowing for the error in calculations of vibrational frequency by such calculations this should correlate with a band at ~865cm^{-1}. This band is not observed after gas phase deposition. This band consists mostly of in plane bending of the CH$_3$ groups (here "plane" refers to the plane of the aromatic moiety). So if the G2 molecule has adsorbed onto the substrate whole and this peak is not observed then this points to the aromatic ring being parallel or close to parallel to the surface.

Further support for this assignment comes from the most intense band in the gas phase spectrum at 763 cm^{-1} which correlates well with the predicted peak at 848 cm^{-1}. This corresponds to the out of plane C-H bending vibration of the aromatic H atoms which has a strong perpendicular component to the dynamic dipole moment. This is similar to what occurs for TP on Au{111}. This mode is observed if the aromatic ring of the molecule is close to parallel to the Au{111} surface. This is due to the surface dipole selection rule (see chapter 2). Other reports of TP[1] mercaptobiphenyls[14] and tertphenylthiols[15] show that aromatic

205

thiols with the SH directly attached to the aromatic ring can have tilt angles of anywhere between 28° and 0°. This peak is observed for both the thiocresol deposition and for the G1 gas phase deposition.

The other six bands observed in the gas phase deposition case are all more difficult to unequivocally assign. The next band at 884cm^{-1} is most likely assigned to 909cm^{-1} which is associated with the CH$_2$ of the vinyl group. The band at 1086 cm^{-1} could be assigned to either the 1066 or 1059cm^{-1} bands predicted by the Gaussian calculation. These bands are both associated with vibrations of the vinyl functionality each of which have dynamic dipole components perpendicular to the plane of the aromatic ring. If the metal surface selection rule is taken into account then both of these bands should be observed in the RAIRS spectrum if the molecule has a flat lying or almost flat lying geometry[16]. The importance of this band is that it indicates that at least a fraction of the vinyl groups are still intact on the surface which has important implications in the design of catalysts based on this system. The band at 1241 cm^{-1} could be related to either of the 1307 or 1329cm^{-1} bands which are both related to CH ring bending vibrations. On the basis of the above arguments, it seems more likely that the band is associated with the 1307 cm^{-1} (~1267 cm^{-1} after correction) which has a component of the dynamic dipole moment perpendicular to the surface.

No bands were resolved in the 1400-1650 cm^{-1} range due to difficulties encountered with gas phase water miscancellation. The final bands observed appear at 3227 and 3254cm^{-1}. It is very difficult to assign these peaks unequivocally since a range of C-H stretching vibrations are predicted by the Gaussian calculation. The overcalculation of vibrational frequencies by Gaussian is more dramatic at higher wavenumbers. As such and bearing in mind the assignments of the other peaks, the 2962 cm^{-1} peak is most likely to derive from one predicted wavenumber (or a combination of predicted wavenumbers) the   C-H stretching modes with a perpendicular dynamic dipole moment. Therefore the gas phase deposited G2 dendrimer, can be assigned, as a species which is almost flat lying. These observations are strikingly similar to what occurs after the deposition of G1 on Au{111}.

Although it is common for aromatic thiols such as TP and thiocresol to be parallel or close to flat lying, larger or longer molecules normally stand upright after gas phase dosing. The molecule appears to be flatlying after G2 deposition this may be because Si containing molecules have been known to chemisorb onto Au{111} surfaces by the Si atom. Work done by Marchenko et al[17]. shows that there is a strong interaction between Si and Au. And in fact it shows that it is possible for a sterically compact tetra-coordinated silicon group to become penta-coordinated and adopt a bipyramidal geometry when in contact with an electron donating atom such as Au. This would mean that a "supervalent" Si may be covalently bonded to the Au making the molecule lie

parallel to the surface. This however may not be possible as the vinyl end groups may sterically hinder the adsorption and this vinyl group is definitely observed on the RAIRS spectra. If this is occurring then the dipole moment from the silicon end of the molecule will be affected. The almost parallel dipole moments will most likely be moved upwards and become either diagonal or almost perpendicular. The gaussian does not show this as it is calculated for a single G2 molecule in the gas phase. Figure 5.19 shows a schematic diagram of how the G2 dipole moment may attach to the substrate if the first silicon atom is also chemically attached onto the Au substrate. It is unlikely that the Si bonded to the allyl groups would adsorb onto the Au due to steric hindrances.
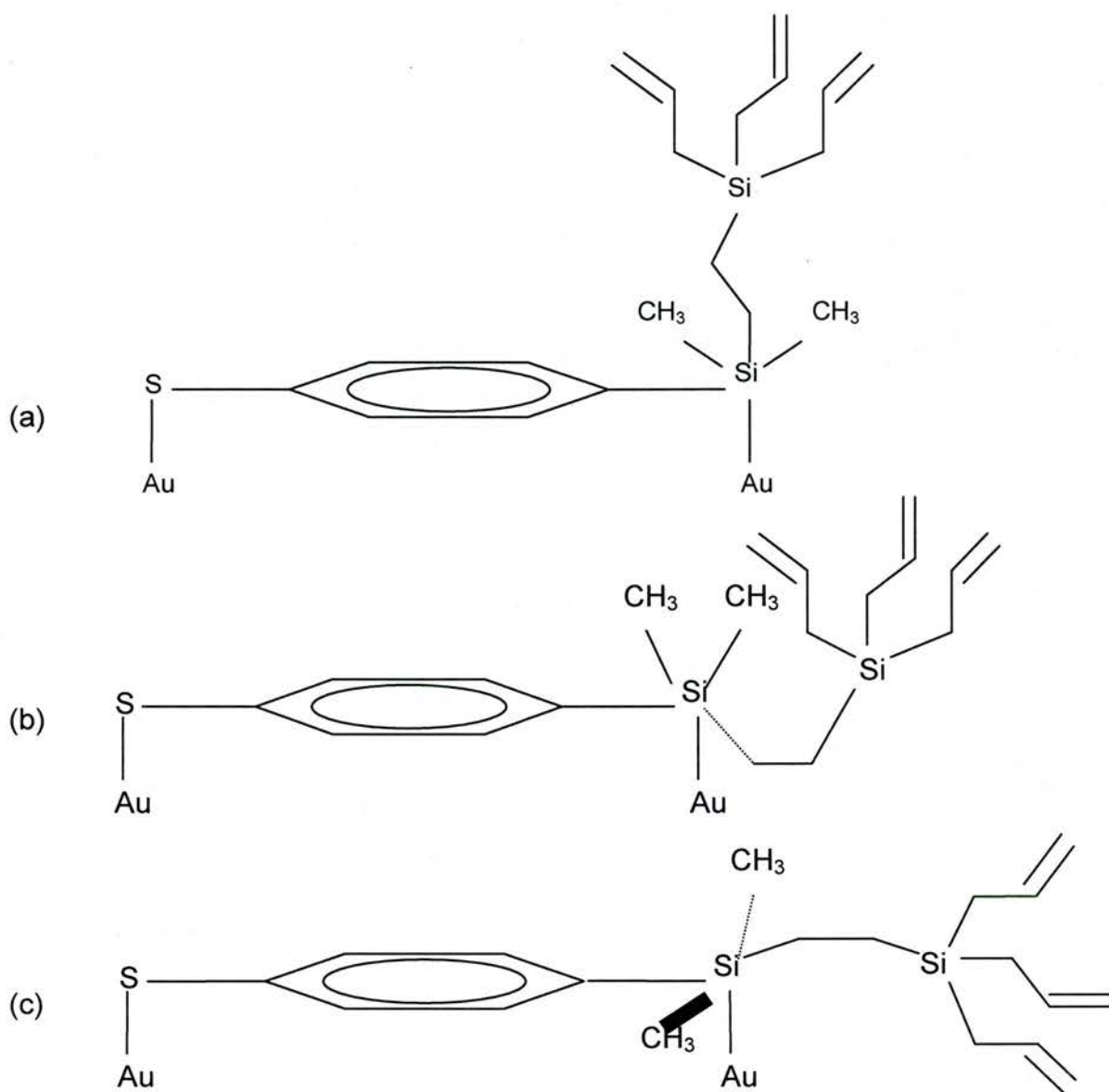
Figure 5.19 Shows three different schematic diagrams of how the G2 molecule might chemisorbed onto the gold by both the Si and S atoms creating a supervalent silicon. Diagram (b) shows steric hinderences. These are only estimations of molecular orientation.

This would mean that a vibration from the whole head of the molecule after Si which before would have been an almost parallel would either now be diagonal or almost perpendicular (examples of parallel, diagonal and perpendicular

209

dipole moments can be seen in figure 4.18 in chapter 4 for G1). This means that the vibrations identified as peak 1 and peak 2 would be observed if the molecule was flat lying. This theory can be supported by the RAIRS data obtained from gas phase deposited G1. As both sets of data omit peaks expected for a completely parallel molecule or a completely perpendicular molecule.

Another clear observation from the table and the Gaussian spectrum is that the peaks with the highest expected relative intensity are not observed in the IR spectra for the G2 on Au. On closer observation these large peaks that are missing at for example $1029cm^{-1}$ and $994cm^{-1}$ are due to C-H bending of the CH_3 molecules directly bonded to the first Si atom. The absence of these peaks is either due to the orientation of the molecule or dissociation of the CH_3. The latter of these is more likely the case. This could then mean that the Si is attached to the surface but not forming a supervalent Si as is suggested above.

5.4.3 STM of Solution Deposition

Figures 5.11 (a-c) show the solution deposition of the G2 thiol dendrimer onto a Au{111} single crystal. From these images one distinct observation can be made. This is the formation of long range order. This may be coupled with the molecularly induced faceting of the steps as observed for G1 (see chapter 4). Figure 5.13 (a-d) show the solution deposition of the G1 thiol dendrimer onto a Au/mica substrate. Again from these images only one observation can be

made. This is the formation of large etch pits (see chapter 1) with some step edge etching.

There are no real similarities between the air and UHV STM data as would be expected. The UHV STM images do not show any etch pits as the air STM images do and the air STM images do not show any evidence of molecular features or faceting. As discussed in chapter one, etch pits are a common occurrence on Au that has been exposed to a dose of a thiol molecule[18], as is step edge etching and the formation of Au islands. The G2 seems to cause larger etch pits than the G1 molecule. One major difference between G2 and the thiocresol and G1 is there is no evidence of Au island formation, as was mentioned in chapters 3 and 4. This effect has been reported before for 4-hydroxythiophenol (4HTP) on Au/mica[19]. The occurrence of etch pits confirms that the G1 molecule is chemisorbing and restructuring the Au/mica substrate.

For the solution deposited G2 on Au{111} single crystal some ordered features are observed which may be molecular features. The periodicity of these features is measured to be 6.4±0.5nm in the diagonal directions and 8.2±0.5nm in the vertical direction. This is completely different from what is reported for TP[1,2,3] and for what is shown in chapter 3 for thiocresol as these exhibit no long or short range periodicity and in chapter 4 for the G1 molecule long range order is observed but no short range order as the order seems to come from the underlying substrate due to molecular induced faceting and the molecules are

211

adsorbed on top of the Au in a random manner. For the G2 however it looks as though the molecule is ordering on the Au however this does not discount that molecular faceting is occurring as for G1 and it may be that the ordering of the molecule may be facilitated by this. It is not possible due to the restrictions of these images to exactly say how the molecules are sitting on the surface but figures 5.20 (a) and (b) below show some examples of what may be happening.
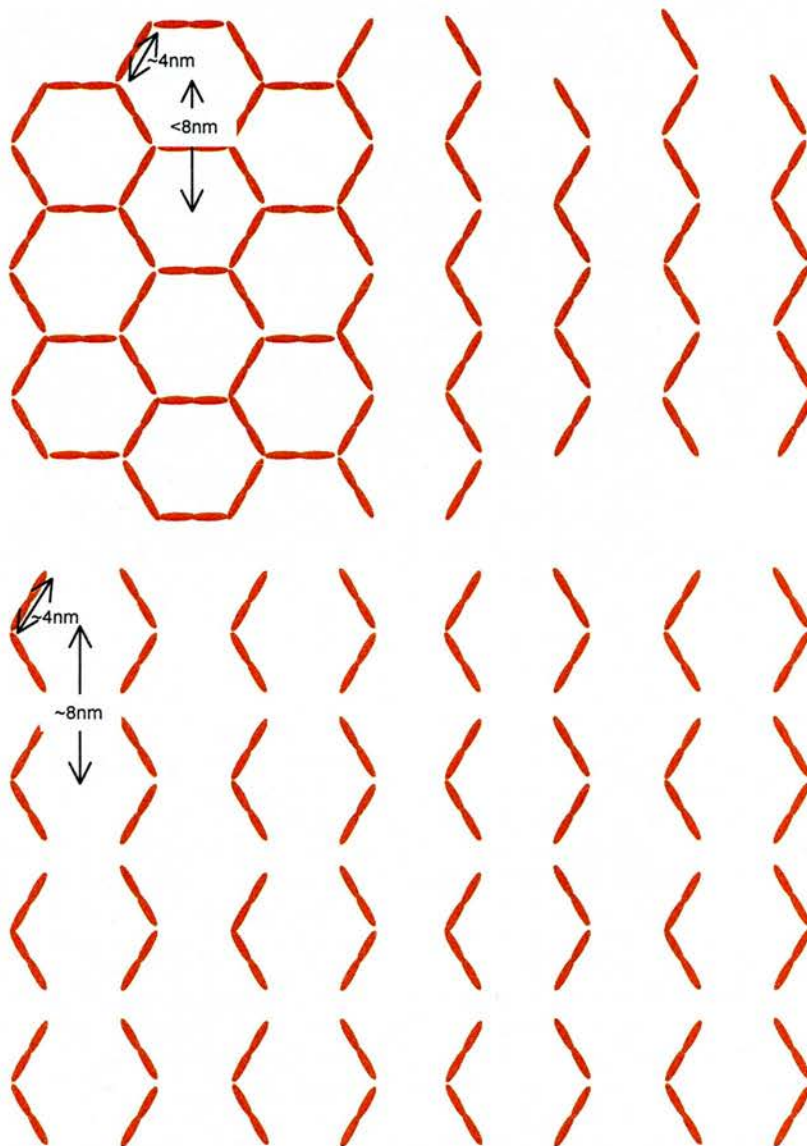
Figure 5.20(a) and (b) Show schematic diagrams of how the molecule may be ordering on the surface after a 16 hour solution deposition onto the Au{111} single crystal.

If any of the above molecular orientations are shown in figure 5.11(a) or (b) they could still be facilitated by an underlying vicinal surface that has been molecularly induced by the G2 molecule. The distance between each hexagon would be approximately 65Å if the angles are 120°. However as the vertical distance is ~8.2nm the hexagons may not be joined together. It is also unknown whether the hexagon is whole as pictured in the first part of figure (a) or not as pictured in the second part of (a). The molecules are most likely linked together through the vinyl groups as the thiol groups will be directly bound to the Au{111}. Exactly which way or which vinyl groups are bonded together cannot be estimated however as some evidence of vinyl groups is observed in the RAIRS data it can be concluded that all three vinyl groups are not used to link the molecules together. Although this is possible it is also possible that the molecules formed a disulphide before they were adsorbed onto the surface in this case the bond between the two molecules may have broken to allow the S-Au bond but the molecules would remain close together on the surface. This positioning is further supported by the presence of bands due to the vinyl groups in the RAIRS data but the omission of bands due to thiol groups. These images are just an approximation as no STM image has given enough detail for a detailed model.

5.4.4 UHV STM Gas Phase Deposition

Reconstruction is observed on figure 5.20(b) and was noticeable on most areas of the Au{111} single crystal after both the 500L and 2000L doses . This is unusual as Dishner et al.[20] reports that normally when a molecule is adsorbed onto a surface the reconstruction is destroyed, however in this case it has not. This may be due to the molecule having a low sticking probability which would mean that it has not chemisorbed onto the area being imaged.

Figures 5.20(a) and (b) are dramatic examples of a phenomenon called "step bunching". According to Jeong et al.[21] highly stepped areas are often rearranged into flat reconstructed terraces with much more sharply inclined regions with closely bunched steps after molecular deposition. Experiments on systems such as GaAs{100}, Pt{111} and Au{111} have shown the that there is a regularity in the size and spacing of these steps and terraces. The figures (a) and (b) show these steps and terraces occurring for the G2 molecule on the Au{111} single crystal, however the array of small terraces is very uniform as in step bunching, the bunches in these images have a periodicity of 8.2±0.5nm and unlike for the G1 molecule there is a large terrace separating the bunches of steps. Although an STM image cannot fully represent the whole surface the occurrence of this step bunching or long range periodicities of steps of steps is not evident for a clean surface. This fact was investigated as thoroughly as possible. This is evident in chapter three for thiocresol as no regular periodicities of steps are evident. The thiocresol experiments were carried out

between the G1 and G2 experiments. Other evidence that this is molecularly induced is that the periodicities between the G2 steps is different (about double the size) than the periodicities of the steps in the G1 case.

The next images figures 5.20(c) to (h) for 5000L and 10000L deposits show no step bunching but as with the G1 molecule gas phase deposited onto the Au{111} single crystal it dose show the occurrence of molecularly induced faceting of vicinal surfaces. As for G1 ,because the periodicity between the terraces is so regular it is very similar to a Au{111} vicinal surface. Surfaces that are vicinal to the {111} plane are normally prepared by the mis-cut of a Au{111} surface plane by a specific angle, for example 3.5° for a {788} surface, with respect to the {111} orientation towards the [$\overline{2}$11] azimuthal direction. Many different Au vicinal surfaces are possible for example {233}, {322}, {455}, {788}, {11,12,12} and {11,9,9} are just a few types, there are other less stable ones. Every vicinal surface exhibits a regular array of steps and terraces of a specific size for example the above vicinal surfaces have terrace sizes of 1.4±0.5nm, 1.3±0.5nm, 3.5±0.5nm, 3.9±0.5nm and 5.6±0.5nm respectively with the {11,9,9} surface having a periodicity of 7nm which is made up of 1x4.2nm terrace and 2x1.4nm terraces. These periodicities lie along the [$\overline{2}$11] direction. Each of these vicinal surfaces apart from {11,9,9} exhibits Au reconstruction with a periodicity of 7.2±0.5nm along the [01 $\overline{1}$] direction. These figures show a high amount of steps with a periodicity in the [$\overline{2}$11] direction of ~8.2nm. This periodicity is not one of a well known vicinal surface and no

reports of a Au surface with this step periodicity. However this type of vicinal surface can be calculated using equation 5.1 below.

$$\tan\theta = \frac{2.35}{82}$$
$$\theta = 1.64$$
$$\cos\theta = \{(x)(x+1)(x+1)\}$$
$$\therefore x = 16$$
$$if \{hkl\}\{abc\} where$$
$$\cos\theta = \frac{ha+kb+lc}{\left[h^2+k^2+l^2\right]^{1/2}\left[a^2+b^2+c^2\right]^{1/2}}$$

Equation 5.1

This equation is calculated using the step height of Au (2.35Å) and the periodicity of the steps in the images (82Å). The vicinal surface calculated in this case and the one most likely is Au{16,17,17}. This vicinal surface would have step sizes of 8.4±0.5nm.

The most striking feature from these figures is the occurrence of features along the step edges that are ~15nm apart in the direction of the step when they are bunched together. However, what is more striking is that these features seem to line up step to step. This may mean that there is some nucleation of these features and so when one occurs it propagates others to occur. This is more evident in figures 5.17 (c) and (d) which are from the 5000L dose as the features are not all over the surface like they are for the 10000L dose. It is unknown why this occurs it could be due to polymerisation similar as to what was described for solution deposition or it could be that groups of molecules, maybe polymerised before deposition, may preferentially adsorbed onto the fcc

nucleation site of the vicinal step as was recorded by Baudot et al. for Co deposited on Au{788}[22,23]. As these molecular groups are large this may hinder the adsorption of another group onto the neighbouring fcc site. This would explain why they look to be in rows as the reconstruction would follow this pattern between steps. It is very clear from figures (c) to (h) that the 10000L dose shows this feature much more dramatically than the 5000L dose and in fact the molecular features seem to be using up almost every second available space.

As with G1 it, considering the periodicity of these features from gas phase deposition that the reconstruction has some influence in the way that the molecules induce the facets causing the substrate to be {16,17,17}. This would explain why the Au/mica substrate does not show this effect. However what is unusual is that it is assumed that once the Au single crystal has been dosed with the thiol the reconstruction will be destroyed. However the reconstruction is still visible after deposition[22]. On investigation there are many reports which show that the reconstruction is not easily destroyed and that it is even present after some thiols have been dosed onto it[24,25]. Therefore it is likely that the reconstruction has had some influence on the deposition.

5.6 Conclusion

Although the synthesis was problematic the analytical studies (nmr, GC) showed that the molecule was successfully synthesised. After adsorption onto the surface by both gas phase and solution phase deposition the RAIRS and XPS data show that the molecule has adsorbed onto the Au surface intact. These studies show that the molecule may is ordering on the Au{111} single crystal surface after solution deposition and after gas phase deposition. However no order was observed for the Au/mica substrate.

Once adsorbed onto the surface from solution deposition some long range order can be observed in the form of pseudo hexagonal patterns. This is may due to molecular induced faceting of the Au{111} substrate which then induces the molecular pattern however the substrate is not observed so it has to be assumed that the patterning is an a flat terrace of the Au{111}.

After gas phase deposition a vicinal surface was observed that is consistent with the Au{16,17,17} surface. This vicinal surface was not observed before dosing and it was not observed in the thiocresol study. The formation of possibly a {16,17,17} surface rather than any other surface could be due to the stability of this vicinal surface however, there is no conclusive proof as to why this surface is preferentially induced. Ordering of molecular features is also observed after gas deposition as well as after solution deposition. These seem

to follow a trend of preferentially adsorbing onto every second fcc nucleation site of the vicinal steps.

The occurrence of these stepped areas, the survival of the reconstruction after the gas phase deposition and what looks like step edge nucleation of the molecule after both gas phase and solution deposition, points to the likelihood that the molecule has low sticking probability and it preferentially adsorbs to the step edges.

References

[1] C. M. Whelan, C. J. Barnes, C. J. H. Walker, N. M. D. Brown. Surface Science **425** (1999) 195

[2] S. Frey, V. Stadler, K. Heister, W. Eck, M. Zharnikov, M. Grunze. Langmuir **17** (2001) 2408

[3] L-J. Wan, M. Terashima, H. Noda, M. Osawa. J. Phys. Chem. B. **104** (2000) 3563

[4] C. J. Murphy and H. W. Post Journal of Organic Chemistry (1961) 1486
[5] Find paper

[6] J Morrison personal communication

[7] C.M. Whelan, C.J. Barnes, C.Grégoire, J.-J. Pireaux. Surface Science **454-456** (2000) 67

[8] S. Contarini, S.P. Howlett, C. Rizzo, B.A. De Angelis. Applied Surface Science, **51** (1991) 177

[9] D. Briggs, M.P. Seah. **1** (1993) second edition, John Willey & Sons.

[10] M.H. Dishner, J.C. Hemminger, F.J. Feher. Langmuir **13** (1997) 4788

[11] M.J. Goldberg, J.G. Clabes,C.A. Kovac. J. Vac. Sci. Technol. A **6** (1988) 991

[12] Y-T. Long, S. Herrwerth, W. Eck, M. Grunze. Phys. Chem. Chem. Phys. **4** (2002) 522

[13] K. Shabtai, S. R. Cohen, H. Cohen, I. Rubinstein. J. Phys. Chem. B. **107** (2003) 5540

[14] J. F. Kang, A. Ulman, S. Liao, R. Jordan, g. Yang, G-Y. Liu. Langmuir **17** (2001) 95

[15] C. Fuxen, W. Azzam, R. Arnold, G. Witte, A. Terfort, C. Wöll. Langmuir **17** (2001) 3689

[16] J.W. Niemantsverdriet Spectroscopy in Catalysis **VCH** (1993) 200

[17] A. Marchenko, N. Katsonis, D. Fichou, C. Aubert, M. Malacria. J. Am. Chem. Soc. **124** (2002) 9998

[18] G. E. Poirier. Chem. Rev. **97** (1997) 1117

[19] Q. Jin, J.A. Rodriguez, C.Z. Li, Y. Darici, N.J. Tao. Surface Science **425** (1999) 101

[20] M. H. Dishner, J. C. Hemminger, F. J. Feher Langmuir **13** (1997) 2318

[21] H-Y. Jeong, J. D. Weeks. Phys. Rev. B. **57** (1998) 3939

[22] V. Repain, G. Baudot, H. Ellmer, S. Rousset. Mat. Sci. Eng. B. **96** (2002) 178

[23] G. Baudot, S. Rohart, V. Repain, H. Ellmer, Y. Girard, S. Rousset. App. Surf. Sci. **212-213** (2003) 360

[24] Z. X. Xie, X. Xu, J. Tang, B. W. Mao. J. Phys. Chem. B. **104** (2000) 17719

[25] Q. Wu, W. H. Shang, J. W. Yan, Z. X. Xie, B. W. Mao. J. Phys. Chem. B **107** (2003) 4065

CHAPTER 6

6.1 Summary of Results

In Chapter 3, the adsorption of thiocresol on Au/mica and a Au{111} single crystal is investigated after both solution phase and gas phase deposition. In the gas phase deposition experiments, TPD, AES and XPS data show that thiocresol adsorbs onto the Au{111} surface presumably as the thiolate. The RAIRS data, supported by Gaussian simulations show that the molecule adopts a geometry with the molecular plane close to parallel to the Au surface. The gas phase deposition STM images show ordering at the step edges at low doses (1000L). The molecules are most likely adopting the ($\sqrt{3} \times \sqrt{3}$)R30° structure. From the STM data for solution deposition no ordering is observed however the images do show dramatic examples of etch pits, step edge etching and formation of gold islands. This however only occurs for solution deposition on Au/mica substrates.

The major difference between the solution deposition and the gas phase deposition is that the molecules order at the step edges after gas phase deposition. However the major similarity between gas phase deposition and solution deposition is that the molecule has a dramatic effect on the step edges.

Chapter 4 reports the successful synthesis of the G1 thiol dendrimer vinyldimethyl-p-thiophenylsilane and its disulphide. The adsorption of G1 from solution phase deposition was investigated on both Au{111} and Au/mica surfaces. In addition, the gas phase deposition of G1 was studied on Au{111}.

After adsorption onto the surface by solution phase deposition, the RAIRS and XPS data show that the molecule has adsorbed onto the Au surface predominantly intact though there is evidence from RAIRS that the Si-CH$_3$ bonds are cleaved which may facilitate a direct interaction between Si and the Au surface. There is some indication from STM for the formation of periodic overlayers following solution phase deposition with a periodicity of 7.2±0.5nm and 5±0.5nm. We were unable to resolve any ordered molecular species with STM.

Gas phase deposition contrasts markedly with solution phase deposition. The number of bands observed in RAIRS is considerably fewer which presumably indicates that the adsorption geometry is much more well-defined following gas phase deposition. Though it cannot be completely ruled out as an artefact due to the limited scanning range of STM, it appears that gas phase adsorption results in the facetting of the Au{111} surface to preferentially form Au{788} facets. The periodicities involved agree with those observed following solution phase deposition on the Au{111} surface. No similar features were observed following solution phase deposition on Au/mica surfaces which may indicate that the formation of molecularly induced facets is related to the presence of the Au{111} herringbone reconstruction.

Chapter 5 reports the successful synthesis of the G2 thiol dendrimer and probably also its disulphide. It is difficult to be certain that the molecule remains intact on the surface due to the poor resolution of the XPS data and the relatively poor quality of the RAIRS data. However, STM clearly shows long range periodic structures of dimensions 8.2±0.5nm x 15±0.5nm, following solution phase deposition, and periodic structures of similar dimensions are also observed following gas phase deposition of G2. As was the case with the G1 dendrimer, no ordered structures were observed following solution phase deposition onto Au/mica. Gaussian simulations predict a very intense IR band related to the Si-CH_3 functionalities. As was the case for G1 adsorption, no such band is observed in the G2 case. This may indicate that the Si-CH_3 bonds are cleaved enabling an interaction between Si and Au. This is further supported by the apparent flat lying nature of the aromatic rings of G2.

As was the case for G1 adsorption (Chapter 4), the G2 molecule appears to induce facetting of the Au{111} substrate but with a longer range periodicity possibly a {16,16,17} or similar vicinal surface.

6.2 Other Experiments

Other molecules were synthesised during this project. The first of these was a new dendrimer shown in figure 6.1. During the attempt to make this new dendrimer papers were found that showed this dendrimer had been made before

by Dong et. al.[1] and attached to Au and investigated using the same surface techniques that are used in this work so progress on this molecule stopped.
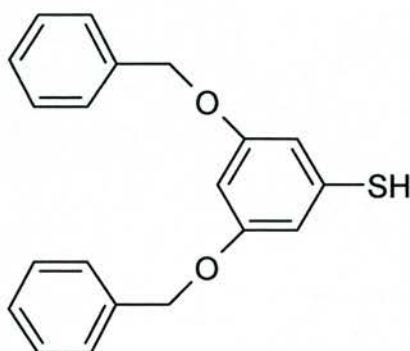

Figure 6.1 The oxygen containing thiol dendrimer which was the aim of the synthesis however this molecule had already been synthesised and adsorbed onto Au before.

We also attempted to synthesise styrene thiol. This was not a novel synthesis[2,3] it has been synthesised before. This synthesis was carried out with the help of Dr. R.A. Aitken. The motivation for the use of styrene thiol was to grow higher generations of dendrimers from the vinyl group of styrene as an alternative to G1 since the synthesis of both G1 and G2 was problematic. This synthesis did not yield styrene thiol due to the strong tendency of this molecule to polymerise. However, the dimer shown in figure 6.2 was successfully synthesised.
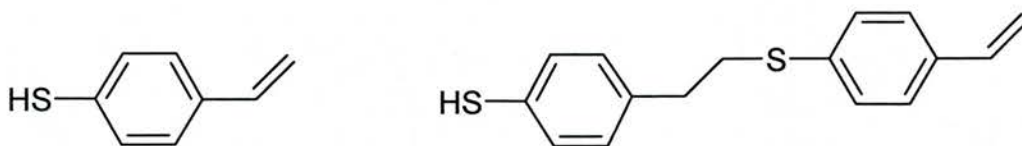
Figure 6.2 Styrene thiol monomer which was the aim of the synthesis and the dimer molecule which was finally produced.

The styrenethiol dimer was adsorbed onto Au{111} and Au/mica. Some RAIRS, STM, XPS and TPD data were taken but are not reported in this thesis.

References

[1] B. Dong, F. Huo, L. Zhang, X. Yang, Z. Wang, X. Zhang, S. Gong, J.Li. Chem. Eur. J. **9** (2003) 2331

[2] C. G. Overberger, A. Lebovits J. Am. Chem. Soc. **78** (1956) 4792

[3] O. Nuyken, M. Hofinger. Polymer Bulletin **11** (1984) 165

Appendix

Spectra 1. Vinyldimethyl-p-bromophenylsilane
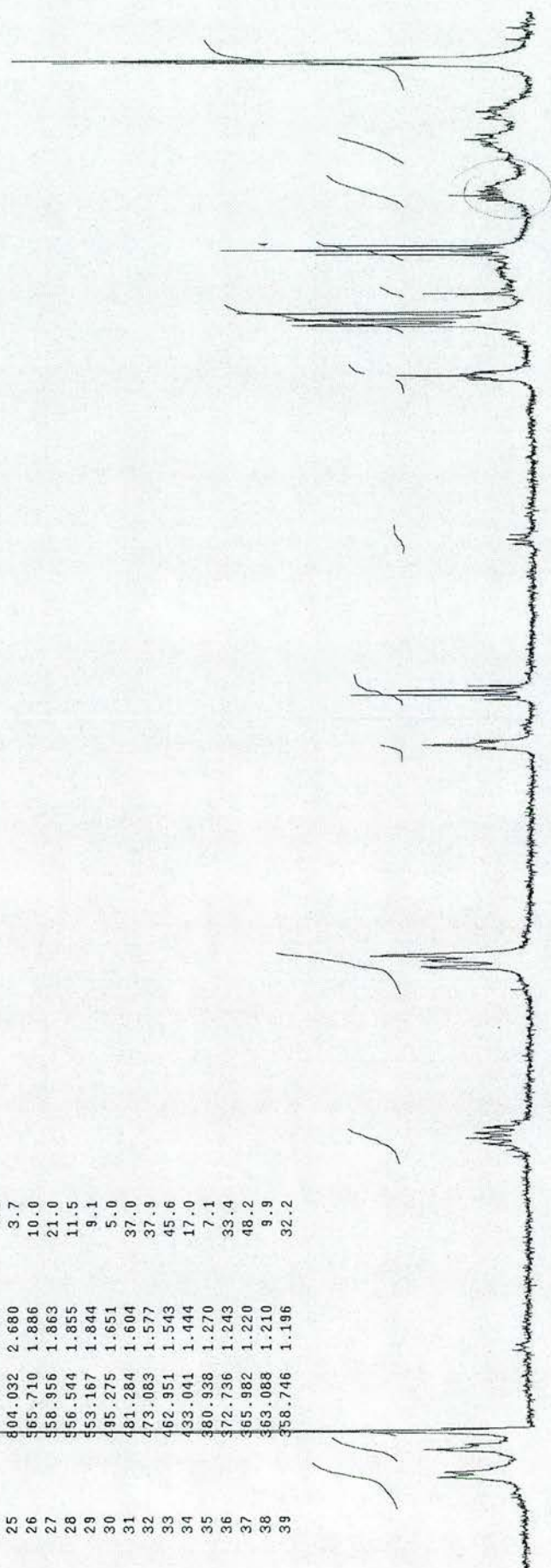
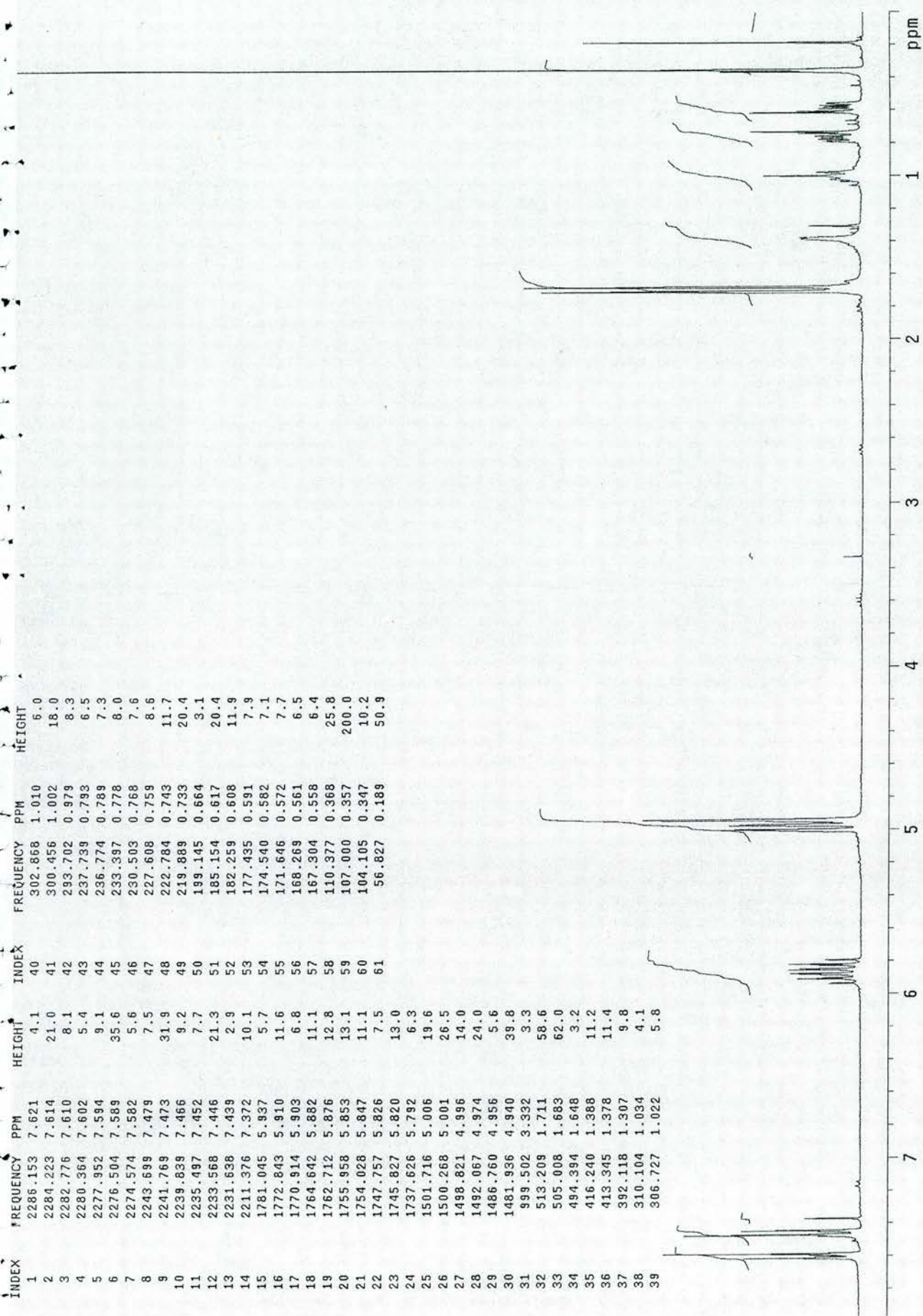Spectra 2. Vinyldimethyl-p-thiophenylsilane

Spectra 3. G2 intermediate 1 NMR

Spectra 4. G2 intermediate 2 NMR

Spectra 5. G2 Thiolatel NMR

Proton NMR spectrum (ppm axis: 7, 6, 5, 4, 3, 2, 1)

Integration values: 6.62 9.03 5.15 5.01 10.53 3.39 3.78 0.74 4.26 13.99 1.91 6.86 6.02 7.07 15.63

#	Freq (Hz)	ppm	Int
2	2245.544	7.485	
3	2210.326	7.368	12.9
4	2180.898	7.270	200.0
5	2178.003	7.260	13.3
6	1740.918	5.803	7.2
7	1732.717	5.776	9.8
8	1724.033	5.747	8.6
9	1713.902	5.713	5.5
10	1715.832	5.720	7.2
11	1503.561	5.012	3.1
12	1468.343	4.895	16.9
13	1459.177	4.864	16.8
14	1450.011	4.834	22.9
15	1451.458	4.838	24.7
16	1127.263	3.758	16.8
17	1120.509	3.735	8.0
18	1121.474	3.738	8.1
19	1057.792	3.526	7.5
20	1050.556	3.502	29.0
21	1043.319	3.478	20.6
22	1036.565	3.455	9.9
23	818.505	2.728	3.3
24	811.269	2.704	4.3
25	804.032	2.680	3.7
26	565.710	1.886	10.0
27	558.956	1.863	21.0
28	556.544	1.855	11.5
29	553.167	1.844	9.1
30	495.275	1.651	5.0
31	481.284	1.604	37.0
32	473.083	1.577	37.9
33	462.951	1.543	45.6
34	433.041	1.444	17.0
35	380.938	1.270	7.1
36	372.736	1.243	33.4
37	365.982	1.220	48.2
38	363.088	1.210	9.9
39	358.746	1.196	32.2

#	Freq (Hz)	ppm	Int
	285.898	0.953	
41	281.556	0.939	8.6
42	279.144	0.931	13.1
43	274.320	0.914	8.2
44	202.437	0.675	8.8
45	195.201	0.651	8.2
46	187.964	0.627	10.7
47	162.878	0.543	9.1
48	152.747	0.509	8.0
49	78.934	0.263	9.0
50	76.040	0.253	74.1
51	75.075	0.250	63.7
52	69.768	0.233	80.4
53	42.269	0.141	23.7
54	24.419	0.081	4.4
55			4.3

PULSE SEQUENCE
Relax. delay 1.000 sec
Pulse 45.0 degrees
Acq. time 2.073 sec
Width 3951.6 Hz
16 repetitions

OBSERVE H1, 299.9859688
DATA PROCESSING
FT size 16384
Total time 1 minute

ehthiol
Pulse Sequence: s2pul
Solvent: CDCl3
Temp. 25.0 C / 298.1 K
GEMINI-300 "gerald"

INDEX	FREQUENCY	PPM	HEIGHT
1	2286.153	7.621	4.1
2	2284.223	7.614	21.0
3	2282.776	7.610	8.1
4	2280.364	7.602	5.4
5	2277.952	7.594	9.1
6	2276.504	7.589	35.6
7	2274.574	7.582	5.6
8	2243.699	7.479	7.5
9	2241.769	7.473	31.9
10	2239.839	7.466	9.2
11	2235.497	7.452	7.7
12	2233.568	7.446	21.3
13	2231.638	7.439	2.9
14	2211.376	7.372	10.1
15	1781.045	5.937	5.7
16	1772.843	5.910	11.6
17	1770.914	5.903	6.8
18	1764.642	5.882	11.1
19	1762.712	5.876	12.8
20	1755.958	5.853	13.1
21	1754.028	5.847	11.1
22	1747.757	5.826	7.5
23	1745.827	5.820	13.0
24	1737.626	5.792	6.3
25	1501.716	5.006	19.6
26	1500.268	5.001	26.5
27	1498.821	4.996	14.0
28	1492.067	4.974	24.0
29	1486.760	4.956	5.6
30	1481.936	4.940	39.8
31	999.502	3.332	3.3
32	513.209	1.711	58.6
33	505.008	1.683	62.0
34	494.394	1.648	3.2
35	416.240	1.388	11.2
36	413.345	1.378	11.4
37	392.118	1.307	9.8
38	310.104	1.034	4.1
39	306.727	1.022	5.8

INDEX	FREQUENCY	PPM	HEIGHT
40	302.868	1.010	6.0
41	300.456	1.002	18.0
42	293.702	0.979	8.3
43	237.739	0.793	6.5
44	236.774	0.789	7.3
45	233.397	0.778	8.0
46	230.503	0.768	7.6
47	227.608	0.759	8.6
48	222.784	0.743	11.7
49	219.889	0.733	20.4
50	199.145	0.664	3.1
51	185.154	0.617	20.4
52	182.259	0.608	11.9
53	177.435	0.591	7.9
54	174.540	0.582	7.1
55	171.646	0.572	7.7
56	168.269	0.561	6.5
57	167.304	0.558	6.4
58	110.377	0.368	12.8
59	107.000	0.357	200.0
60	104.105	0.347	10.2
61	56.827	0.189	50.9

PULSE SEQUENCE
Relax. delay 1.000 sec
Pulse 45.0 degrees
Acq. time 2.073 sec
Width 3951.6 Hz
16 repetitions

OBSERVE   H1, 299.985378

DATA PROCESSING
FT size 16384
Total time 1 minute

ehden2

Pulse Sequence: s2pul

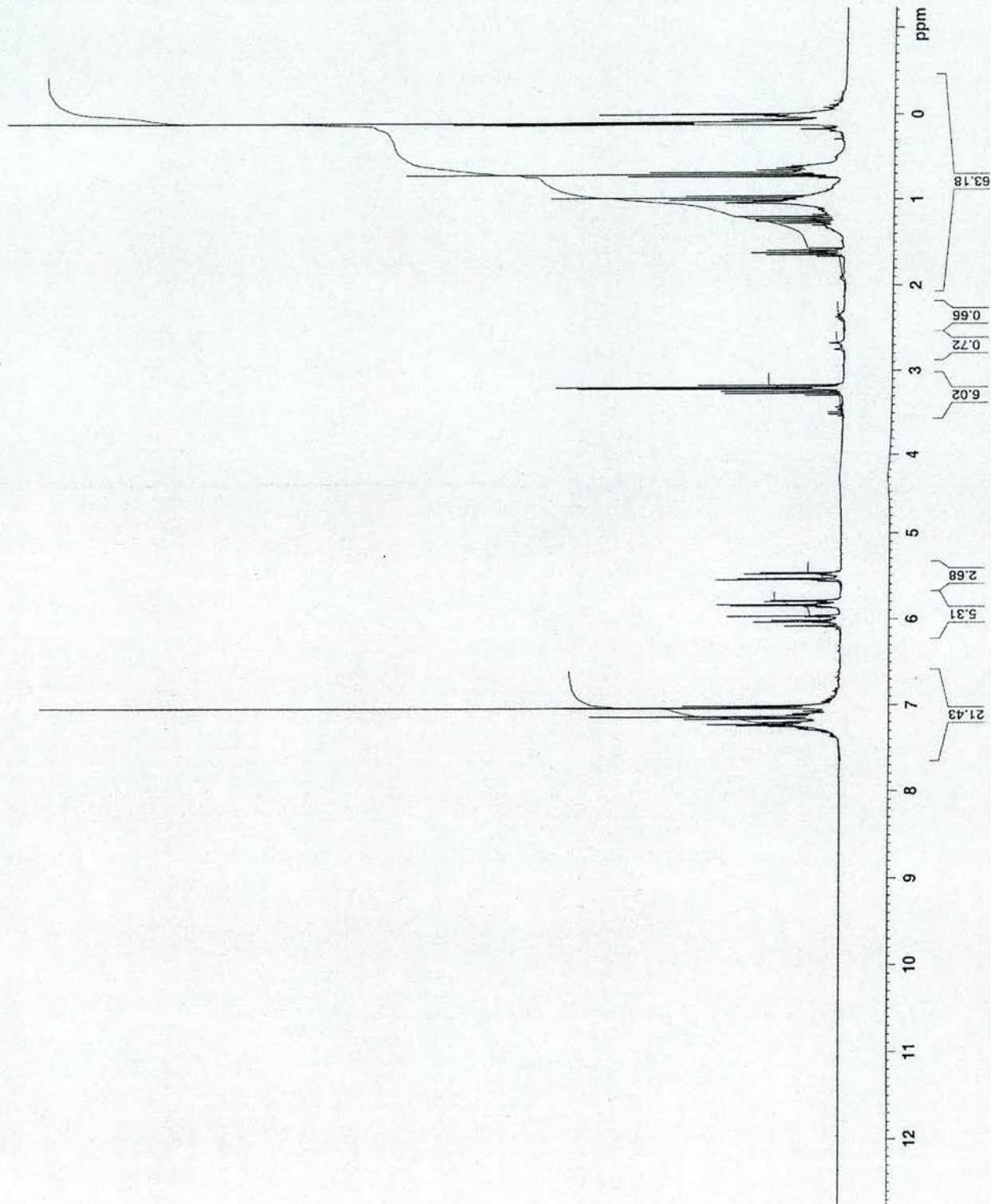Solvent: CDC13
Temp. 25.0 C / 298.1 K
GEMINI-300 "gerald"

ppm

INDEX	FREQUENCY	PPM	HEIGHT
1	2293.872	7.647	23.2
2	2291.942	7.640	7.4
3	2287.600	7.626	9.0
4	2285.670	7.619	37.5
5	2243.699	7.479	33.3
6	2241.769	7.473	9.3
7	2235.497	7.452	24.2
8	2211.858	7.373	14.9
9	412.863	1.376	13.7
10	409.003	1.363	9.4
11	405.626	1.352	9.8
12	403.696	1.346	9.5
13	398.872	1.330	7.8
14	395.495	1.318	21.8
15	318.306	1.061	20.4
16	314.929	1.050	9.9
17	310.104	1.034	10.6
18	308.175	1.027	9.6
19	304.315	1.014	8.3
20	300.456	1.002	11.5
21	130.639	0.435	18.4
22	127.744	0.426	200.0
23	56.827	0.189	33.0

ppm

BRUKER

silicon thiol

63.18

0.66

0.72

6.02

2.68

5.31

21.43

ppm

0 1 2 3 4 5 6 7 8 9 10 11 12

eh1

Pulse Sequence: s2pul

Solvent: CDCl3
Temp. 25.0 C / 298.1 K
GEMINI-300 "gerald"

34.51

21.42

6.01

5.65   6.06

OBSERVE   H1, 299.9859739

DATA PROCESSING
FT size 131072
Total time 1 minute

12.52
13.83

PULSE SEQUENCE
Relax. delay 1.000 sec
Pulse 45.0 degrees
Acq. time 8.292 sec
Width 3951.6 Hz
8 repetitions